(12)

AAE

AERONAUTICAL AND ASTRONAUTICAL ENGINEERING DEPARTMENT

AN EXPERIMENTAL STUDY OF CW HF CHEMICAL LASER AMPLIFIER PERFORMANCE AND ZERO POWER GAIN

L. H. Sentman, P. Theodoropoulos, R. Waldo,
T. Nguyen and R. Snipes

ENGINEERING EXPERIMENT STATION, COLLEGE OF ENGINEERING, UNIVERSITY OF ILLINOIS, URBANA

(12)

Aeronautical and Astronautical Engineering Department

University of Illinois at Urbana-Champaign

Urbana, Illinois

✓

Technical Report AAE-TR-87-6,

UILU-Eng-87-0506

AN EXPERIMENTAL STUDY OF CW HF CHEMICAL LASER AMPLIFIER PERFORMANCE AND ZERO POWER GAIN

L. H. Sentman, P. Theodoropoulos, R. Waldo,
T. Nguyen and R. Snipes

Prepared for

Defense Advanced Research Projects Agency

1400 Wilson Blvd.

Arlington, VA 22209

August, 1987

SECURITY CLASSIFICATION OF THIS PAGE (When Data Entered)

REPORT DOCUMENTATION PAGE

READ INSTRUCTIONS BEFORE COMPLETING FORM

1. REPORT NUMBER: AAE 87-6 UILU ENG 87-0506	2. GOVT ACCESSION NO.: AD-A185 241
3. RECIPIENT'S CATALOG NUMBER:	
4. TITLE (and Subtitle): An Experimental Study of cw HF Chemical Laser Amplifier Performance and Zero Power Gain	5. TYPE OF REPORT & PERIOD COVERED: Technical Report
	6. PERFORMING ORG. REPORT NUMBER:
7. AUTHOR(s): L. H. Sentman, P. Theodoropoulos, R. Waldo, T. Nguyen and R. Snipes	8. CONTRACT OR GRANT NUMBER(s): N00014-85-K-0326
9. PERFORMING ORGANIZATION NAME AND ADDRESS: Aeronautical and Astronautical Engineering, University of Illinois at Urbana-Champaign, Urbana, IL 61801	10. PROGRAM ELEMENT, PROJECT, TASK AREA & WORK UNIT NUMBERS:
11. CONTROLLING OFFICE NAME AND ADDRESS: Defense Advanced Research Projects Agency, 1400 Wilson Boulevard, Arlington, VA 22209	12. REPORT DATE: August 1987
	13. NUMBER OF PAGES:
14. MONITORING AGENCY NAME & ADDRESS (if different from Controlling Office): Office of Naval Research, Resident Representative, Room 286, 536 South Clark Street, Chicago, IL 60605	15. SECURITY CLASS. (of this report): UNCLASSIFIED
	15a. DECLASSIFICATION/DOWNGRADING SCHEDULE:

16. DISTRIBUTION STATEMENT (of this Report)

UNLIMITED

17. DISTRIBUTION STATEMENT (of the abstract entered in Block 20, if different from Report)

18. SUPPLEMENTARY NOTES

19. KEY WORDS (Continue on reverse side if necessary and identify by block number)

Chemical laser
Chemical laser amplifier performance
Zero power gain

20. ABSTRACT (Continue on reverse side if necessary and identify by block number)

The multiline and single-line amplifier performance of a two channel Helios CL II laser was studied. Flow channel aperturing of the input beam was found to cause a significant reduction in the measured amplification ratio. The absorption of the multiline input beam by SF_6 was found to be negligible (< 0.5%/cm). Maximum multiline and single line amplification was obtained when the input beam was passed through the amplifier at the X_c corresponding to maximum zero power gain. Single-line amplification ratios were considerably lower than multiline

DD FORM 1 JAN 73 1473 EDITION OF 1 NOV 65 IS OBSOLETE

SECURITY CLASSIFICATION OF THIS PAGE (When Data Entered)

20. ABSTRACT

cont'd → amplification ratios obtained for the same input power. The $P_2^{\Pi}(6)$ amplification ratios were lower than the $P_1^{\Pi}(6)$ amplification ratios, even though the $P_2^{\Pi}(6)$ zero power gain was considerably higher than the $P_1^{\Pi}(6)$ zero power gain. The data suggested that about 1/3 of the oscillator output needs to be input to obtain amplifier output equal to the device's oscillator performance.

Low pressure (5-7 torr) $P_2(J)$ peak zero power gains were about 1.55 times larger than the $P_1(J)$ peak zero power gains. The zero power gain zones of the $P_1(J)$ lines were about 1.3 times longer than those of the $P_2(J)$ lines. The zero power gains of all the $P_1(J)$ lines peaked 1.5 - 2.0 mm downstream of the H_2 injectors while the zero power gains of the $P_2(J)$ lines peaked 1.0 mm downstream of the H_2 injectors. The lines with the highest zero power gains were $P_1(5)$ and $P_1(6)$ for the 1→0 vibrational band and $P_2(5)$ and $P_2(6)$ for the 2→1 vibrational band. High pressure (10-12 torr) did not affect the peak $P_1(6)$ zero power gain but caused a 22.5% decrease in the peak $P_2(5)$ and $P_2(6)$ gains. The gain zones were shortened by 46.7%. Zero power gain measurements obtained with vertically polarized, horizontally polarized and unpolarized beams showed that polarization does not affect zero power gain.

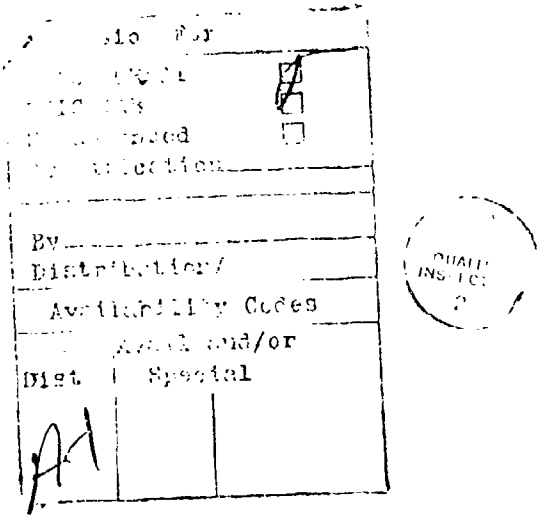

TABLE OF CONTENTS

I. INTRODUCTION

This research is an integrated experimental and theoretical investigation of the multiline issues associated with assessing the impact of temporal variations in a cw HF device on the capability of achieving a phased output beam from multiple laser cavities. The objectives of this research are to fully characterize the output of an oscillator-amplifier (MOPA) configuration as a function of the oscillator input beam, time-dependent oscillations, mode beats, and determine if the coupling between the oscillator and amplifier perturbs the oscillator output; these studies are to be carried out for first one and then two amplifiers driven by the same oscillator. To accomplish these objectives, the zero power gain distribution of the different lines in the amplifier must be known because it provides essential information required in conducting MOPA experiments and interpreting their results.

The objectives of this study were to perform a preliminary experimental investigation of the performance of a cw HF amplifier, to experimentally determine the zero power gains of several lines in the amplifier and to examine the effect of polarization on zero power gain. A single channel Helios CL I cw HF chemical laser was used as the oscillator and a two channel Helios CL II cw HF chemical laser was used as the amplifier. The flow channel in the single channel Helios CL I laser is identical to one of the flow channels in the two channel Helios CL II laser. Thus, when the CL I is run at one half the mass flow rates of the CL II, the flow fields in the oscillator and amplifier are identical.

Comparison of the 0% and the 50% aperturing data for the same oscillator/amplifier flow rate combinations showed that aperturing of the input beam by the amplifier flow channel causes a reduction of 16.0% in the amplification ratio. For this reason, all data were taken with no flow

channel aperturing of the input beam. The absorption of the input beam due to SF_6 was measured and it was found to be quite small (< 0.5%/cm), and thus its effects on amplifier performance were neglected.

Multiline amplification experiments showed that maximum amplification occurs when the input beam is passed through the amplifier at the X_c location corresponding to peak amplifier gain. This is consistent with the results of previous studies[1] in the sense that when the CL II is run as an oscillator with a stable resonator, peak power is obtained at an X_c that is close to the X_c for maximum amplification. The effect of input intensity on the amplification ratio was clearly demonstrated when higher amplification ratios were obtained when both the oscillator and the amplifier were run at the Run 34 flow rates than when both were run at the Run 36 flow rates. Investigation of the MOPA performance as a function of input power showed that about 1/3 of the oscillator output must be input to the amplifier to obtain amplifier output equal to the CL II's oscillator performance.

Single-line amplification experiments showed that maximum amplification occurs when the input beam is passed through the amplifier at the X_c for maximum zero power gain. The single-line amplification ratios were considerably lower than the multiline amplification ratios that were measured using the same input power, because in the multiline case the total input power was distributed among the different lines. The $P_2(6)$ amplification ratios measured were lower than the $P_1(6)$ amplification ratios, even though the $P_2(6)$ zero power gain was found to be considerably higher than the $P_1(6)$ zero power gain.

Comparison of the $P_1(J)$ and the $P_2(J)$ zero power gain data shows that the $P_2(J)$ peak zero power gains are about 1.55 times larger than the $P_1(J)$ peak zero power gains and that the length of the gain zone of the $P_1(J)$ lines is

about 1.3 times larger than that of the $P_2(J)$ lines. The zero power gains of all the $P_1(J)$ lines peaked .5 - 2.0 mm downstream of the H_2 injectors while the zero power gains of all the $P_2(J)$ lines peaked 1.0 mm downstream of the H_2 injectors. The lines with the highest zero power gains were $P_1(5)$ and $P_1(6)$ for the 1→0 vibration band and $P_2(5)$ and $P_2(6)$ for the 2→1 vibrational band.

Comparison of zero power gain data obtained 0.75 mm above, 0.75 mm below, and at the centerline of the flow channel shows that the zero power gain values obtained 0.75 mm above and 0.75 mm below the center of the flow channel are almost identical and higher than the values of the zero power gain measured on the flow channel centerline.

High pressure zero power gain measurements were made for lines $P_1(6)$, $P_2(5)$ and $P_2(6)$. Comparison of low and high pressure zero power gain data shows that high pressure zero power gain zones are considerably shorter than low pressure zero power gain zones. The peak zero power gain of $P_1(6)$ was not affected by high pressure but the peak zero power gains of $P_2(5)$ and $P_2(6)$ were decreased by about 22.5%.

Comparison of zero power gains obtained with a vertically polarized, a horizontally polarized and an unpolarized beam showed that polarization does not affect zero power gain. To obtain an unpolarized beam, non-Brewster windows were used on both the oscillator and the amplifier. The non-Brewster windows on the amplifier acted as a Fabry-Perot resonator, causing the amplifier to lase on lines $P_2(4)$ and $P_2(5)$. The fact that the lines $P_2(4)$ and $P_2(5)$ lased with the non-Brewster windows on the amplifier suggests that $P_2(4)$ and $P_2(5)$ have the highest gains, which is in agreement with the experimental results that showed $P_2(5)$ to have the highest zero power gain followed by lines $P_2(4)$ and $P_2(6)$ whose gains were found to be about equal.

Comparison of the experimental zero power gains with the zero power gains

calculated using the Blaze II computer simulation[2] of the Helios laser showed that the calculated $P_1(J)$ peak zero power gains were about 9% smaller than the experimental ones, while the calculated $P_2(J)$ peak zero power gains were about 13% larger than the experimental ones. The calculations predicted gain zones that are about 30% longer than the ones obtained experimentally. The calculated $P_1(J)$ zero power gains peaked 4.0 mm downstream of the H_2 injectors, while the experimental $P_1(J)$ zero power gains peaked 1.5 to 2.0 mm downstream of the H_2 injectors. The calculated $P_2(J)$ zero power gains peaked 2.0 mm downstream of the H_2 injectors and the experimental ones peaked 1.0 mm downstream of the H_2 injectors. The Blaze II computer simulation of the laser predicted peak zero power gain lines that are two J's lower than the data.

Section II presents preliminary multiline and single-line amplifier data, and the effects of flow channel aperturing and SF_6 absorption on amplifier performance. In Section III, low and high pressure zero power gain data for several lines for the Run 34 and the Run 36 flow rates in the amplifier, and the effects of polarization on zero power gain are given. In Section IV, several concluding remarks are presented.

II. PRELIMINARY AMPLIFIER EXPERIMENTS

2.1 EXPERIMENTAL PROCEDURE

The oscillator used in these experiments is a single channel Helios CL I laser, while the amplifier is a two channel Helios CL II laser. The flow channel of the CL I laser is identical to one of the flow channels of the CL II laser. This permits the flow field of the oscillator and amplifier to be identical when the CL I laser is run at one half the flow rates of the CL II amplifier.

Figure 1 shows a schematic of the layout of the master oscillator/power amplifier (MOPA) experiments. The oscillator performance was determined by comparing P_1 (the power measured at location 1) to existing data[3]. The transmissivity of the turning mirror #2 and telescope combination (TMT) was obtained by measuring the power at locations 2 and 3, and is given by

$$TMT = \frac{P_3}{P_2} \qquad (2.1\text{-}1)$$

The power input to the amplifier is P_4, and is given by,

$$P_{IN} = P_4 = P_3 \cdot TLW = P_2 \cdot TMT \cdot TLW \qquad (2.1\text{-}2)$$

where TLW is the transmissivity of the left amplifier Brewster window which was measured.

The gain or loss in the amplifier's media is given by,

$$\alpha = \frac{1}{I}\frac{dI}{dz} \qquad (2.1\text{-}3)$$

where I is the intensity and z is the coordinate along the optical axis of the amplifier cavity. If it is assumed that α is independent of z, then,

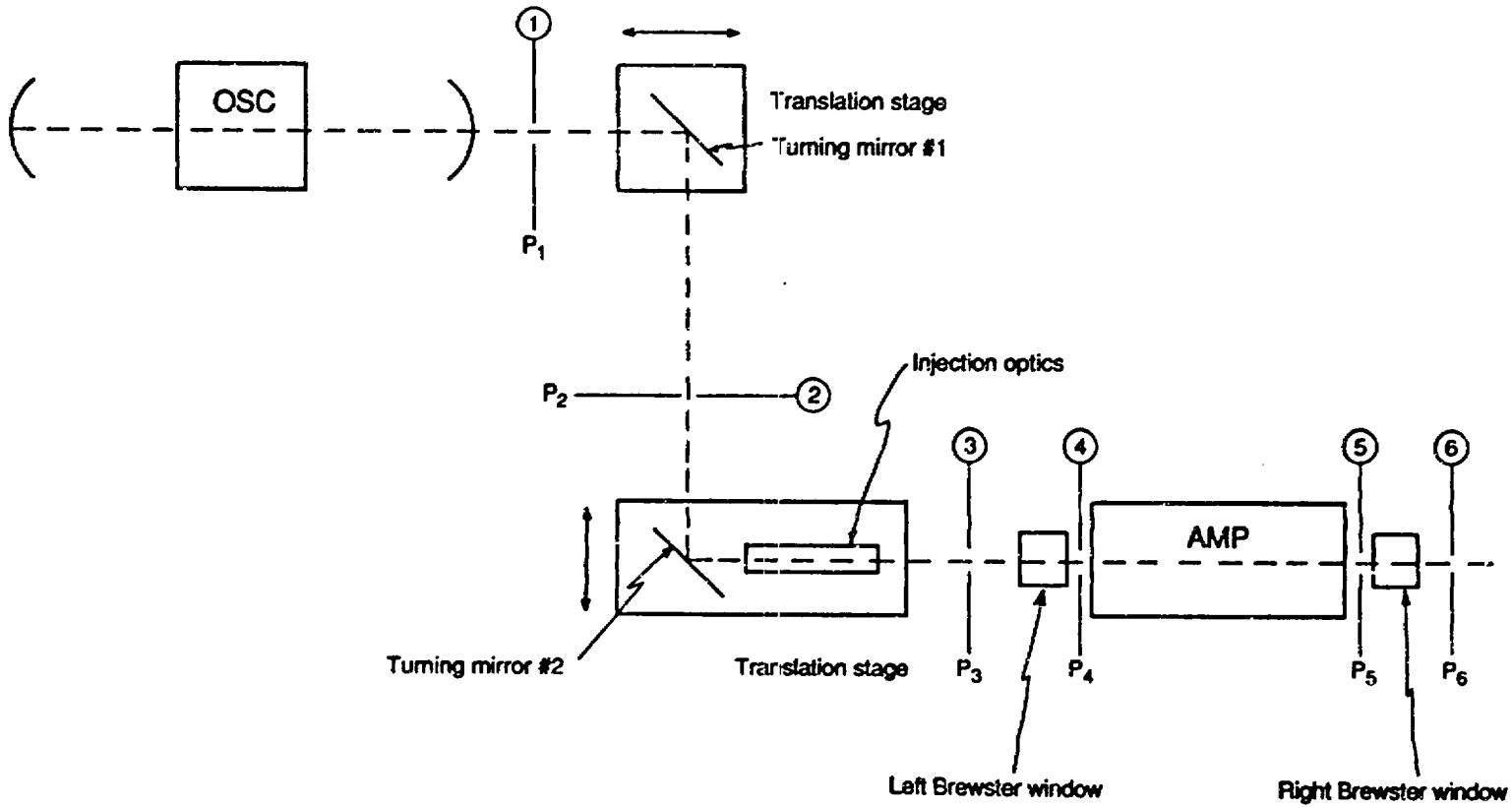

Figure 1. Schematic of the MOPA experimental layout showing the positions at which the power was measured or calculated in order to determine oscillator performance, amplifier input power, and amplifier output power.

$$\alpha \int_0^{Le} dz = \int_{I_{IN}}^{I_{OUT}} \frac{dI}{I} = \int_{I_4}^{I_5} \frac{dI}{I} \qquad (2.1\text{-}4)$$

where Le is the effective length of the mixed region in the amplifier, given by Blaze II (a rotational equilibrium Fabry-Perot model) as 24.4 cm, $I_{IN} = I_4$ is the amplifier input intensity, and $I_{OUT} = I_5$ is the amplifier output intensity. After the integration is carried out, Eq. (2.1-4) gives

$$\alpha = \frac{1}{Le} \ln \frac{I_5}{I_4} \qquad (2.1\text{-}5)$$

where $$I_5 = \frac{P_5}{A_5} \qquad (2.1\text{-}6a)$$

and $$I_4 = \frac{P_4}{A_4} \qquad (2.1\text{-}6b)$$

If the input and output beam cross sectional areas (A_4 and A_5 respectively) are assumed to be equal, (2.1-5) and (2.1-6) can be combined to obtain

$$\alpha = \frac{1}{Le} \ln \frac{P_5}{P_4} = \frac{1}{Le} \ln \frac{P_{OUT}}{P_{IN}} \qquad (2.1\text{-}7)$$

If the amplification ratio, AR, is defined as

$$AR = \frac{P_{OUT}}{P_{IN}} \qquad (2.1\text{-}8)$$

then $$\alpha = \frac{1}{Le} \ln AR \qquad (2.1\text{-}9)$$

The experiment was set up so that the H_2 supply to the amplifier could be turned on and off, Fig. 2. When the input beam was not apertured by the flow channel and the H_2 was turned off,

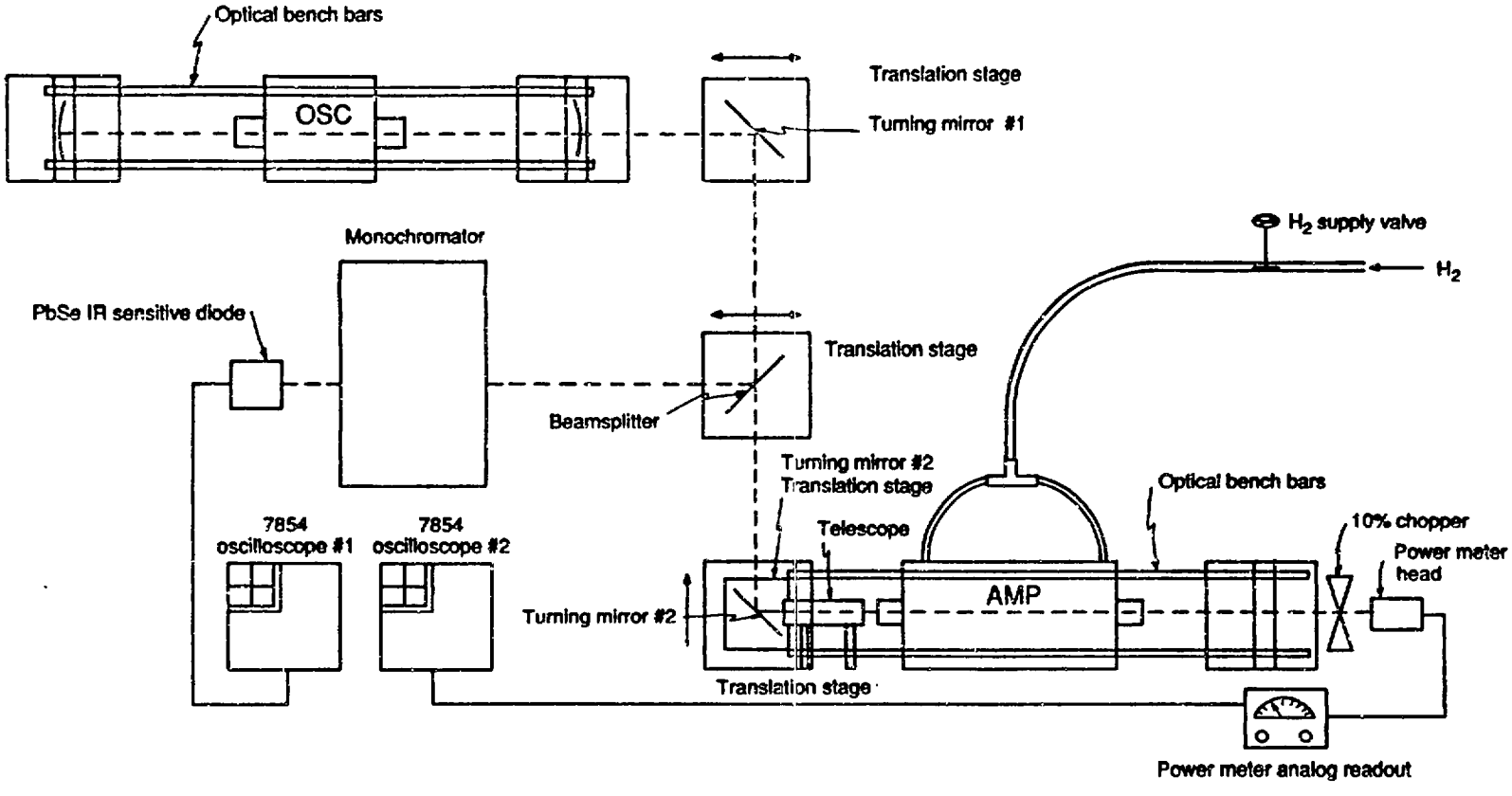

Figure 2. Schematic of the MOPA experimental layout used for amplification measurements and to identify the wavelengths of the lasing lines when the oscillator was run single line.

$$P_5 = P_4 = P_{IN} \tag{2.1-10}$$

and $$P_{6\ H_2\ OFF} = P_5\ TRW = P_4\ TRW = P_{IN}\ TRW \tag{2.1-11}$$

where TRW is the transmissivity of the right Brewster window. When the H_2 was turned on,

$$P_{6\ H_2\ ON} = P_5 \cdot TRW = P_{OUT} \cdot TRW \tag{2.1-12}$$

Then the amplification ratio can be expressed as

$$AR = \frac{P_{OUT}}{P_{IN}} = \frac{P_{6\ H_2\ ON}}{TRW} \frac{TRW}{P_{6\ H_2\ OFF}} = \frac{P_{6\ H_2\ ON}}{P_{6\ H_2\ OFF}} \tag{2.1-13}$$

When the input beam was apertured by the flow channel,

$$P_{IN} = P_4 \cdot TAP \tag{2.1-14}$$

where TAP is the transmissivity of the amplifier flow channel. TAP was determined by measuring the power at locations 3 and 6 with no flow in the amplifier. Then,

$$TAP = \frac{P_5}{P_4} = \frac{P_6}{TRW \cdot P_3 \cdot TLW} \tag{2.1-15}$$

The amplification ratio when there was flow channel aperturing of the input beam is given by

$$AR = \frac{P_{OUT}}{P_{IN}} = \frac{P_{6\ H_2\ ON}}{TRW \cdot P_4 \cdot TAP} \tag{2.1-16}$$

But P_{IN} is also given by

$$P_{IN} = \frac{P_{6\ H_2\ OFF}}{TRW} \tag{2.1-17}$$

and thus

$$AR = \frac{P_{OUT}}{P_{IN}} = \frac{P_{6\ H_2\ ON}}{TRW} \frac{TRW}{P_{6\ H_2\ OFF}} = \frac{P_{6\ H_2\ ON}}{P_{6\ H_2\ OFF}} \qquad (2.1\text{-}18)$$

Since Eqs. (2.1-13) and (2.1-18) are the same, the amplification ratio is given by the same equation when the input beam is and is not apertured by the flow channel.

The total multiline and single-line power was measured by placing a Scientech Model 362 power meter at locations 1, 2, 3 and 6. In the cases where the total power of the amplified beam ($P_{6\ H_2\ ON}$) exceeded nine watts (the power meter can measure up to ten watts), a chopper was used to reduce the total power input to the power meter head by 90%, Fig. 2. The chopper was always placed after the amplifier for two reasons. If placed before the amplifier, the chopper causes a discontinuous sampling of the amplifier media, that is, when the beam is blocked, the flow recovers its zero power gain which influences the measured amplification ratio. Second, the beam shape is distorted and the beam diameter is increased when the beam passes through the chopper. This results in undesirable flow channel aperturing (Section 2.3) which influences the measured amplification ratio.

Fluctuations of the oscillator output power sometimes made it difficult to accurately read the analog scale of the power meter. This problem was solved by connecting the power meter to a 7854 digitizing Tektronix oscilloscope which was used to measure the area under the power meter signal after the signal was averaged one hundred times, Fig. 2. The 7854 digitizing oscilloscope was also used to measure a "zero area" when there was no input to the power meter. This zero area was needed to correct the $P_{6\ H_2\ ON}$ and $P_{6\ H_2\ OFF}$ areas. The amplification ratio is then given by Eq. (2.1-13) and by the ratio of the area obtained from the power meter signal with H_2 in the amplifier on minus the zero area obtained with no signal, to the area

obtained from the power meter signal when the H_2 in the amplifier was off minus the zero area obtained with no signal,

$$AR = \frac{A_{6\ H_2\ ON} - A_{ZERO\ H_2\ ON}}{A_{6\ H_2\ OFF} - A_{ZERO\ H_2\ OFF}} \tag{2.1-19}$$

The amplification ratios obtained from these two methods were compared for consistency. Because of power fluctuations in the input beam to the amplifier, the amplification ratios obtained from areas are more accurate than those obtained from reading the analog scale of the power meter. For this reason, the gains were always calculated using the amplification ratios obtained from the areas. Absolute values of the input and output powers were obtained from

$$P_{IN} = \frac{P_{6\ H_2\ OFF}}{TRW} \tag{2.1-20}$$

$$P_{OUT} = \frac{P_{6\ H_2\ ON}}{TRW} \tag{2.1-21}$$

The pressure in both the oscillator and the amplifier was adjusted by flow control valves. Cavity pressures in the 5-7 torr range were achieved in both lasers by keeping the oscillator valve entirely open and the amplifier valve partially open. The pressure in both cavities was measured by a digital readout connected to two Baratron pressure gauges which in turn were connected to a centerline pressure tap in each laser cavity which was 5 mm downstream of the H_2 injectors.

The beam was injected into the amplifier by using a two-lens telescope, Figs. 2 and 3. The first lens is a CaF_2 plano-convex with a focal length of 250 mm, while the second lens is a CaF_2 plano-concave with a focal length of

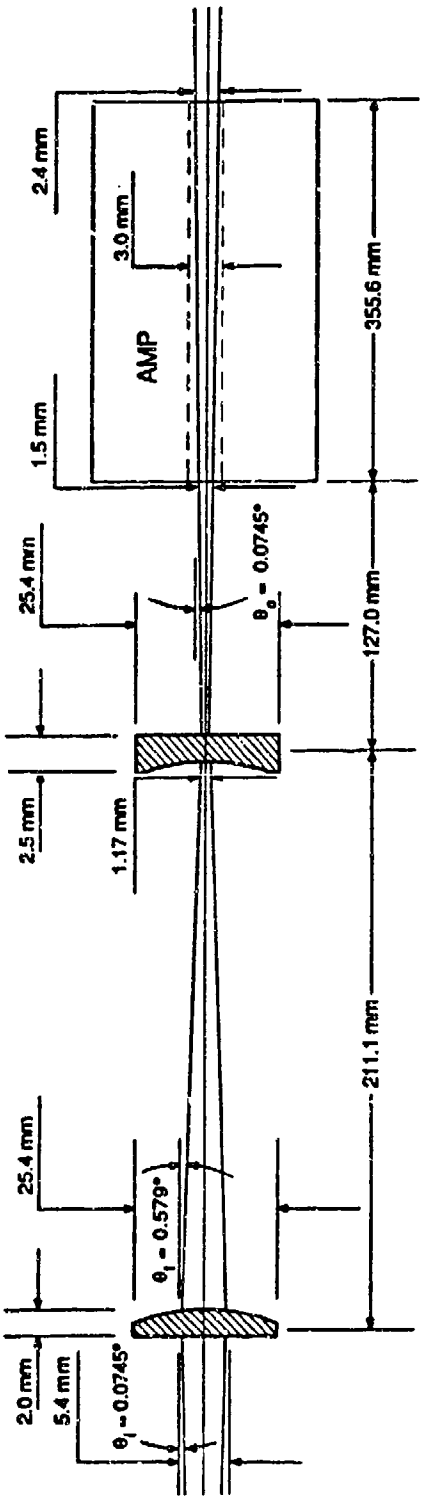

Figure 3. Schematic of the two telescope lenses used to reduce the beam diameter and pass it through the amplifier without flow channel aperturing.

-50 mm. The first lens was used to focus the beam down to about 1.5 mm diameter, while the second lens was used to produce a nearly parallel input beam. The lens did not remove the inherent oscillator beam divergence of about 2 milliradians. The telescope was attached to four translation stages which in turn were fastened to the rod structure of the CL II optical bench to permit a precise vertical and horizontal alignment of the input beam with respect to the amplifier flow channel, Fig. 4. This optical injection system provided a 1.5 mm diameter beam at the inlet of the amplifier and a 2.4 mm diameter beam at the exit of the amplifier, thus avoiding flow channel aperturing (the flow channels of both the oscillator and the amplifier are 3.0 mm high) which will be shown later to have a negative effect on amplifier performance.

2.2 AMPLIFIER AND OSCILLATOR ALIGNMENT

Since the two channel Helios CL II laser that was used as the amplifier has a 3.0 mm flow channel height and is 355.6 mm long, a precise alignment of all the optical elements involved (i.e. turning mirrors #1 and #2, as well as the two telescope lenses, Fig. 2) was necessary in order to pass the multiline or single-line beam produced by the oscillator through the amplifier without flow channel aperturing and maintain control of the location and direction of the beam with respect to the amplifier H_2 injectors. This alignment problem was separated into two parts by always having the input beam follow the same path from turning mirror #1 to turning mirror #2. When this was accomplished, once the injection optics were aligned to pass the beam through the amplifier parallel to the H_2 injectors, changes in the position of the oscillator output beam could be corrected with turning mirror #1 without having to realign the injection optics.

To ensure that the input beam always followed the same path from mirror

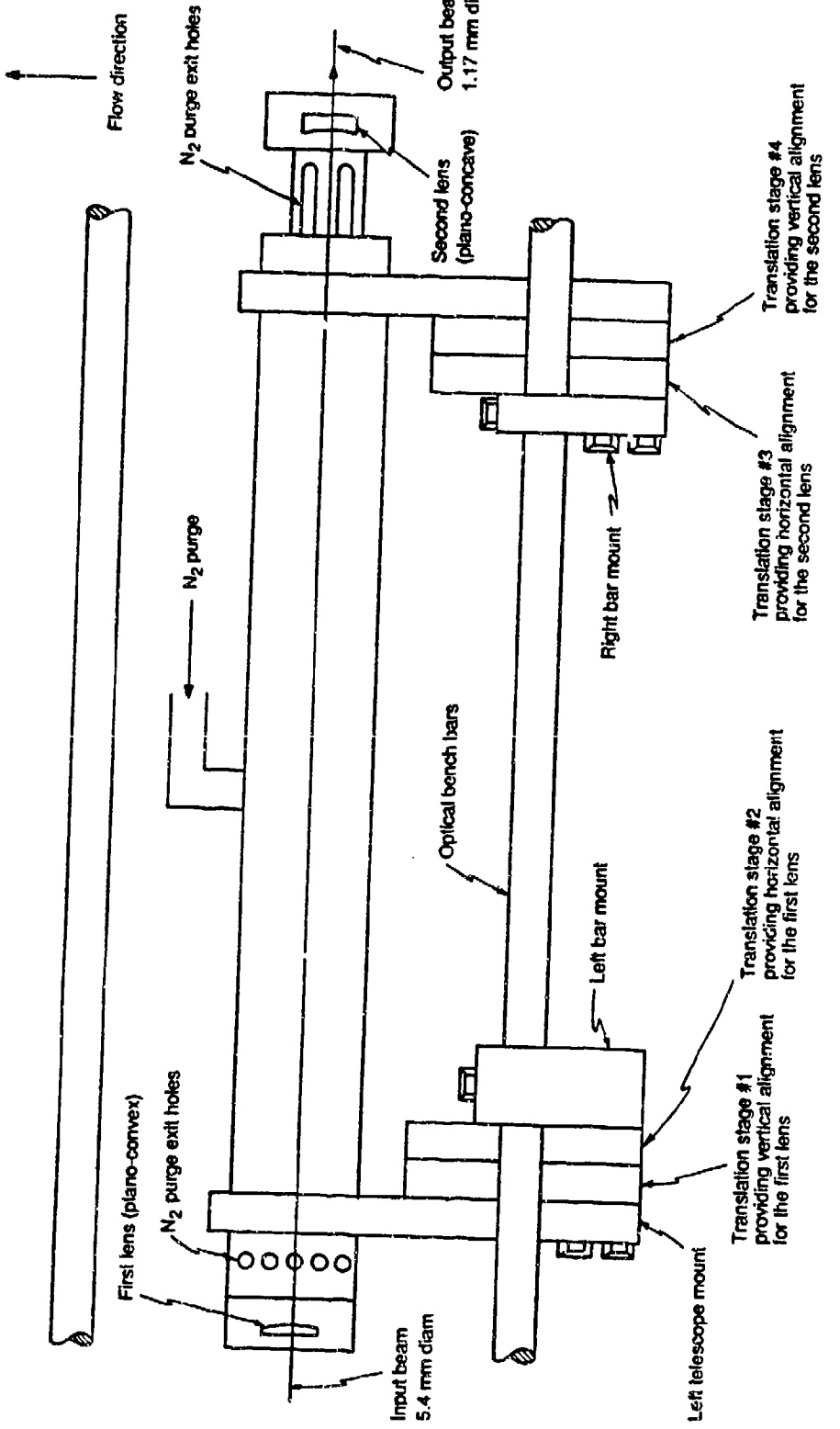

Figure 4. Schematic of the telescope support and alignment mechanisms.

#1 to mirror #2, it was necessary to design and manufacture a special gig for holding burnblocks. The gig was made so that the holes in its base could be aligned with the holes of the optical table, Fig. 5. The alignment of turning mirrors #1 and #2 can be best explained if an x-y coordinate system is defined on the surface of the optical table, Fig. 6. Turning mirror #1 was first aligned as follows: the gig with a burnblock on it was placed at location B (which can be represented by the point (x,y_1)), and mirror #1 was rotated until the beam from the CL I would hit the burnblock somewhere close to the center. At this point a burn was taken. Then the gig was moved to location A (point (x,y_2)), where a new burn was taken. Turning mirror #1 was adjusted so that next time the center of the burns taken at locations A and B would be closer together. This was repeated until the centers of the two burns were the same. Turning mirror #2 was aligned by placing the gig with a burnblock at locations C (point (x_1,y)) and D (point (x_2,y)) and following the above procedure. In this case however, it was also necessary to align the beam with the H_2 injectors of the amplifier. This was accomplished by translating turning mirror #2 in a direction perpendicular to the amplifier's optical axis until the beam was aligned with the amplifier's H_2 injectors. The alignment of the beam with respect to the H_2 injectors was checked by taking paper-burns at the inlet and exit of the amplifier.

The next optical element to be aligned was the first telescope lens (plano-convex). The lens was first placed on the left side of the telescope and a paper-burn was taken at the inlet of the amplifier. Then depending on the location of the beam with respect to the amplifier's H_2 injectors, the first and second telescope translation stages were adjusted in an effort to align the beam with the H_2 injectors at the inlet of the amplifier. This process was repeated until the beam was aligned with the H_2 injectors. The

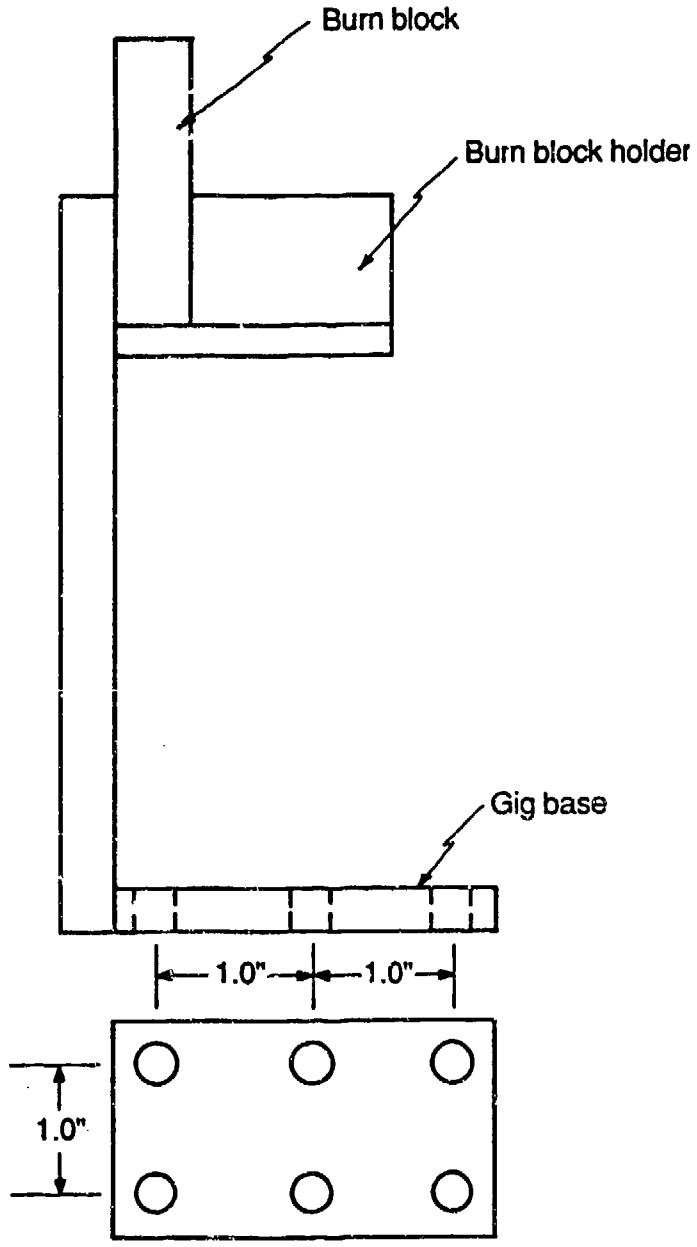

Figure 5. Schematic of the gig used to align turning mirrors #1 and #2.

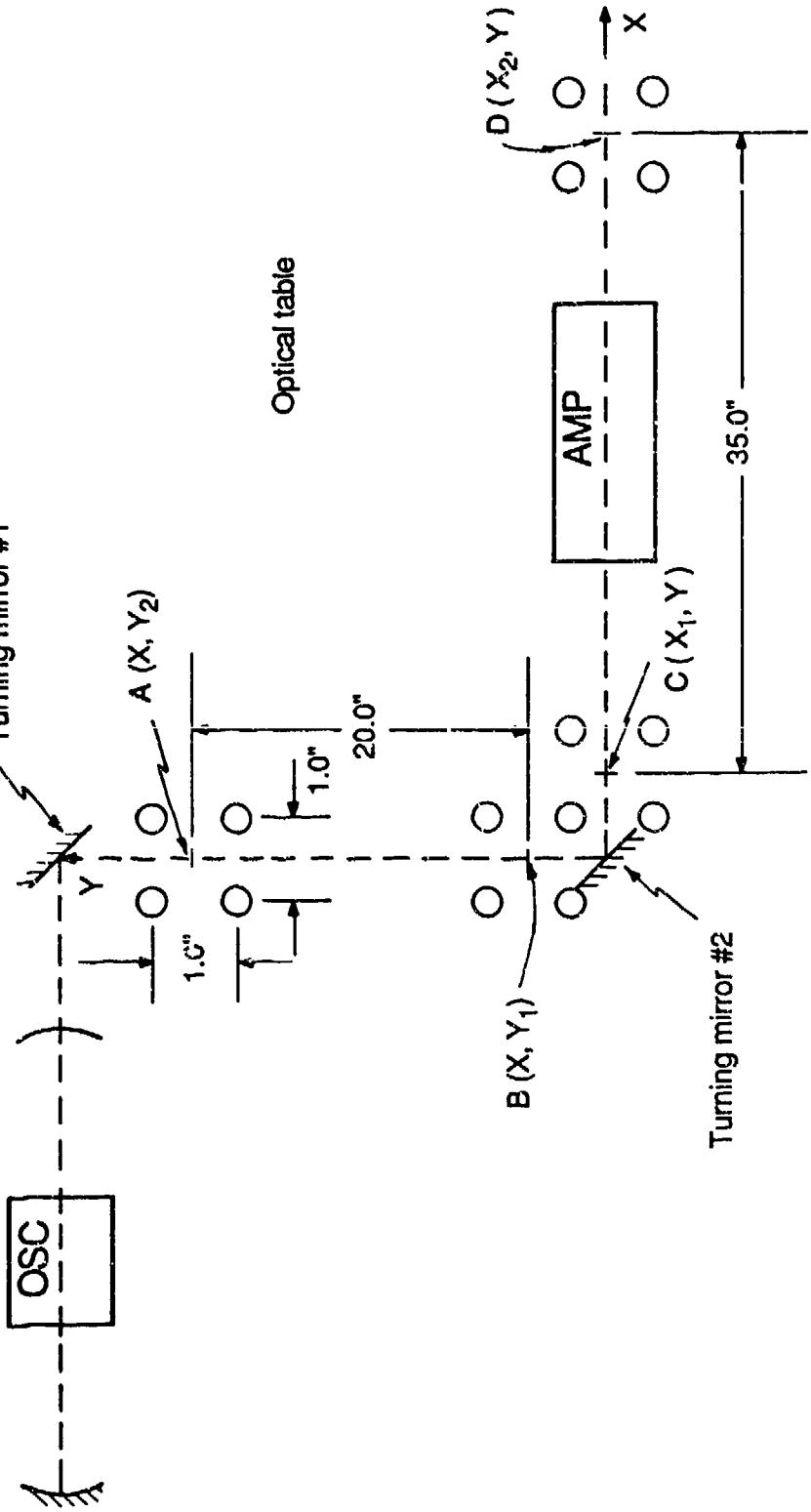

Figure 6. Schematic of the MOPA experimental layout showing the positions at which the gig was placed in order to align turning mirrors #1 and #2.

alignment of the beam with respect to the H_2 injectors was then checked at the exit of the amplifier by taking a paper-burn. In this case, however, the beam was too wide and it was difficult to decide whether the beam was aligned with the H_2 injectors or not. It is important to note that if turning mirrors #1 and #2 were aligned correctly, there should not be a problem with the alignment of the plano convex lens when the alignment was checked at the exit of the amplifier; the beam should be aligned with the H_2 injectors. If the paper-burn at the exit of the amplifier suggested that the beam was not aligned with the H_2 injectors, the alignment of turning mirrors #1 and #2 was checked and corrected and the plano convex lens realigned until the beam was aligned with the H_2 injectors at both the inlet and exit of the amplifier.

Finally, the second telescope lens (plano-concave) was aligned by following a procedure identical to the one described for the first telescope lens. After this lens was aligned, a beam of 1.5 mm diameter was obtained at the amplifier inlet and one of 2.4 mm diameter was obtained at the amplifier exit, thus avoiding flow channel aperturing.

During the course of these experiments, the oscillator was run both multiline and single-line. The multiline stable resonator alignment is described in Ref. 4 and the single-line oscillator alignment is described in the following paragraph.

The CL I single-line cavity was aligned with the help of a He-Ne laser. A grating was used in place of the multiline output mirror, Fig. 7. A beam director was used to receive the single-line beam, which was the zero order reflection from the grating, and direct it parallel to the cavity axis. The grating was installed in the far mirror mount and the rod structure of the CL I optical bench was moved until the He-Ne beam was centered on the grating surface. Then the ETR was installed in the near mirror mount (the mirror was

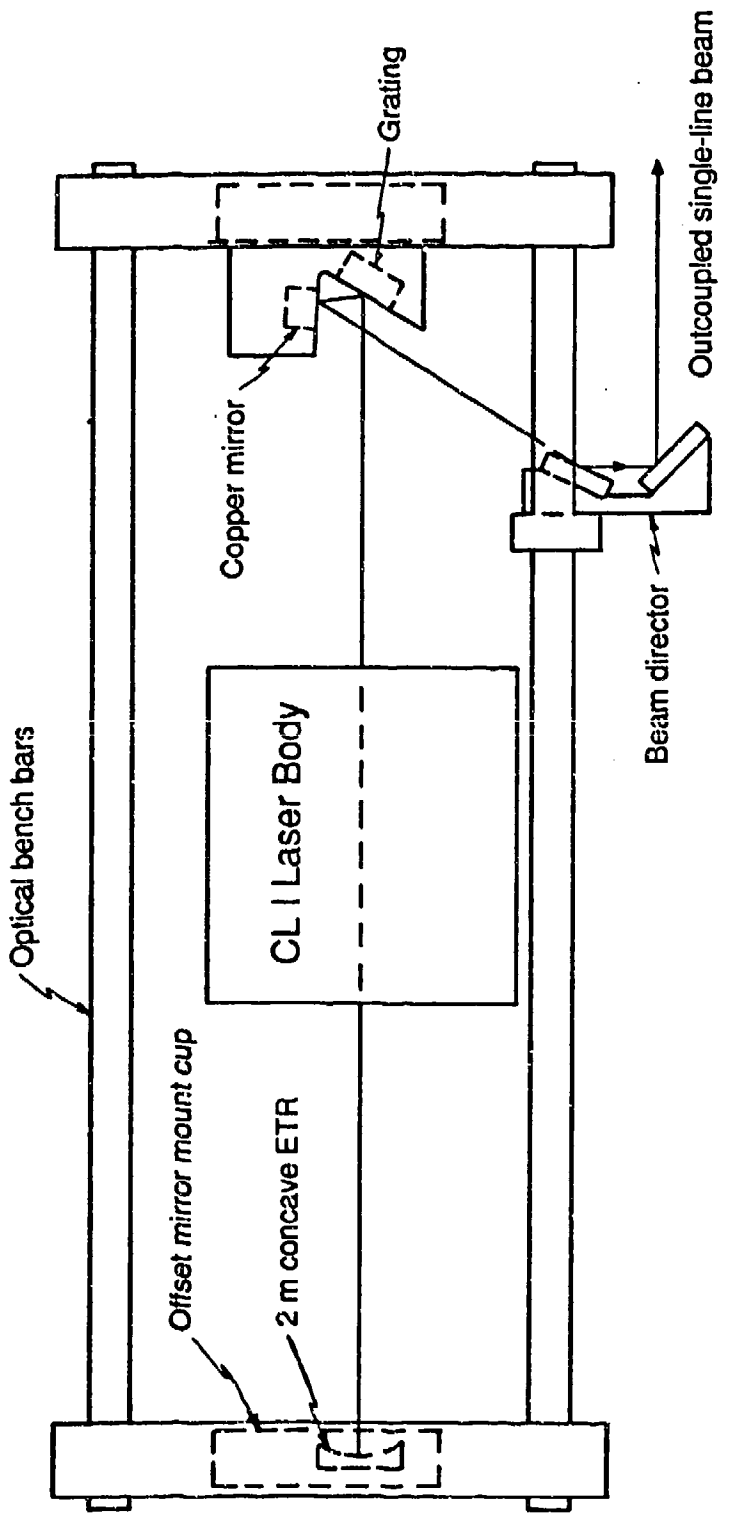

Figure 7. Schematic of the single-line optics used on the Helios CL I laser.

mounted in an offset mirror mount cup) and the mirror cup was rotated until the beam was centered on the back surface of the ETR. At this point the cavity rod structure was secured in place. The offset mirror cup with the ETR was then removed, which allowed the He-Ne beam to go through the CL I and strike the grating. Various orders of the He-Ne beam were observed, and the grating in the mirror mount was rotated so that these orders were placed on the fine line between the two halves of the laser body. The grating was then locked in place by tightening the lock ring. The beam director was then installed on the cavity side rods (the side towards which the grating was offset) and the zero-order reflection of the He-Ne beam from the grating was found by sweeping the grating in the horizontal direction (the zero-order remains stationary when the grating is rotated, while all other orders move). The beam director was then adjusted so that it would receive the zero-order beam. Finally, the offset mirror mount cup with the ETR was installed in the near mirror mount, and the back reflection of the ETR was returned on the incident beam. At this point the cavity was aligned.

Identification of the different lines which lased was accomplished by passing the single-line beam through a scanning monochromator, Fig. 2. Table 1 presents the output power, the readings of the horizontal micrometer of the grating and the monochromator readings corresponding to each line that lased at the Run 34 flow rates.

2.3 EFFECT OF FLOW CHANNEL APERTURING ON AMPLIFIER PERFORMANCE

The effect of flow channel aperturing on amplifier performance was investigated by measuring the multiline amplification ratio without flow channel aperturing and with 50% flow channel aperturing and comparing the results.

Multiline amplification experiments with zero aperturing were conducted

Line	Grating Micrometer Reading	Monochromator Reading λ/2 (nm)	Actual Wavelength λ (μm)	Power (Watts)
$P_1(2)$	2.328	1283.8	2.5788	0.300
$P_1(3)$	2.449	1298.4	2.6085	0.900
$P_1(4)$	2.577	1313.8	2.6398	1.400
$P_1(5)$	2.708	1330.6	2.6728	1.600
$P_1(6)$	2.852	1347.8	2.7075	1.850
$P_2(3)$	2.908	1358.0	2.7275	0.700
$P_1(7)$	3.000	1366.0	2.7441	1.475
$P_2(4)$	3.040	1374.0	2.7605	1.200
$P_1(8)$	3.150	1385.0	2.7826	0.420
$P_2(5)$	3.180	1391.8	2.7953	1.550
$P_2(6)$	3.330	1410.0	2.8319	1.550
$P_2(7)$	3.482	1429.0	2.8706	1.250
$P_2(8)$	3.643	1449.6	2.9112	0.530
$P_2(9)$	3.800	1477.0	2.9540	0.350

Table 1. Grating micrometer reading, monochromator reading, wavelength and power for each line that lased in the CL I with the single line optics for the Run 34 flow rates at 5.4 torr.

for Run 34 in both the oscillator and the amplifier, for Run 34 in the oscillator and Run 36 in the amplifier, and for Run 36 in both the oscillator and the amplifier. Amplification ratios as a function of the location of the optical axis of the input beam with respect to the H_2 injectors for the above combinations of oscillator/amplifier flow rates are shown in Figs. 8-10.

Multiline amplification experiments with 50% aperturing of the input beam by the flow channel were conducted for the above oscillator/amplifier flow rate combinations. Aperturing of the input beam was obtained by adjusting the distance between the two telescope lenses so that 50% of the input power was chopped by the amplifier flow channel. The data are presented in Figs. 11-13 as a function of the location of the optical axis of the input beam with respect to the H_2 injectors.

Comparison of the 0% aperturing data, Figs. 8-10, with the 50% aperturing data, Figs. 11-13, for the same oscillator/amplifier flow rate combinations, reveals that aperturing of the input beam by the amplifier flow channel causes a significant reduction (an average of 16.0%) in the amplification ratio. Since the reduction in amplifier performance resulting from flow channel aperturing is undesirable, all data were taken with no flow channel aperturing of the input beam.

2.4 ABSORPTION DUE TO THE SPECIES IN THE PRIMARY FLOW

The absorption of the multiline input beam by gases flowing in the primary stream was investigated by starting with no gases flowing in the CL II and measuring the amplifier output power after turning on each gas. The absorption of each gas was measured as a function of the location of the optical axis of the input beam. It was found that He and O_2 did not absorb, but SF_6 did.

The SF_6 absorption was measured for two oscillator/amplifier flow rate

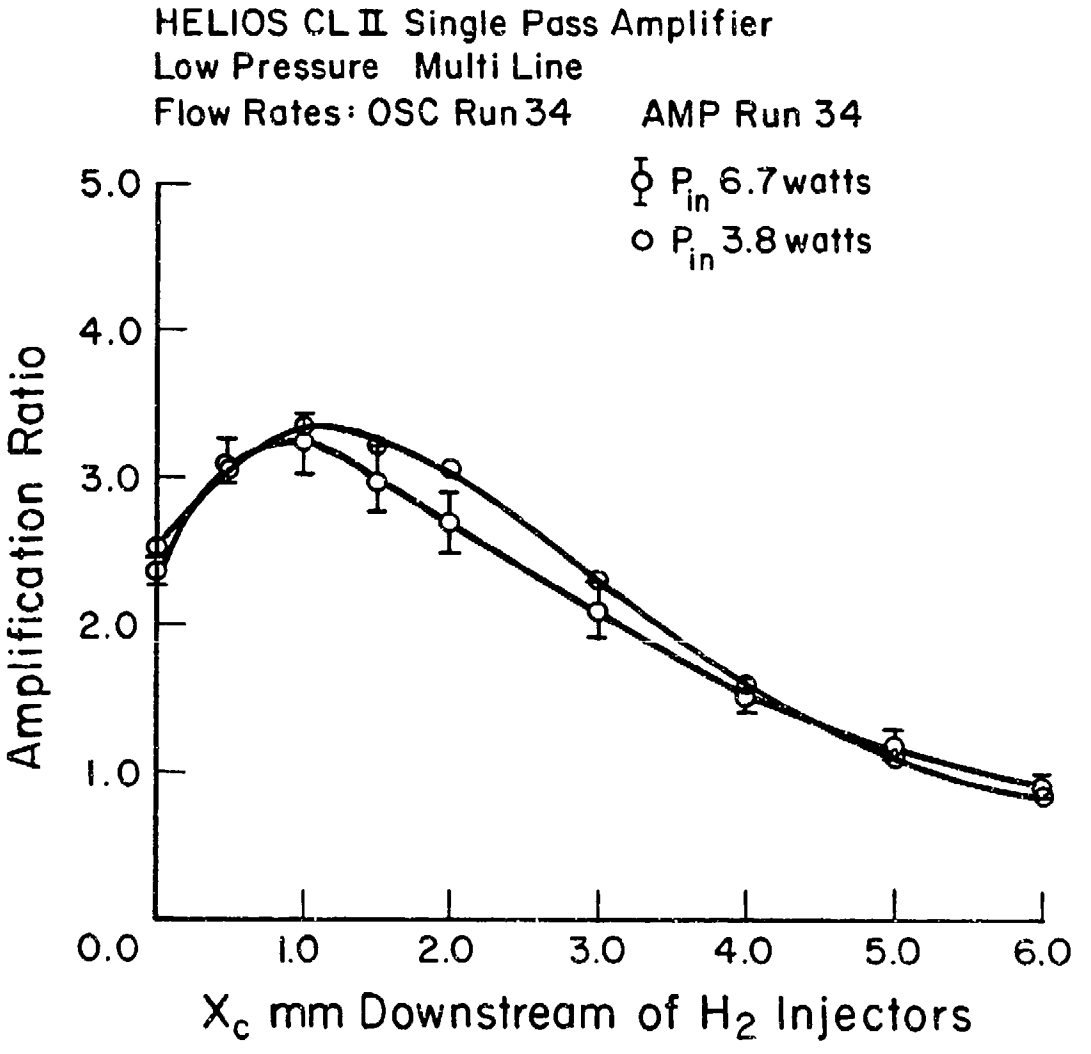

Figure 8. Amplification ratio as a function of the location of the axis of the input beam with respect to the H_2 injectors for zero flow channel aperturing of the input beam.

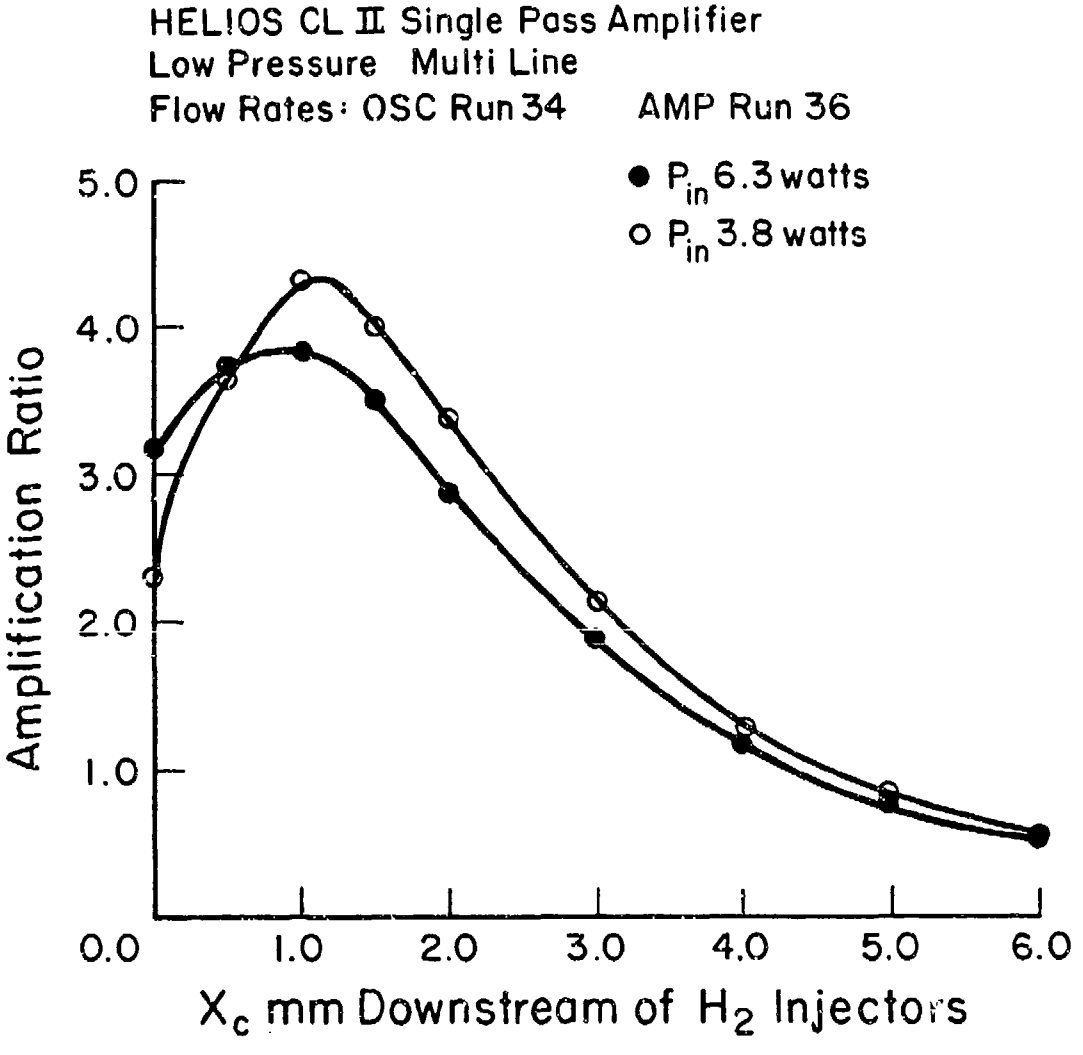

Figure 9. Amplification ratio as a function of the location of the axis of the input beam with respect to the H_2 injectors for zero flow channel aperturing of the input beam.

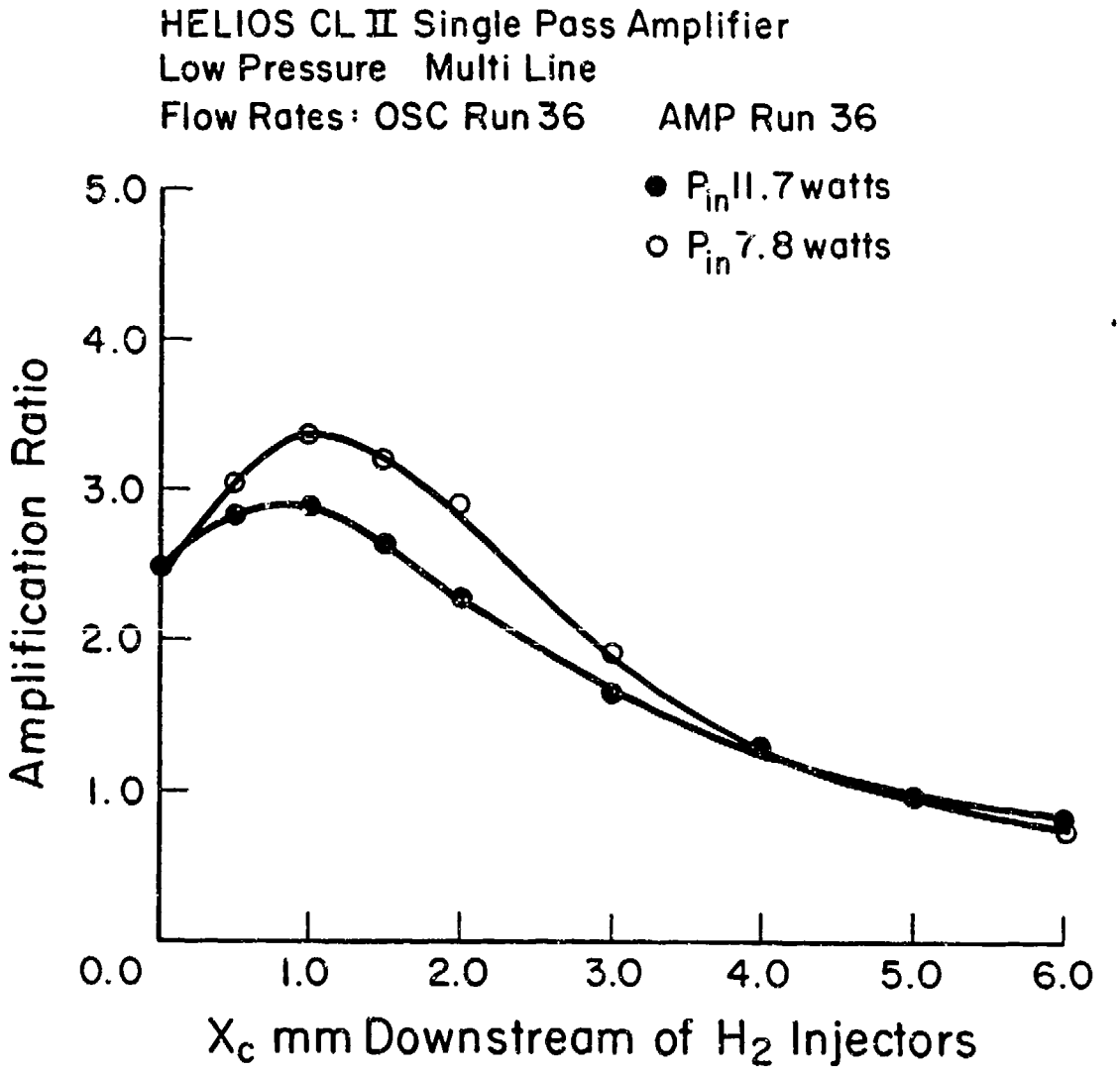

Figure 10. Amplification ratio as a function of the location of the axis of the input beam with respect to the H_2 injectors for zero flow channel aperturing of the input beam.

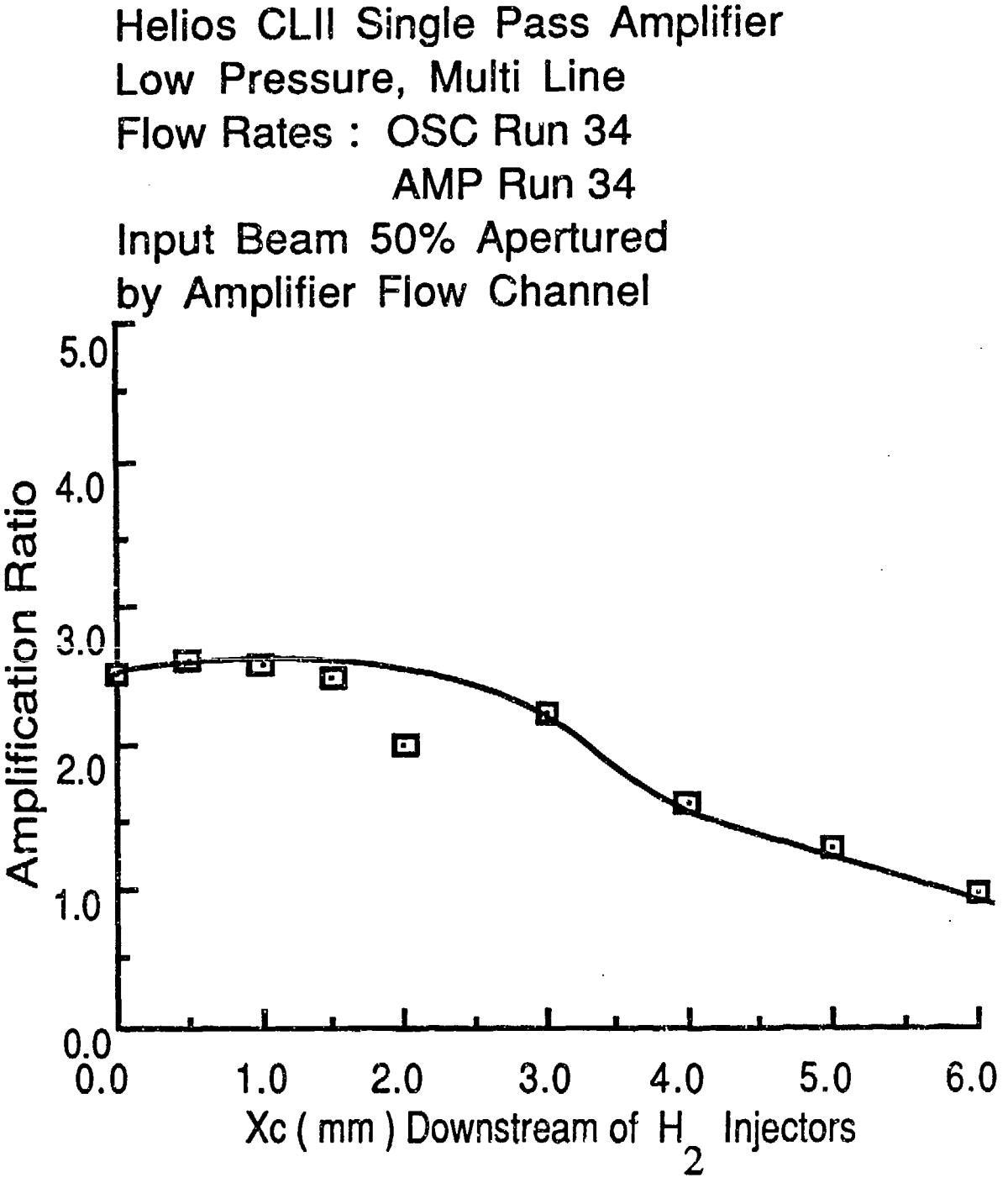

Figure 11. Amplification ratio as a function of the location of the axis of the input beam with respect to the H_2 injectors for 50% flow channel aperturing of the input beam. P_{IN} = 4.3 watts.

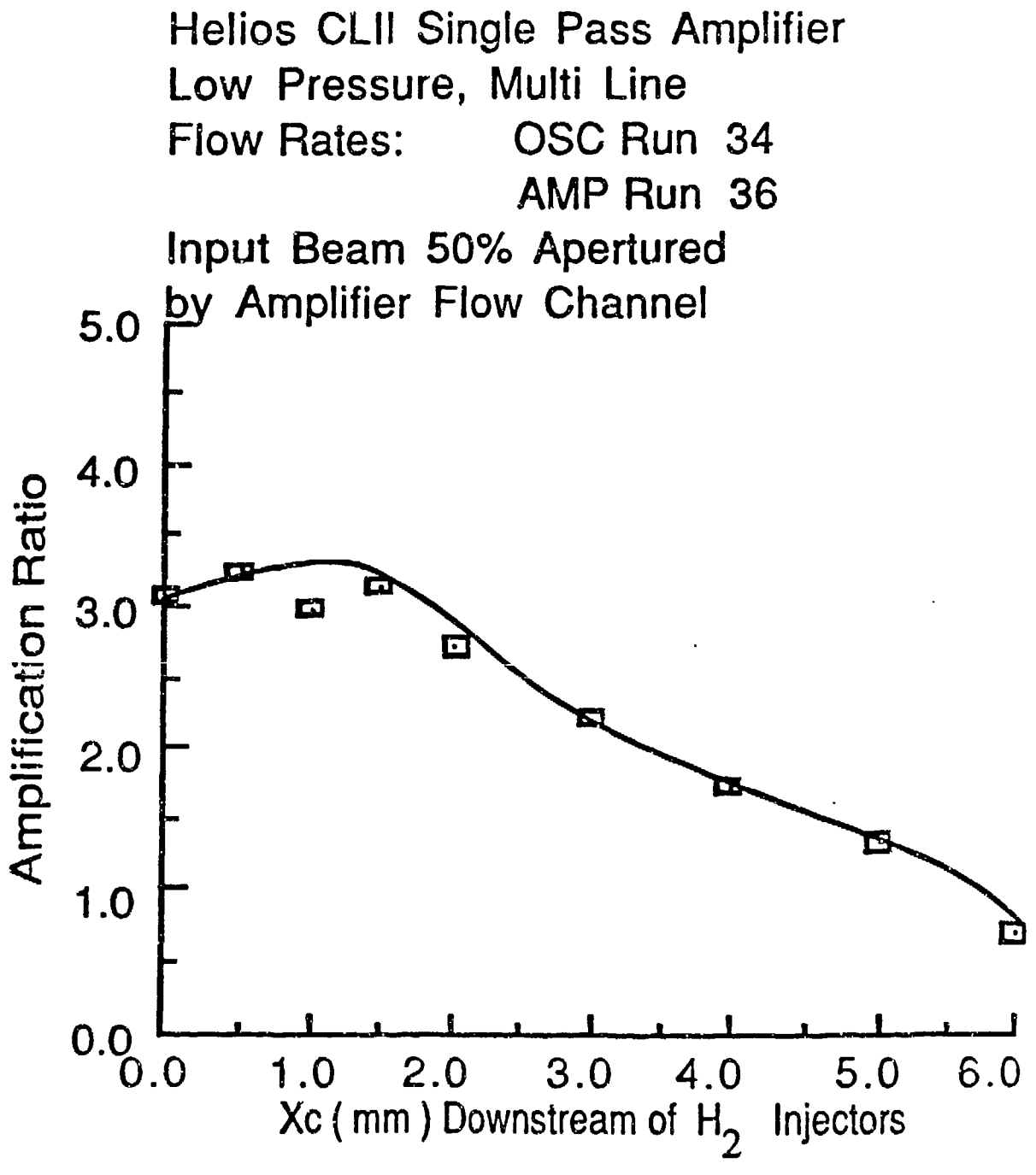

Figure 12. Amplification ratio as a function of the location of the axis of the input beam with respect to the H_2 injectors for 50% flow channel aperturing of the input beam. P_{IN} = 4.3 watts.

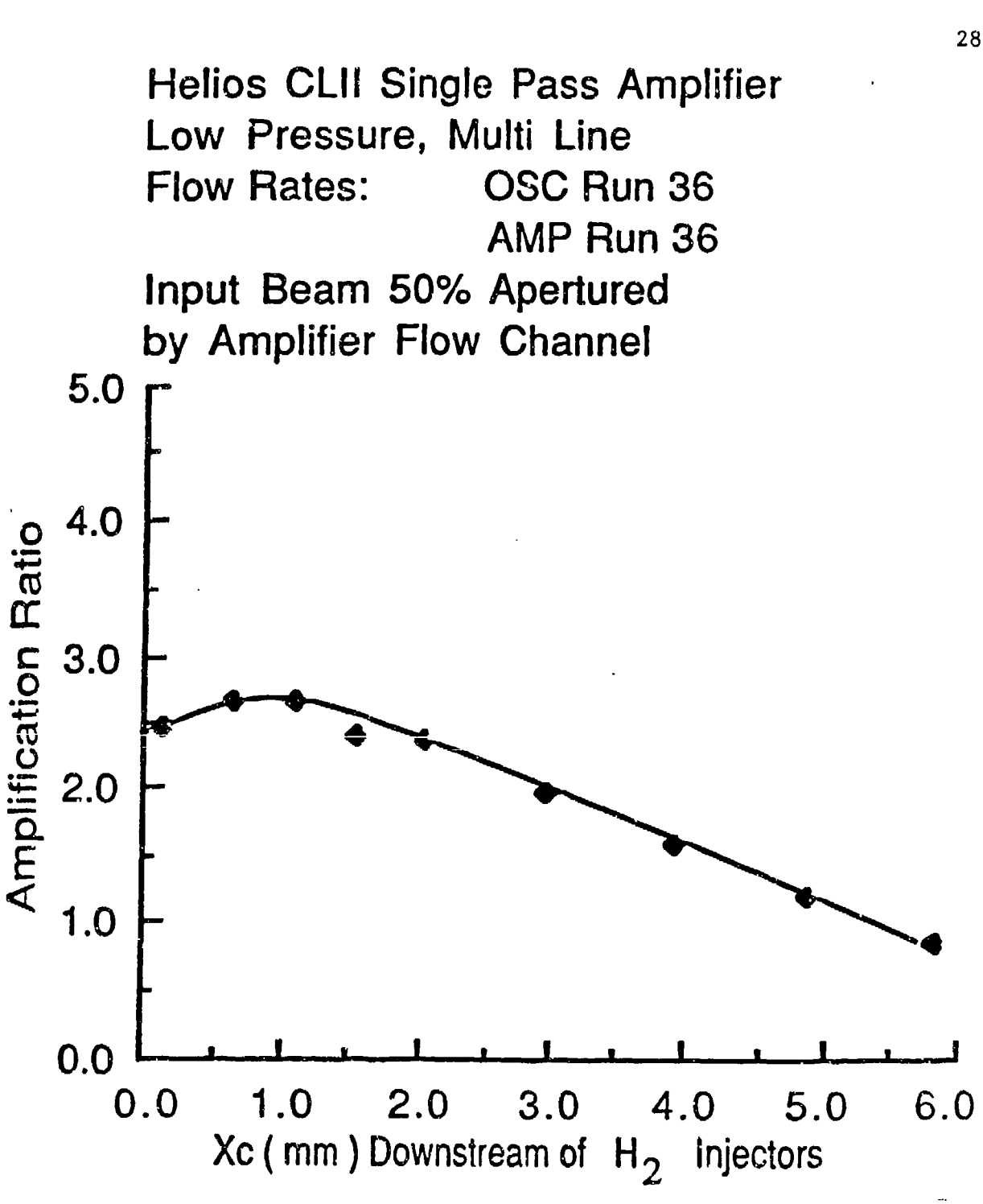

Figure 13. Amplification ratio as a function of the location of the axis of the input beam with respect to the H_2 injectors for 50% flow channel aperturing of the input beam. P_{IN} = 7.6 watts.

combinations and the data are presented in Tables 2 and 3. The absorption due to SF_6 is given by

$$SF_6 \text{ Absorption} = \frac{1}{Le} \ln \frac{(A_{SF_6 \text{ ON}} - A_{\text{ZERO } SF_6 \text{ ON}})}{(A_{SF_6 \text{ OFF}} - A_{\text{ZERO } SF_6 \text{ OFF}})} \qquad (2.4\text{-}1)$$

An examination of the values of SF_6 absorption given in Tables 2 and 3 showed that, in both cases, the absorption due to SF_6 is quite small (< 0.5%/cm). Thus the effects of SF_6 absorption on amplifier performance could be neglected.

2.5 MULTILINE AMPLIFIER PERFORMANCE

Multiline amplification experiments were conducted for three different oscillator/amplifier flow rate combinations: Run 34 in both the oscillator and the amplifier, Run 34 in the oscillator and Run 36 in the amplifier, and Run 36 in both the oscillator and the amplifier. Amplification ratios as a function of the location of the optical axis of the input beam for the above combinations of oscillator/amplifier flow rates are shown for two different values of P_{IN} in Figs. 8-10. The peak amplification ratios occurred in all three cases at an X_c that is both close to the value of X_c for peak power when a stable resonator is used on the CL II, and close to the values of X_c at which the peak zero power gains of the $P_1(J)$ and $P_2(J)$ lines were measured (Section 3.5). This means that maximum amplification is obtained when the input beam is passed through the amplifier at the X_c location corresponding to peak amplifier gain. Thus for maximum amplification, the input beam intensity distribution has to be matched to the gain distribution in the amplifier in the sense that the input beam intensity peak and the amplifier gain peak should be located at the same X_c.

Table 4 presents the amplifier input powers, output powers and

CL II X_c (mm)	P_{6SF_6} ON		P_{6SF_6} OFF		SF_6 Absorption (cm^{-1})
	Power (Watts)	Area (μ)	Power (Watts)	Area (μ)	Based on Area
0.0	6.80	106.31	6.85	106.52	- 0.0000808
0.5	6.60	101.95	6.70	104.86	- 0.0011533
1.0	6.75	104.98	6.90	107.45	- 0.000953
1.5	6.60	102.50	6.75	104.92	- 0.000956
2.0	6.75	107.81	6.75	106.71	0.000000
3.0	6.60	104.86	6.80	105.85	- 0.0003928
4.0	6.75	104.37	6.80	104.54	- 0.0000668
5.0	6.50	101.86	6.70	101.87	- 0.0000041
6.0	6.65	104.29	6.70	104.55	- 0.000102

Table 2. Multiline SF_6 absorption as a function of the location of the optical axis of the input beam with respect to the H_2 injectors for the Run 34 flow rates at 5.4 torr in both the oscillator and the amplifier.

CL II X_c (mm)	P_{6SF_6} ON		P_{6SF_6} OFF		SF_6 Absorption (cm^{-1})
	Power (Watts)	Area (μ)	Power (Watts)	Area (μ)	Based on Area
0.0	14.0	51.144	14.5	54.376	- 0.0025115
0.5	14.0	55.287	14.5	56.788	- 0.00109774
1.0	14.0	53.245	14.3	52.865	0.00029344
1.5	14.0	55.923	14.3	52.912	0.00226835
2.0	14.0	44.755	14.5	50.184	- 0.00469239
3.0	13.8	47.913	14.5	54.149	- 0.0050145
4.0	13.6	48.796	13.8	54.491	- 0.00452408
5.0	13.6	48.159	13.7	49.681	- 0.00127579
6.0	13.4	50.532	13.5	55.045	- 0.0035057

Table 3. Multiline SF_6 absorption as a function of the location of the optical axis of the input beam with respect to the H_2 injectors for the Run 36 flow rates at 6.5 torr in both the oscillator and the amplifier.

CL II X_c (mm)	CL I - Run 34 CL II - Run 34			CL I - Run 34 CL II - Run 36			CL I - Run 36 CL II - Run 36		
	P_{IN} (Watts)	P_{OUT} (Watts)	AR Based On Area	P_{IN} (Watts)	P_{OUT} (Watts)	AR Based On Area	P_{IN} (Watts)	P_{OUT} (Watts)	AR Based On Area
0.0	6.928	17.054	2.450	6.640	20.603	3.180	12.258	31.614	2.460
0.5	6.822	21.850	3.250	6.683	24.696	3.740	12.258	35.525	2.840
1.0	6.992	23.087	3.300	6.608	25.581	3.860	12.258	36.240	2.910
1.5	7.141	21.669	2.980	6.822	23.630	3.520	12.790	34.289	2.620
2.0	7.035	19.186	2.690	6.683	19.186	2.900	12.790	29.311	2.270
3.0	7.248	13.675	1.920	6.822	12.790	1.880	12.790	21.850	1.650
4.0	6.928	11.938	1.420	6.502	7.536	1.170	12.258	15.881	1.290
5.0	6.928	7.461	1.116	6.395	4.796	0.779	12.258	11.863	0.960
6.0	6.502	5.393	0.849	6.150	3.379	0.530	11.938	9.593	0.810
0.0	3.997	9.060	2.479	3.997	9.593	2.296	8.239	19.825	2.445
0.5	3.997	12.524	3.048	4.104	15.455	3.633	8.527	25.048	3.044
1.0	3.997	14.123	3.334	4.104	17.587	4.316	8.314	27.180	3.372
1.5	4.157	14.283	3.187	4.157	16.787	3.985	8.314	26.860	3.202
2.0	4.157	13.323	3.050	4.263	14.656	3.356	8.527	23.982	2.882
3.0	4.104	9.699	2.289	4.338	9.060	2.128	8.527	16.521	1.907
4.0	3.997	6.395	1.599	4.263	4.903	1.254	8.314	10.659	1.288
5.0	3.944	4.370	1.066	4.050	3.411	0.817	8.314	7.674	0.955
6.0	3.730	3.020	0.827	4.050	2.238	0.538	7.781	5.756	0.743

Table 4. Multiline input power, output power and amplification ratio a function of P_{IN} and the location of the optical axis of the input beam with respect to the H_2 injectors for low pressure for various flow rate combinations in the oscillator and the amplifier.

amplification ratios for Figs. 8-10. Comparison of Figs. 8 and 10 shows that higher amplification ratios were obtained when both the oscillator and the amplifier were run at the Run 34 flow rates than when both were run at the Run 36 flow rates. The amplifier gain (and therefore the amplification ratio) depends on the amplifier flow rates and the input power. Increasing the amplifier flow rates caused the amplifier gain to increase. Increasing the input power caused the input intensity to increase which decreases the amplifier gain because it stimulates emission of radiation. In the case of Fig. 10, even though the amplifier was run at the Run 36 flow rates, the higher input intensity decreased the gain to lower values than those of Fig. 8, resulting in lower amplification ratios. Thus amplification ratio depends on the balance between amplifier flow rates and input power.

2.6 SINGLE LINE AMPLIFIER PERFORMANCE

Single-line amplification ratios for lines $P_1(6)$ and $P_2(6)$ are presented in Figs. 14 and 15. Table 5 presents data for input power, output power and amplification ratio as a function of the location of the optical axis of the input beam for lines $P_1(6)$ and $P_2(6)$. This data was obtained using the single-line optics on the CL I. The CL I SF_6 and H_2 flow rates were increased until the single-line input power was approximately equal to the total multiline input power for Run 34 in the oscillator. The console pressures at which this happened were 15 psig for He, 27 psig for O_2, 60 psig for SF_6 and 45 psig for H_2. The set of gas flow rates corresponding to these console pressures was called Run *.

Figure 14 shows that the $P_1(6)$ amplification ratio reaches its maximum value at an X_c of 1.5 mm, which is the same X_c at which the $P_1(6)$ amplifier zero power gain is maximum (Section 3.5). In the case of $P_2(6)$, Fig. 15 shows that the maximum amplification ratio occurs 1.0 mm downstream of the H_2

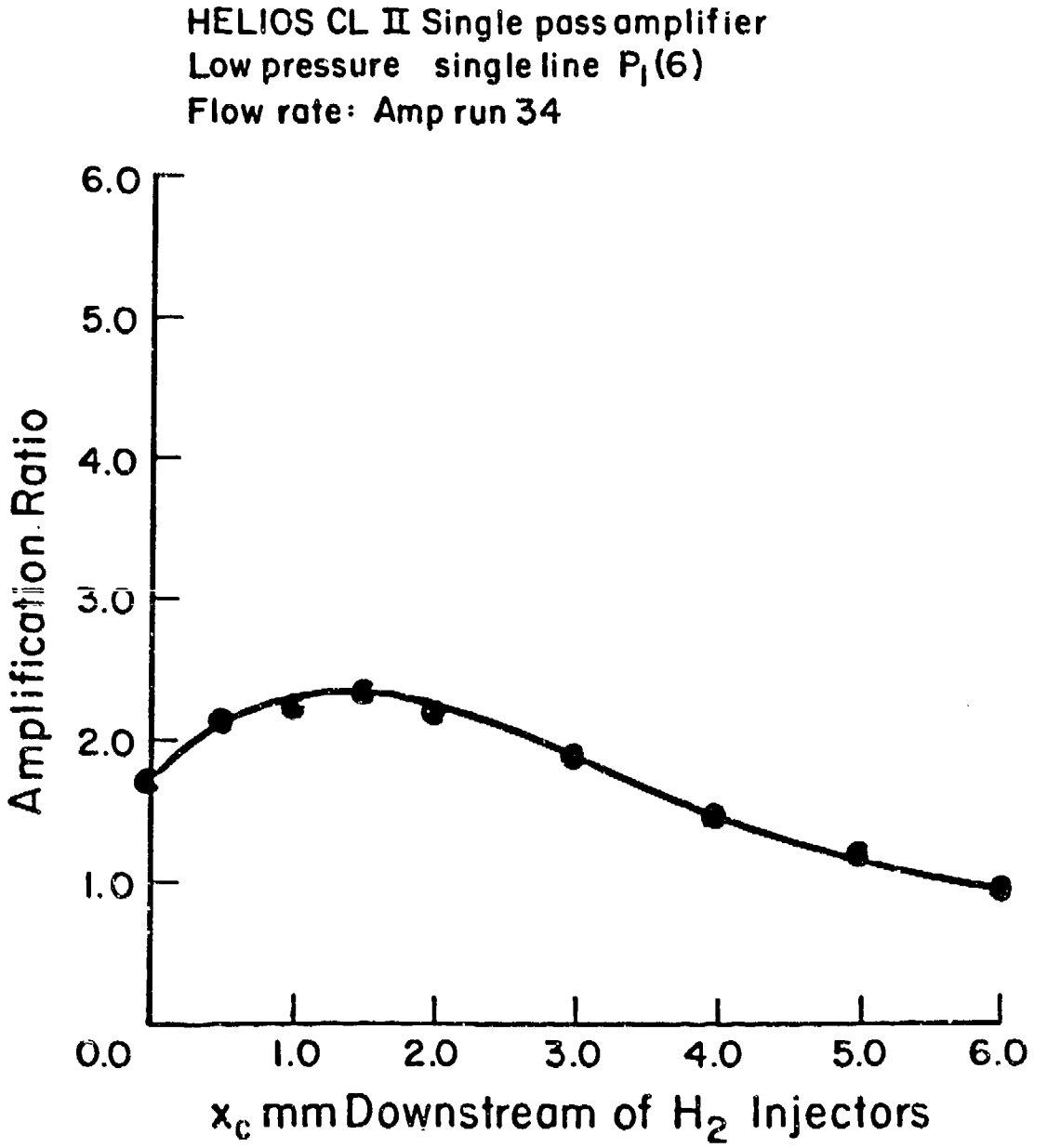

Figure 14. Amplification ratio as a function of the location of the axis of the input beam with respect to the H_2 injectors for zero flow channel aperturing of the input beam. P_{IN} = 2.8 watts.

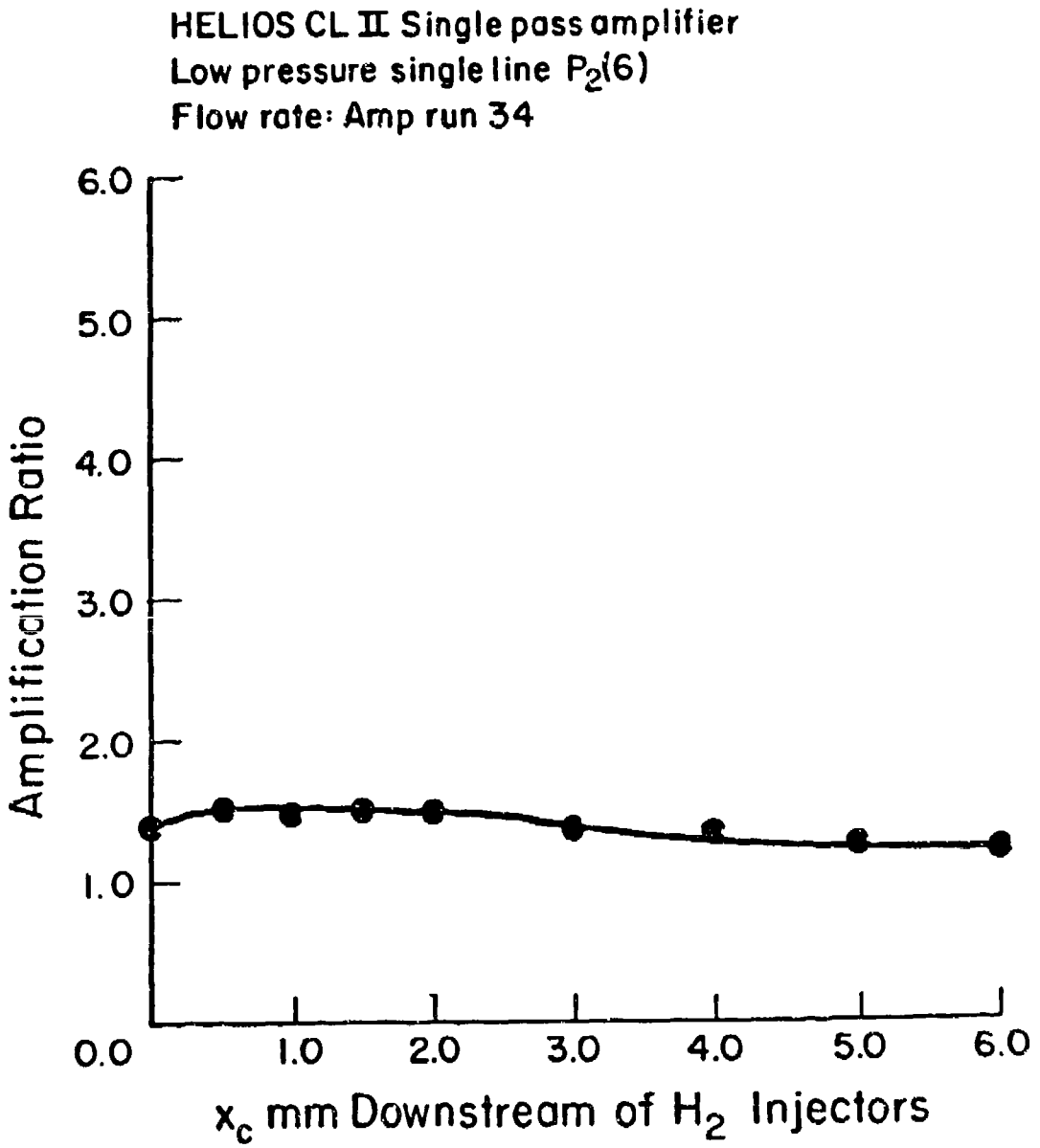

Figure 15. Amplification ratio as a function of the location of the axis of the input beam with respect to the H_2 injectors for zero flow channel aperturing of the input beam. P_{IN} = 2.7 watts.

CL II	$P_1(6)$			$P_2(6)$		
X_c (mm)	P_{IN} (Watts)	P_{OUT} (Watts)	AR Based On Area	P_{IN} (Watts)	P_{OUT} (Watts)	AR Based On Area
0.0	3.073	5.369	1.701	2.899	4.018	1.400
0.5	3.038	6.568	2.145	2.931	4.157	1.529
1.0	3.091	6.981	2.233	2.931	4.317	1.480
1.5	2.966	7.000	2.339	2.878	4.370	1.510
2.0	3.038	6.893	2.214	2.878	4.402	1.490
3.0	2.931	5.756	1.905	2.984	4.317	1.370
4.0	2.931	4.370	1.482	2.931	3.890	1.330
5.0	2.825	3.304	1.191	2.793	3.464	1.240
6.0	3.038	2.825	0.940	2.771	3.251	1.190

Table 5. Input power, output power and amplification ratio for lines $P_1(6)$ and $P_2(6)$ as a function of the location of the optical axis of the input beam with respect to the H_2 injectors for the Run * flow rates in the oscillator and the Run 34 flow rates in the amplifier.

injectors, which is the location at which the $P_2(6)$ zero power gain reaches its maximum value (Section 3.5). This indicates that maximum single-line amplification ratios are obtained when the input beam is passed through the amplifier at the X_c for maximum zero power gain.

When Figs. 14 and 15 are compared to Fig. 8, it is seen that, for the same input power, single-line amplification ratios are considerably lower than multi-line amplification ratios. This is a result of the fact that in the multiline case, the total input power was distributed among the different lasing lines, which means that the input intensity on each line was less than the input intensity in the single line case. This fact results in higher amplification ratios for each line, because each line's gain in the amplifier gets depressed less than in the single-line case for the same total input power.

It is interesting to note that the $P_2(6)$ amplification ratios in Fig. 15 are lower than the $P_1(6)$ amplification ratios in Fig. 14, while the $P_2(6)$ zero power gain is considerably higher than the $P_1(6)$ zero power gain (Section 3.5), and that $P_2(6)$ amplification ratios are less sensitive to X_c than $P_1(6)$ amplification ratios are. The reasons for this behavior are not understood at the present time.

2.7 MULTILINE MOPA PERFORMANCE AS A FUNCTION OF INPUT POWER

From a MOPA system view point, a question of considerable interest is the following. What fraction of a device's output when it is run as an oscillator must be input to the device when it is run as an amplifier in order to obtain an amplifier output equal to the device's oscillator output? Table 6 presents data for input power, output power and amplification ratio at the X_c for peak amplification, for Run 34 in both the oscillator and the amplifier, for Run 34 in the oscillator and Run 36 in the amplifier, and for Run 36 in both the

CL I - Run 34 CL II - Run 34			CL I - Run 34 CL II - Run 36			CL I - Run 36 CL II - Run 36		
P_{IN} (Watts)	P_{OUT} (Watts)	AR Based On Area	P_{IN} (Watts)	P_{OUT} (Watts)	AR Based On Area	P_{IN} (Watts)	P_{OUT} (Watts)	AR Based On Area
6.992	23.087	3.300	6.608	25.581	3.860	12.258	36.240	2.91
3.997	14.123	3.334	4.104	17.587	4.316	8.314	27.180	3.372

Table 6. Multiline input power, output power and amplification ratio at the X_c for peak amplification for low pressure for various flow rate combinations in the oscillator and the amplifier.

oscillator and the amplifier. Figure 16 shows the amplifier data plotted as P_{OUT} versus P_{IN} at the X_c for peak amplification. On such a plot, at large input powers that immediately saturate the amplifier, P_{OUT} would be only slightly larger than P_{IN}. At lower input powers, larger amplification would occur. The anticipated behavior is indicated by the dashed line in Fig. 16. Since the CL II gives 27 to 37 watts for Run 34 and 40 to 50 watts for Run 36 when run as an oscillator, the data suggest that about 1/3 of the oscillator output needs to be input to obtain amplifier output equal to the CL II's oscillator performance. Future experiments will obtain the data necessary to extend this curve to larger values of P_{IN}.

2.8 SUMMARY

Comparison of the 0% and 50% aperturing data for the same oscillator/amplifier flow rate combinations showed that aperturing of the input beam by the amplifier flow channel causes a significant reduction (an average of 16.0%) in the amplification ratio. For this reason, all data were taken with no flow channel aperturing of the input beam.

The absorption of the multiline input beam by the gases flowing in the primary stream was investigated. It was found that He and O_2 did not absorb, but SF_6 did. The absorption due to SF_6 was quite small (< 0.5%/cm), and thus its effects on amplifier performance were neglected.

Multiline amplification experiments showed that the peak amplification ratios occurred at an X_c that is both close to the value of X_c for peak power when a stable resonator is used on the CL II, and close to the values of X_c at which the peak zero power gains of the $P_1(J)$ and $P_2(J)$ lines were measured (Section 3.5). Thus, to obtain maximum amplification, the input beam should be passed through the amplifier at the X_c location corresponding to peak amplifier gain. Higher amplification ratios were obtained when both the

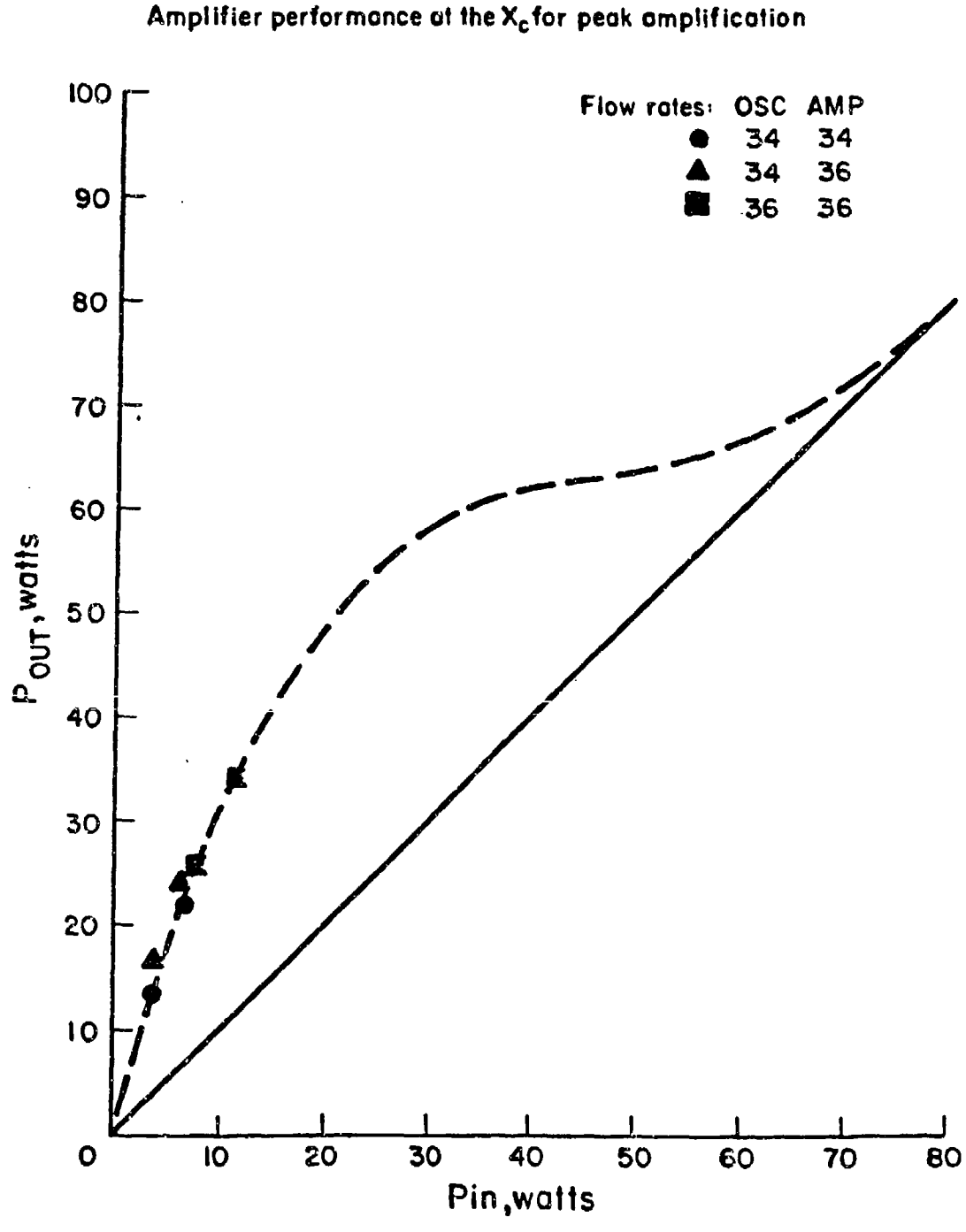

Figure 16. P_{OUT} versus P_{IN} at the X_c for peak amplification for several oscillator/amplifier flow rate combinations.

oscillator and the amplifier were run at the Run 34 flow rates than when both were run at the Run 36 flow rates. This was a consequence of the higher input intensity that was used in the case of the Run 36 flow rates.

Single-line amplification experiments showed that the peak $P_1(6)$ amplification ratio is located at an X_c of 1.5 mm, which is the same X_c at which the $P_1(6)$ amplifier zero power gain is maximum (Section 3.5). In the case of $P_2(6)$, the maximum amplification ratio occurs 1.0 mm downstream of the H_2 injectors, which is again the location at which the $P_2(6)$ zero power gain reaches its maximum value (Section 3.5). Thus, to obtain maximum single-line amplification, the input beam should be passed through the amplifier at the X_c for maximum zero power gain. The single-line amplification ratios are considerably lower than the multi-line amplification ratios that were measured using the same input power. This is a result of the fact that in the multiline case, the total input power was distributed among the different lasing lines, which means that the input intensity on each line was less than the input intensity in the single-line case. This fact results in higher amplification ratios for each line, because each line's gain in the amplifier was depressed less than in the single-line case for the same total input power. The $P_2(6)$ amplification ratios measured are lower and less sensitive to X_c than the $P_1(6)$ amplification ratios, even though the $P_2(6)$ zero power gain is considerably higher and more sensitive to X_c than the $P_1(6)$ zero power gain.

The multiline MOPA performance was investigated as a function of input power and it was found that about 1/3 of the oscillator output needs to be input to obtain amplifier output equal to the CL II's oscillator performance.

III. ZERO POWER GAIN EXPERIMENTS

Zero power gain is the gain in a laser when the intensity is equal to zero. From a practical point of view, zero power gain is the gain in a laser when the intensity is low enough that it does not perturb the media. This low intensity (input in this case) results in a radiation term that is negligible compared to the other terms in the species equations.

The zero power gains of different lines in the CL II laser were measured as a function of distance downstream from the H_2 injectors. Knowledge of the zero power gain distribution of each line in the CL II will provide essential information required to interpret the master oscillator/power amplifier experiments.

The amplifier gain is inversely proportional to input power. An increase in input power results in an increase in input intensity which in turn stimulates more radiation and therefore drives the gain down. As the input power decreases, the gain in the amplifier increases until at some point ($P_{IN\ ZPG}$), it becomes equal to the zero power gain. Further decrease of the input power does not have any effect on the gain measured because the intensity is so low that it does not perturb the media. This is the criteria for determining when the zero power gain region has been reached. A power equal to or lower than $P_{IN\ ZPG}$ is then chosen for measuring zero power gain.

3.1 EXPERIMENTAL EVALUATION OF PbSe DETECTOR PERFORMANCE IN MEASURING ZERO POWER GAIN

The first step in the zero power gain experiments was a determination of the input power required to measure the zero power gain of each line. To accomplish this objective, it was necessary to find a way of varying the input power from about 1.0 watt to 0.0001 watts. This was done by gradually reducing the CL I SF_6 flow rate and by placing mirrors of different

reflectivities in front of turning mirror #2, so that only a given percentage of the incoming power could pass through, Fig. 17.

Initially, the power meter coupled with a 7854 Tektronix oscilloscope was used to measure the $P_1(6)$ amplification ratio as a function of input power. Figure 18 presents power meter amplification ratio data obtained at the (x,y) for maximum amplification (Section 3.5). At relatively high input powers (above 0.1 watts), the power meter performance was satisfactory. At powers less than 0.1 watts, the decreased SF_6 flow rates in the CL I caused its output power to fluctuate, which resulted in a fluctuating signal. Since the response time of the power meter is slow, it could not follow the fast fluctuations of the signal which resulted in errors in the amplification ratios obtained at these low input powers. Thus, at low input powers, amplifier performance could not be measured using the power meter.

Since amplifier performance could not be accurately measured with the power meter at low input powers, an Infared Industries 500 Series Lead Selenide (PbSe) detector[5] was tried. The input beam to the detector was modulated by a 50% chopper, resulting in a chopping frequency of about 870 Hz. A Stanford Research Systems SR510 lock-in amplifier was used, Fig. 17, to amplify the detector signal which was then displayed on the 7854 oscilloscope. The 870 Hz chopping frequency provided the reference frequency required by the lock-in amplifier. The PbSe detector was connected in series with a load resistor and a d.c. bias voltage and its output was monitored across the detector resistor, Fig. 19. Figure 20 shows that with the circuit of Fig. 19, the detector output voltage is a linear function of the detector resistance. Since the detector resistance decreases linearly as the power incident on the detector increases, the output voltage across the detector is linearly proportional to the power incident on the detector. Since the

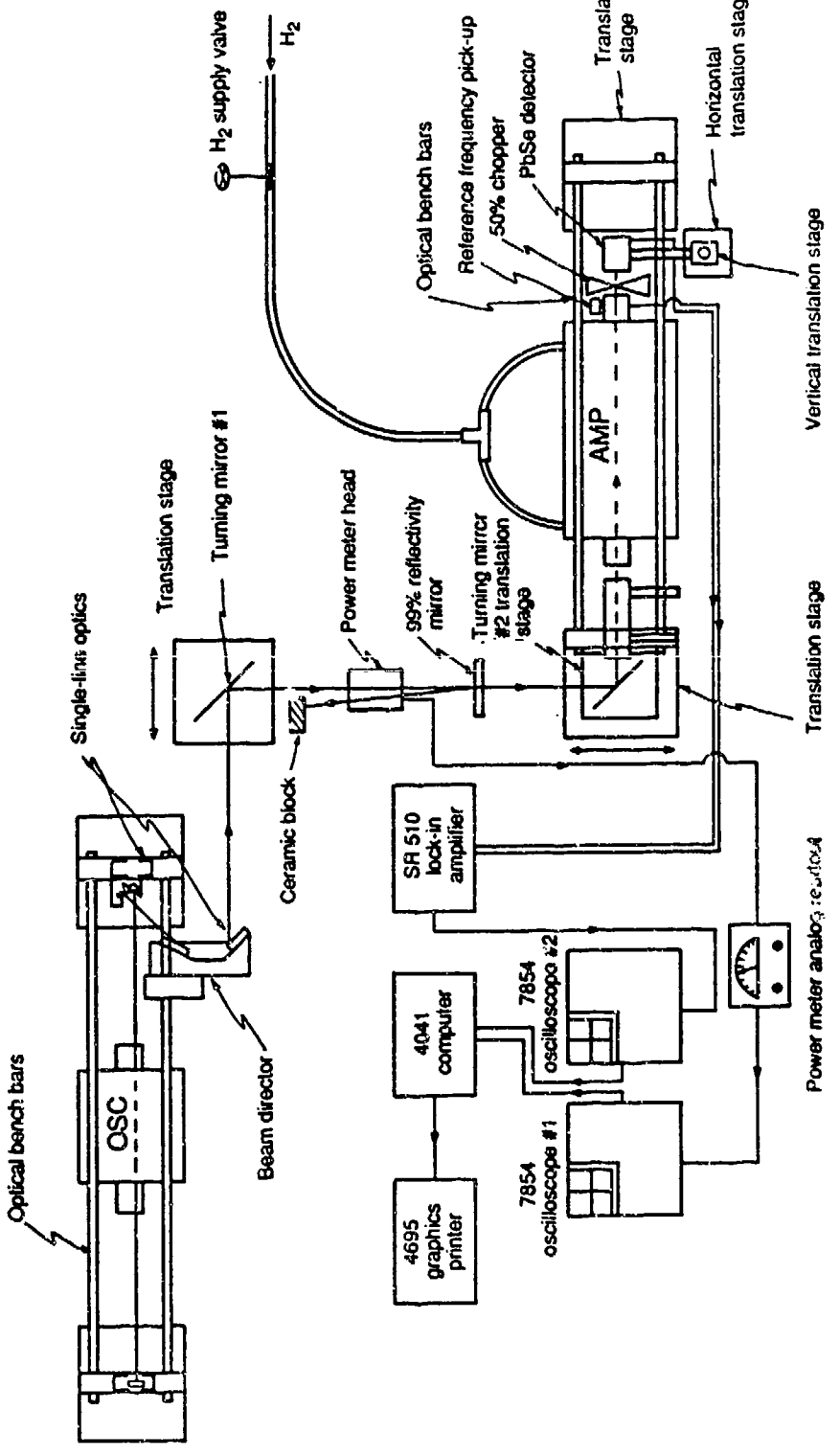

Figure 17. Schematic of the experimental layout used to measure gain with a PbSe detector and a lock-in amplifier.

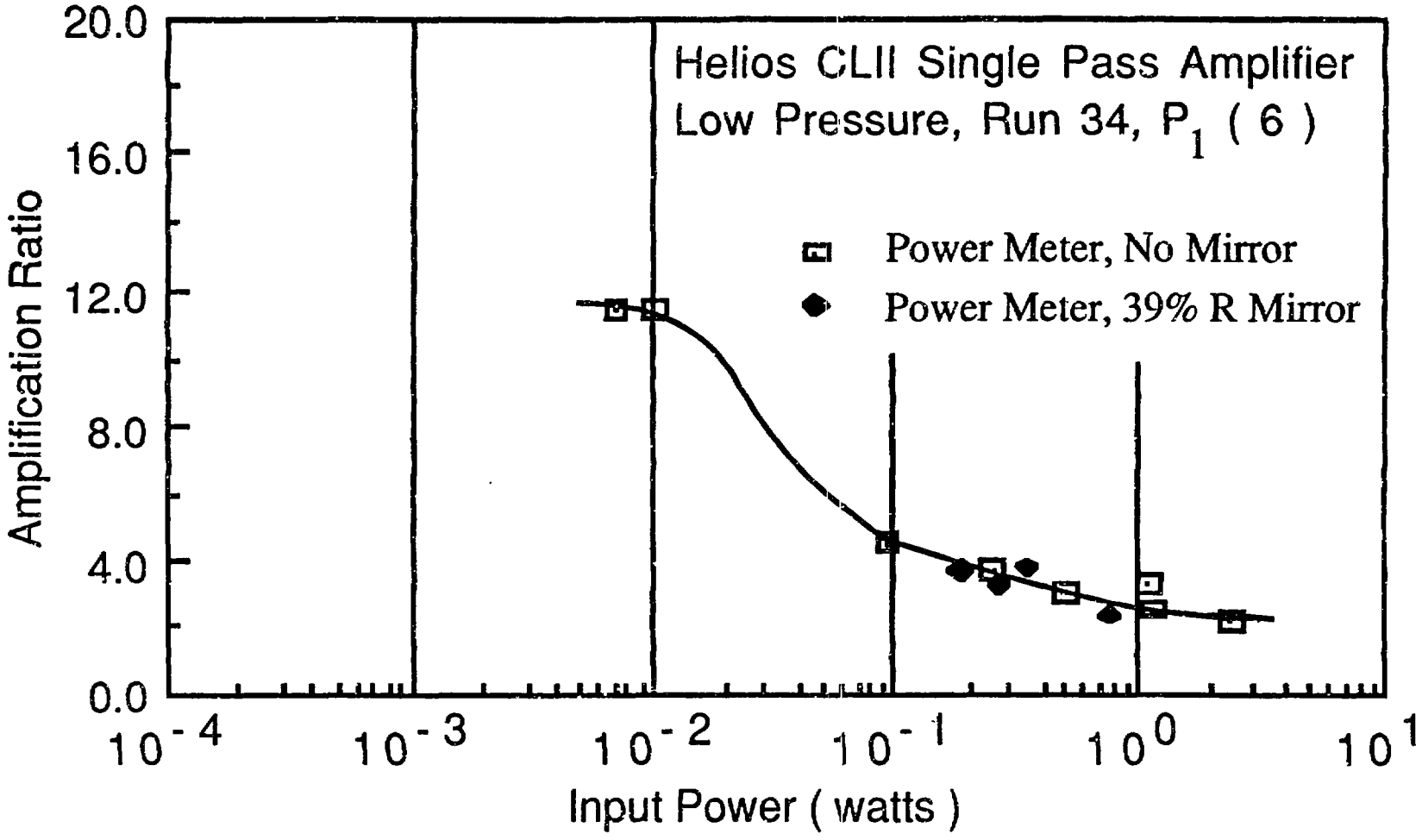

Figure 18. Variation of amplification ratio with input power. The input power was varied by gradually reducing the CL I SF_6 flow rate and by placing a 39% reflectivity mirror in front of turning mirror #2.

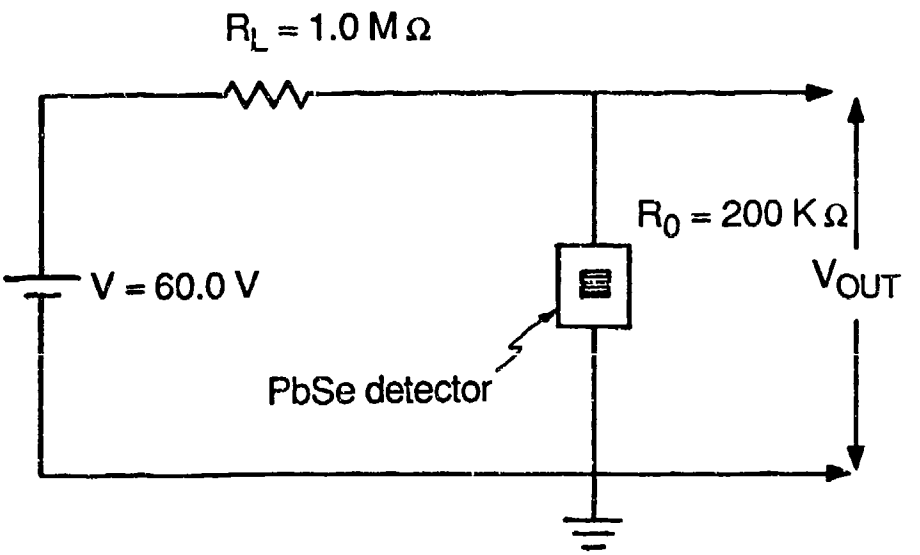

Figure 19. Lead selenide detector circuit.

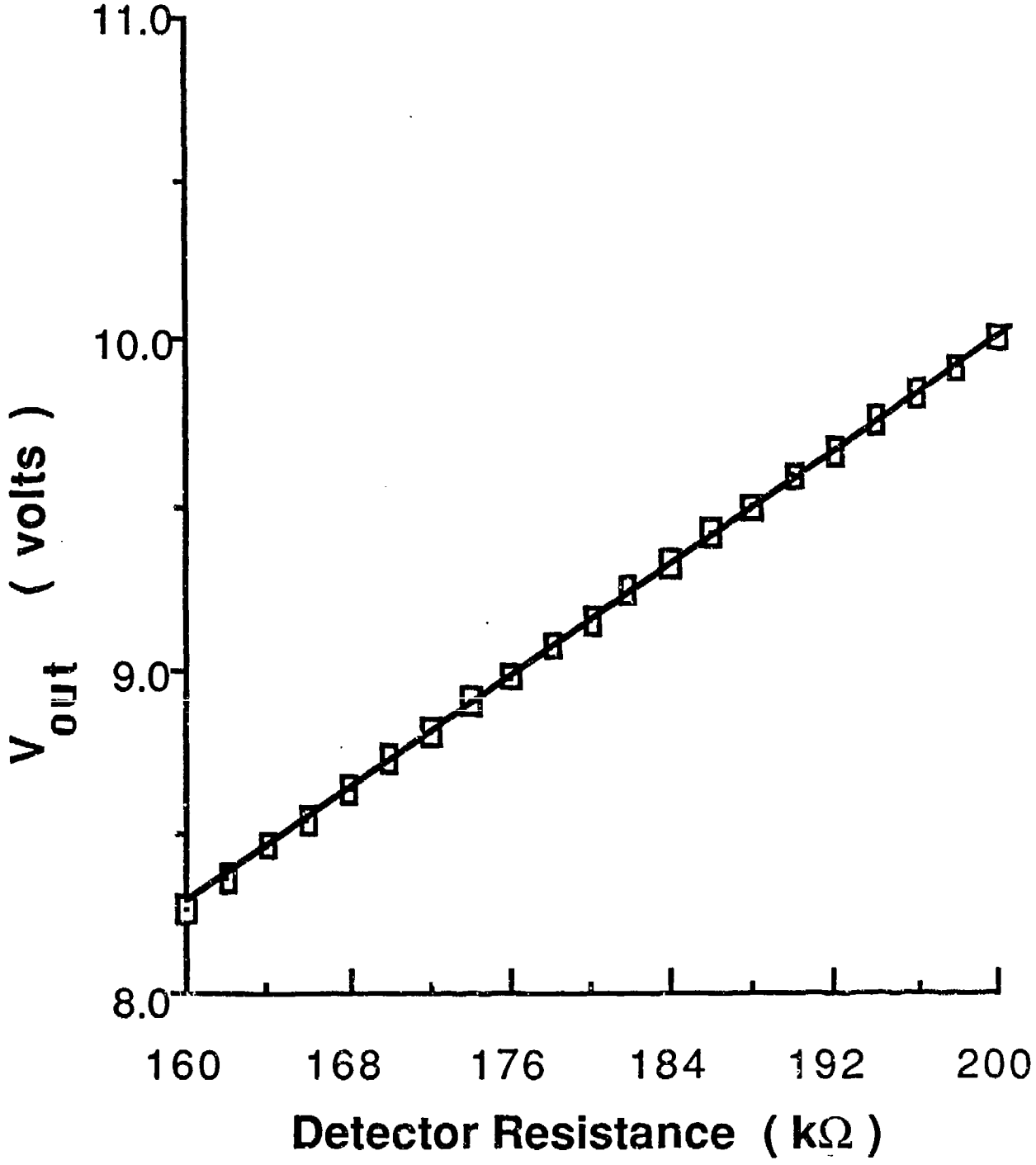

Figure 20. Lead selenide detector output voltage as a function of detector resistance.

resistance, R_D, is a linear function of input power,

$$R_D = R_0 - C\,P_{IN} \tag{3.1-1}$$

where R_0 is the detector resistance for no input power and C is a proportionality constant. The detector output voltage is then

$$V_{OUT} = I\,(R_0 - C\,P_{IN}) \tag{3.1-2}$$

or $$V_{OUT} = V_{OUT_0} - IC\,P_{IN} \tag{3.1-3}$$

where I is the current which can be assumed constant, while V_{OUT_0} is the detector output voltage for zero input power. If P_{IN_1} represents the input power to the detector with H_2 ON and P_{IN_2} the input power with H_2 OFF, the amplification ratio is given by

$$AR = \frac{P_{IN_1}}{P_{IN_2}} = \frac{V_{OUT_0} - V_{OUT_1}}{V_{OUT_0} - V_{OUT_2}} \tag{3.1-4}$$

where P_{IN_1} and P_{IN_2} have been obtained from Eq. (3.1-3). Eq. (3.1-4) can be written as

$$AR = \frac{\Delta V_1}{\Delta V_2} \tag{3.1-5}$$

where ΔV_1 and ΔV_2 are shown in Fig. 21. These voltage differentials were obtained by averaging the signal one hundred times and reading the P-P voltage.

Two circular plates with pin-holes drilled at their centers were placed in front of the detector to form a pin-hole telescope in order to decrease the power incident on the detector and increase the optical resolution. The power incident on the detector must be less than 0.012 watts[5]. Powers higher than

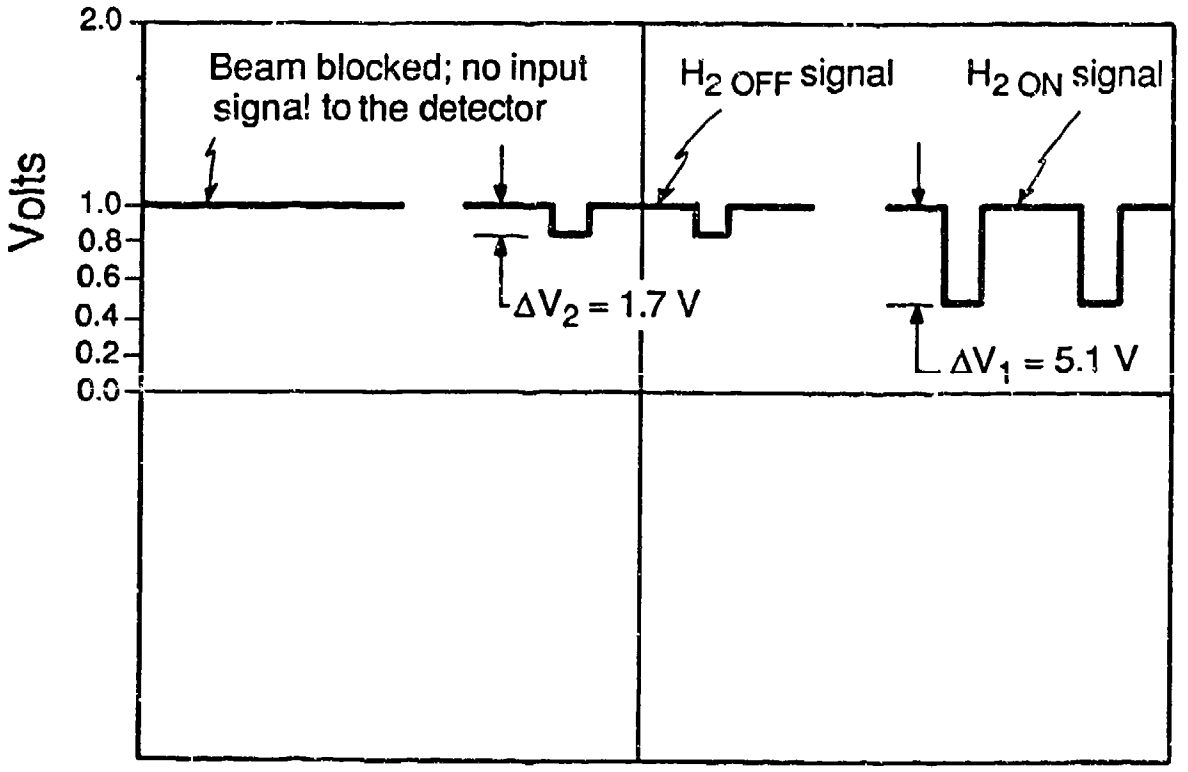

Figure 21. The $H_{2\ ON}$, the $H_{2\ OFF}$ and the signal obtained from the PbSe detector when the beam was blocked. The detector output voltage decreases as the input power increases. The amplification ratio can be calculated from the voltage differentials ΔV_1 and ΔV_2.

0.012 watts can cause saturation of the detector, which means that the linear relationship between incident power and output voltage is not valid. Operation of the detector under saturation conditions will result in false readings and can be harmful to the detector. It was found experimentally that the best combination of incident power and optical resolution was obtained when the pin-hole placed close to the detector had a diameter of 0.25 mm while the other one had a diameter of 1.00 mm. The use of the pin-hole telescope resulted in good optical resolution and low input power, but often times it was difficult to align.

Data obtained with the pin-hole telescope/PbSe detector combination are presented in Fig. 22. At high input powers there is good agreement between the detector and power meter data, but at low input powers there is no agreement at all. Figure 22 shows that the highest $P_1(6)$ amplification ratio obtained with the detector is about 10.0, while Fig. 18 shows that with the power meter, amplification ratios up to 11.5 were measured. It appeared that it was impossible to obtain accurate and consistent data with this PbSe detector/circuit combination because the necessary electronics needed to process the signal were missing.

The simple PbSe detector unit was then replaced with a ROFIN Optical Spectrum Analyzer, Fig. 23. Figure 24 presents amplification ratio versus input power data obtained with the spectrum analyzer and the PbSe detector at the location in the amplifier at which maximum amplification was obtained. The high-power part of the plot was obtained with the PbSe detector, while the low-power part of the plot was obtained with the spectrum analyzer. In this case, consistent and repeatable data were obtained and the zero power gain r ·ion (the flat part of the AR versus input power curve) was reached for the

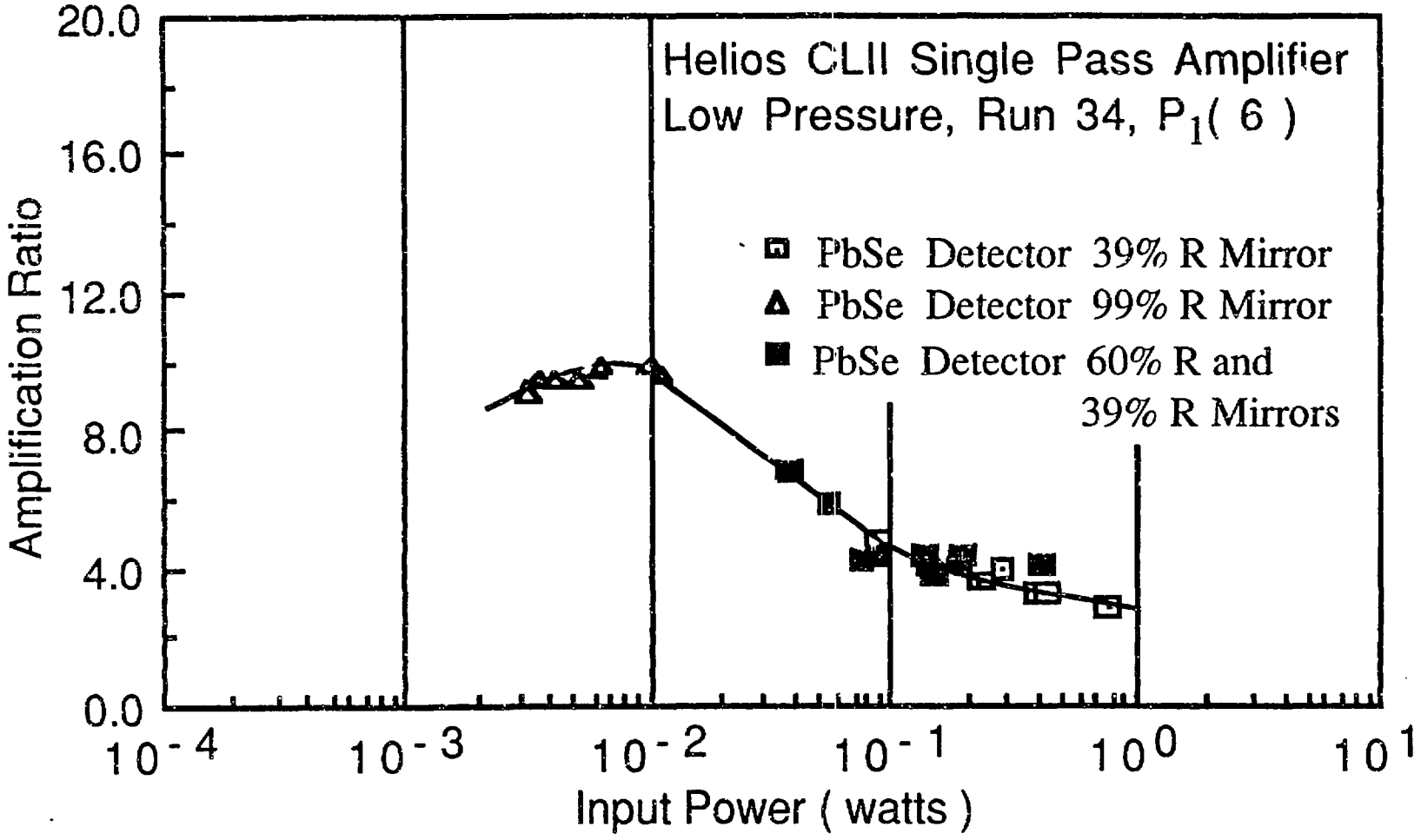

Figure 22. Variation of amplification ratio with input power. The input power was varied by gradually reducing the CL I SF_6 flow rate and by placing mirrors of different reflectivities in front of turning mirror #2.

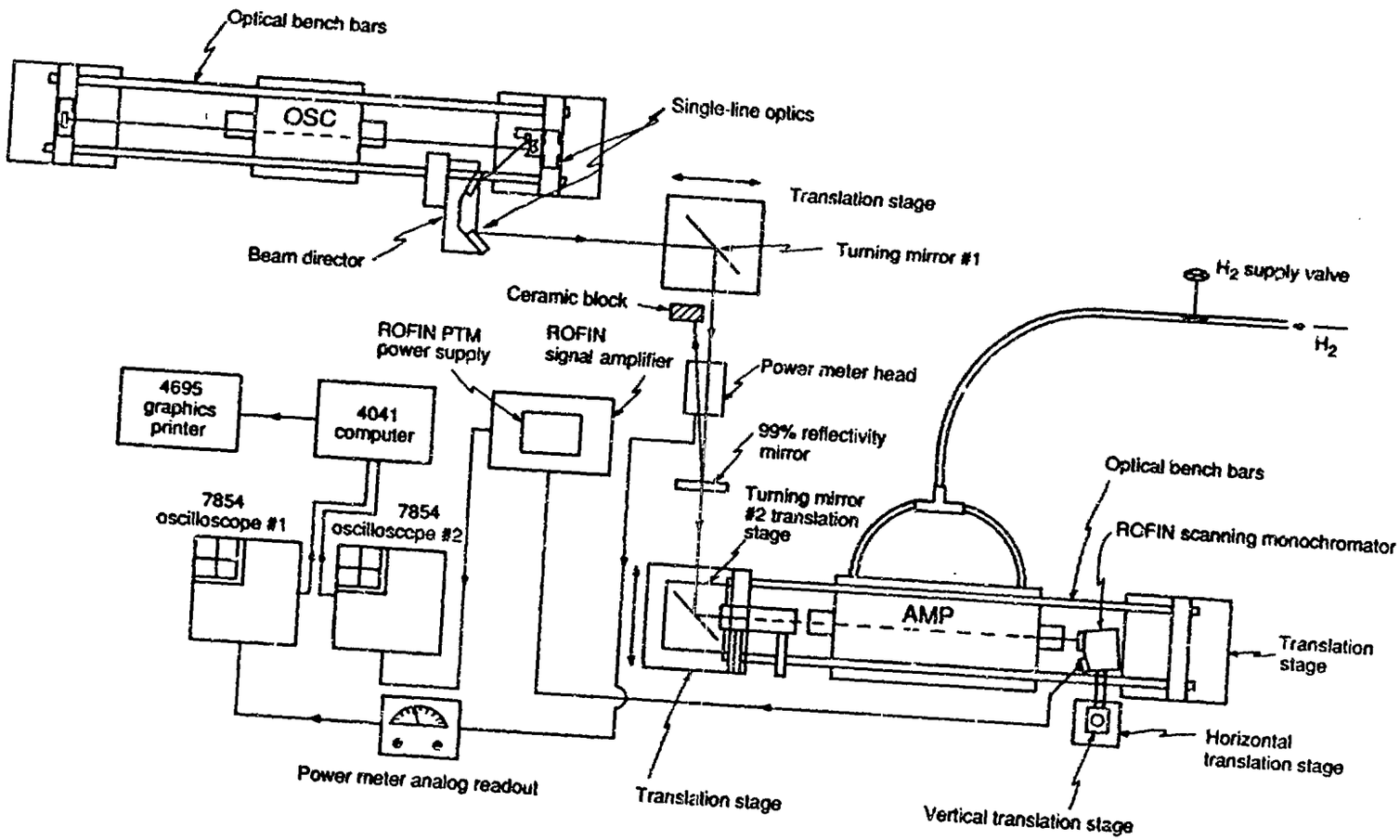

Figure 23. Schematic of the experimental layout used to measure gain with a ROFIN spectrum analyzer.

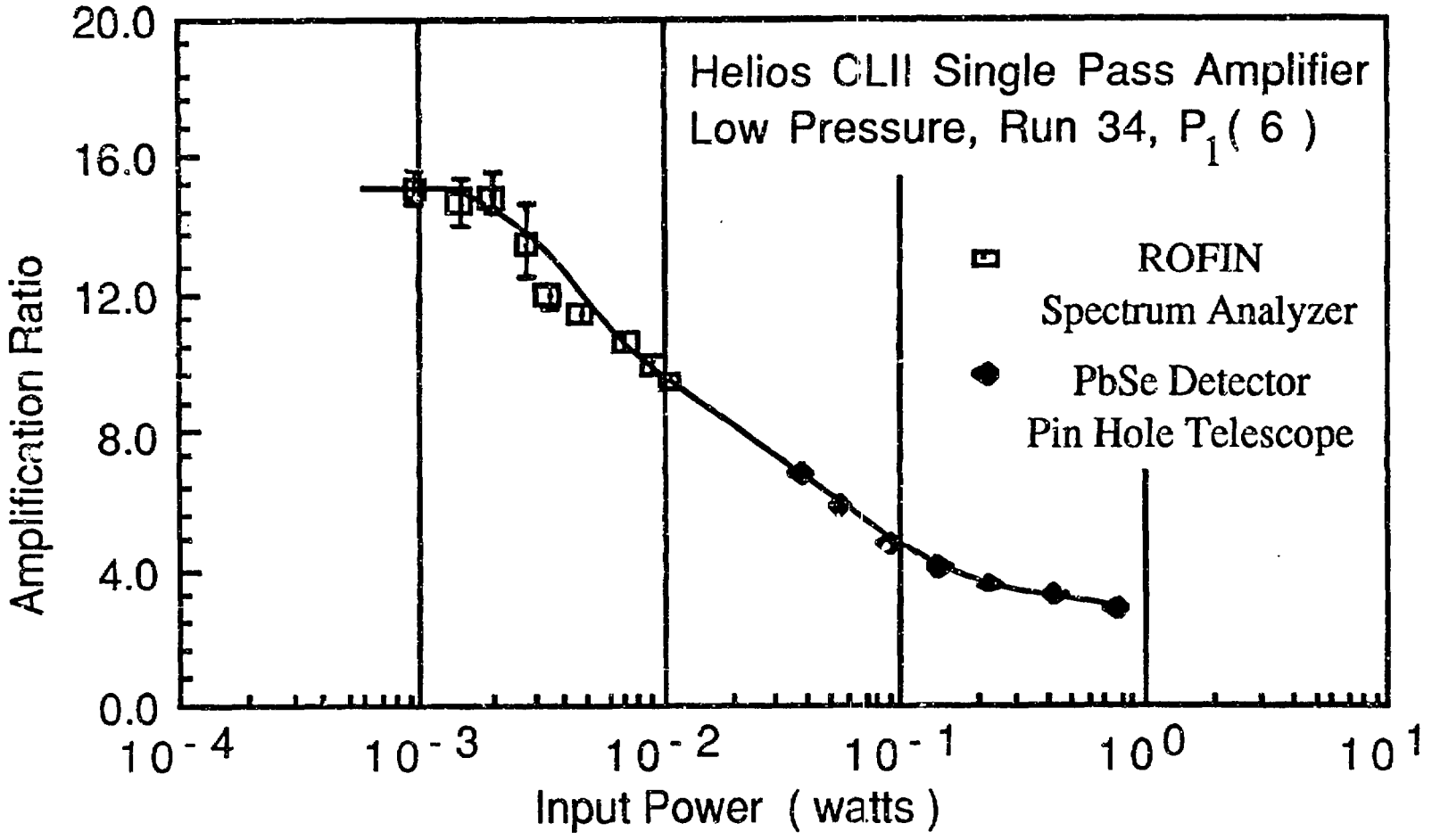

Figure 24. Variation of amplification ratio with input power. The zero power gain region is reached when $P_{IN} < 0.002$ watts. Error bars smaller than the symbols are not shown.

first time. Therefore the spectrum analyzer was used for the zero power gain measurements.

3.2 EXPERIMENTAL PROCEDURE

The main differences between the experimental procedure used in the zero power gain experiments and that used in the preliminary amplifier experiments are three. First, for the zero power gain experiments, the oscillator was run single-line. Second, the oscillator in this case had to be run at much lower powers than before because zero power gain can be measured only if the input power is low enough that the gain in the amplifier is not perturbed by the input beam. Low CL I output powers were obtained by greatly reducing the CL I SF_6 flow rate, while holding the flow rates of the rest of the gases in the CL I equal to the values corresponding to Run 34. The input power was further reduced by placing a ZnSe 99% reflectivity mirror in front of turning mirror #2. Third, because of the low amplifier input powers involved (of the order of 0.001 watt), a ROFIN RSO 6000 Series Optical Spectrum Analyzer coupled to a Tektronix MP2501 data acquisition system, Fig. 23, was used to measure the relative strength of the $P_{OUT\ H_2\ ON}$ and $P_{OUT\ H_2\ OFF}$ signals as well as to identify the different lines. The MP2501 data acquisition system consists of two 7854 Tektronix digitizing oscilloscopes, a 4041 computer, 4105 display terminal, two P6202A FET probes, and a 4695 graphics printer. The RSO 6000 Series Optical Spectrum Analyzer consists of three main elements, the scanning monochromator, the PMT power supply and the signal amplifier. The spectral data were displayed in real time on a 7854 Tektronix oscilloscope.

The heart of the spectrum analysis system is a unique type of scanning monochromator[6]. It uses a continuously rotating diffraction grating driven by a d.c. motor at approximately 600 r.p.m., Fig. 25. Light incident on the input slit is dispersed into its component wavelengths by the diffraction

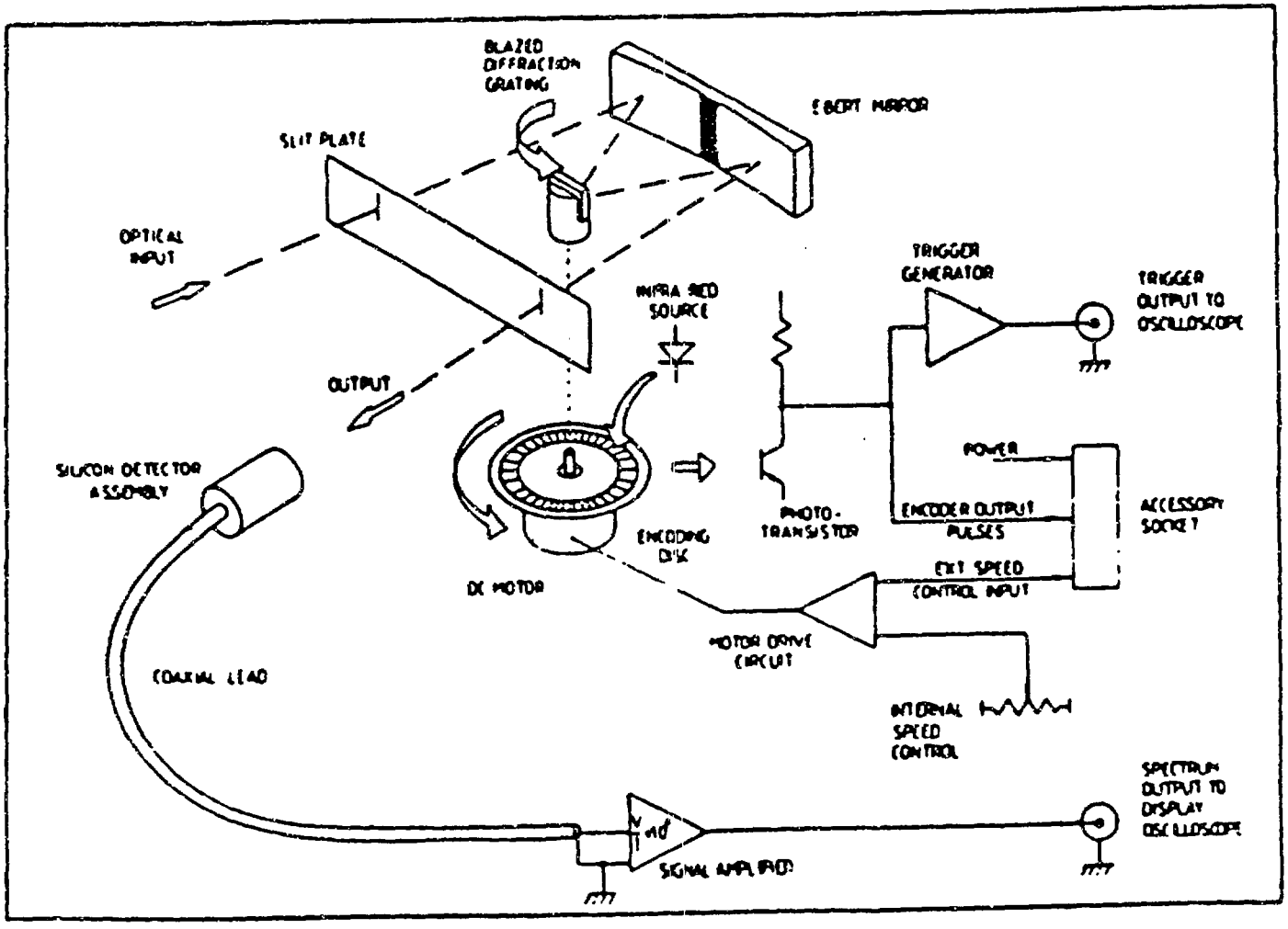

Figure 25. Schematic block diagram of the basic scanning monochromator.

grating and then sequentially swept past the output slit where a lead selenide detector converts the optical signal into a corresponding electrical signal. The signal is then amplified and displayed on the oscilloscope, where its peak to peak voltage was measured by averaging the signal 800 times. The signal was averaged 800 times because of the fluctuations caused by the low SF_6 flow rates in the CL I. The number of times that the signal had to be averaged (800 in this case) was obtained experimentally; it is the lowest number that resulted in consistent and repeatable data.

In order to increase the optical resolution and decrease the input power to the lead selenide detector (the highest recommended input power by Infared Industries Inc. for this kind of PbSe detector is 0.012 watts), a plate with a 0.25 mm diameter pin-hole was placed 18.0 mm in front of the 150 μm slit on the scanning monochromator inlet.

The amplification ratio was determined by taking the ratio of $V_{H_2\ ON}$ to $V_{H_2\ OFF}$, Fig. 26. The gain was then calculated from the amplification ratio as follows;

$$\alpha = \frac{1}{Le} \ln \frac{V_{H_2\ ON}}{V_{H_2\ OFF}} \qquad (3.2\text{-}1)$$

where Le is the effective length of the mixed flow, which was given by the computer simulations[2,7] as 24.4 cm.

There is a critical input power (P_{IN} zero power gain), below which the gain in the amplifier is equal to the zero power gain and is independent of P_{IN}, and above which the gain in the amplifier is inversely proportional to P_{IN}. In order to determine the input power level required for zero power gain measurements, the gain in the amplifier was measured as a function of decreasing input power at the location of maximum amplification until the

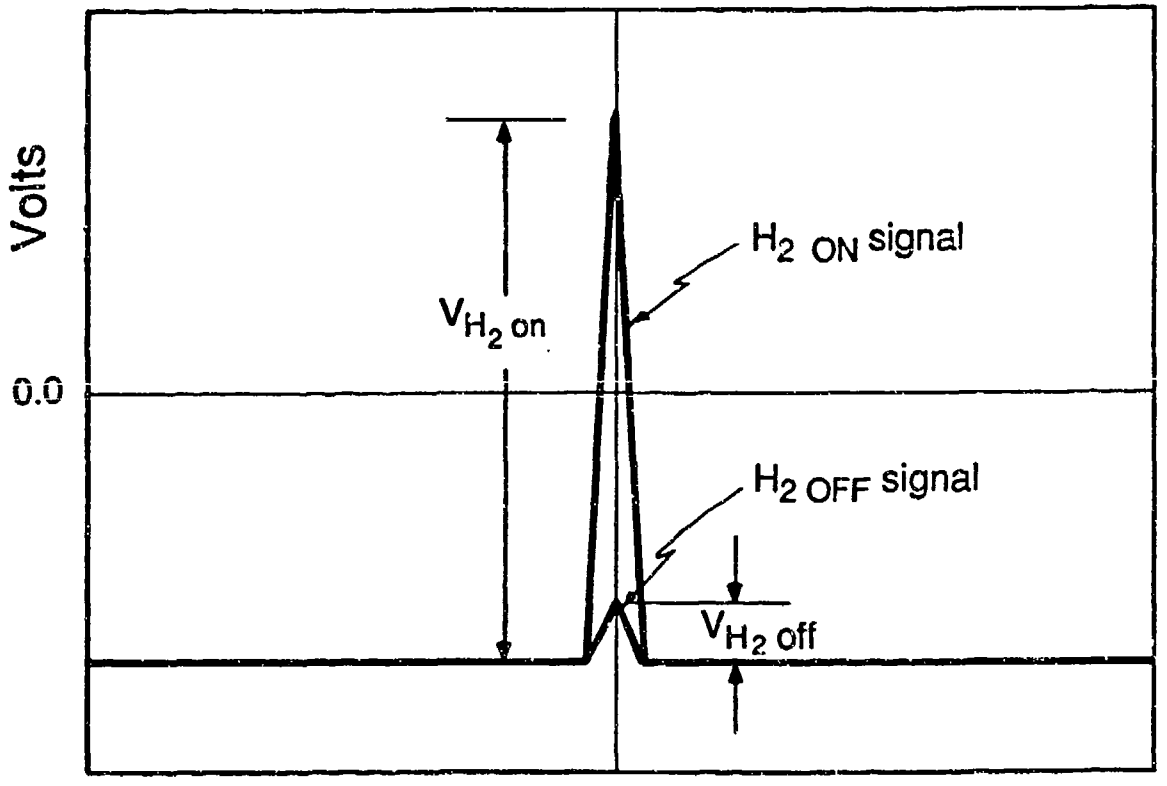

Figure 26. Schematic of $H_{2\ ON}$ and $H_{2\ OFF}$ signals obtained with the spectrum analyzer.

level part of the gain versus P_{IN} plot was reached. This was done for all lines whose zero power gains were to be measured. Absolute values of the input power were obtained by using the power meter to measure the power before turning mirror #2, and then correcting for the turning mirror, telescope and left Brewster window losses (which were measured).

3.3 ALIGNMENT OF SCANNING MONOCHROMATOR

Turning mirrors #1 and #2 as well as the telescope were aligned with the H_2 injectors as described in Section 2.2. The slit and the pin-hole of the scanning monochromator were then aligned with the H_2 injectors of the amplifier as follows. With the Brewster window at the exit of the amplifier and the pin-hole out, the scanning monochromator box was set on a horizontal and a vertical translation stage and was aligned with respect to the CL II laser body and the amplifier rod assembly, Fig. 27. The monochromator was then translated both in the vertical and the horizontal direction, until a signal was obtained on the oscilloscope. The slit was aligned with the H_2 injectors by using a piece of paper to partially block the beam (the power was so low that the paper would not burn) at the exit of the amplifier while observing the signal on the oscilloscope. This way the field of view of the slit at the exit of the amplifier was determined. The field of view of the slit was then centered on the H_2 injectors at the exit of the amplifier by translating the monochromator as necessary in the vertical and horizontal directions.

The next step was to align the pin-hole. The pin-hole was placed on the monochromator box and secured at a distance of 18 mm in front of the slit. A plexiglass plate with a 0.5 mm diameter pin-hole was placed at the CL II exit, such that the 0.5 mm diameter pin-hole was aligned both vertically and horizontally with the H_2 injectors. First the vertical translation stage of

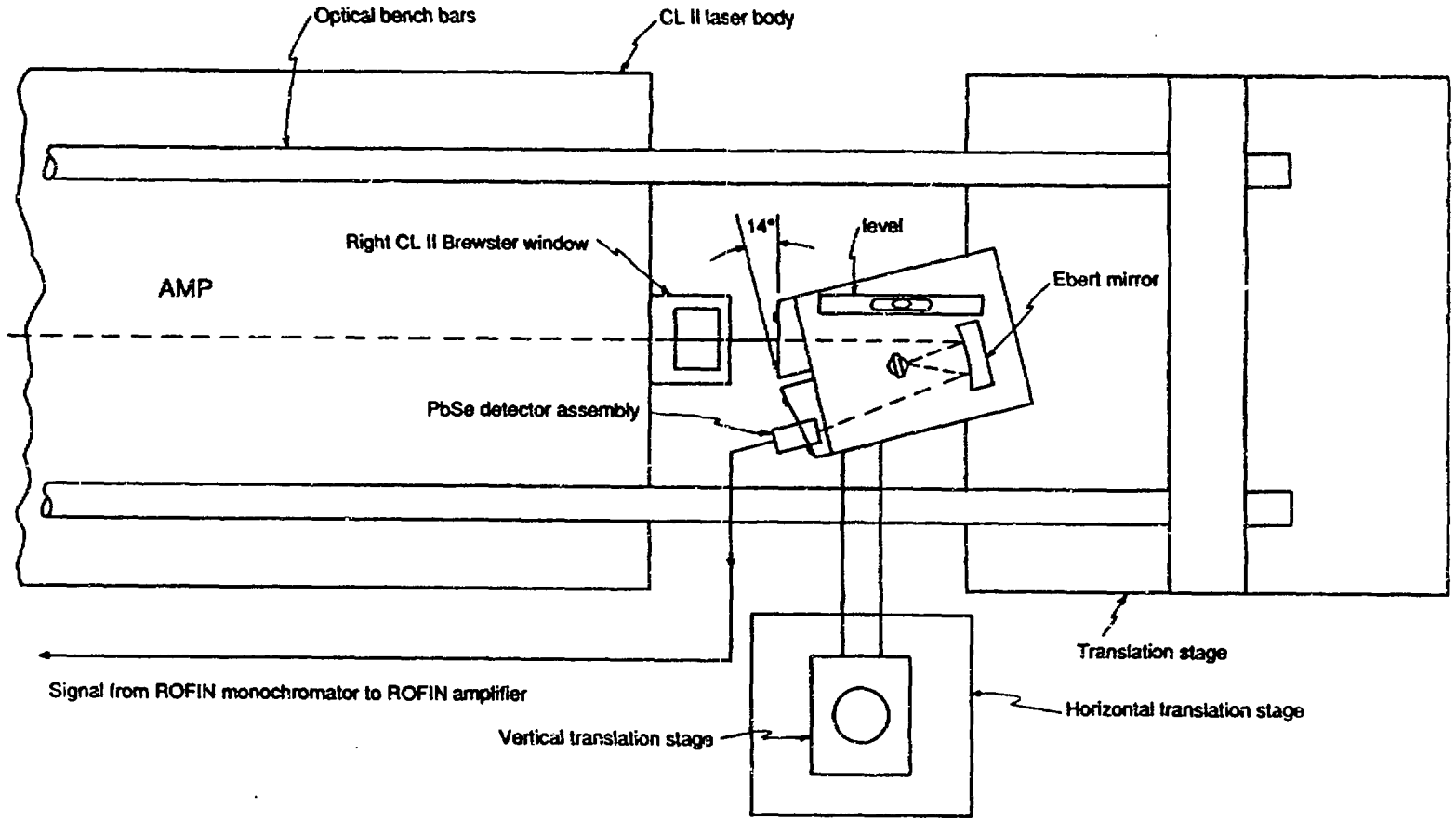

Figure 27. Position of the monochromator with respect to the CL II laser body. The vertical and the horizontal translation stages shown provide independent vertical and horizontal movement of the monochromator.

the monochromator and then the horizontal one were aligned so that the signal on the oscilloscope was maximized. The signal was also maximized by slightly moving the pin-hole with respect to the slit, in whatever direction required to maximize the signal. When a maximum signal was obtained, the pin-hole was locked to the monochromator box. The PbSe detector was rotated in its base until the signal was maximized, and then secured in place. At this point, the monochromator was aligned horizontally but not vertically. The Brewster window was placed at the exit of the CL II and the beam size in the vertical direction was measured by translating the monochromator vertically and recording the readings of the vertical translation stage at the points where the signal on the oscilloscope appeared and disappeared. The monochromator height was then aligned according to experimental requirements; for example, if it was desired to take gain measurements 0.75 mm below the top of the flow channel (the height for maximum amplification), the monochromator was moved from the highest point of the beam, a distance equal to 1/4 of the size of the beam in the vertical direction.

3.4 CALIBRATION OF THE SPECTRUM ANALYZER

The spectrum analyzer had to be calibrated in order to correctly identify the different lines. This was accomp d with the help of a calibration table that came with the instrument. This table was used to provide the wavelength corresponding to each cursor reading of the spectrum analyzer. The wavelengths of all the lasing lines were compared to the wavelengths presented in this table and it was found that only the $P_2(6)$ wavelength (2.8319 μm) matched a wavelength in the calibration table (the corresponding cursor reading was 1423). Thus, this line was chosen as the reference for the calibration of the instrument.

The single-line optics on the CL I were aligned so that $P_2(6)$ was lasing.

The oscillator output beam was then passed through the amplifier and the scanning monochromator was aligned with the incoming beam as described in Section 3.2, so that a signal was obtained on the 7854 oscilloscope connected to the spectrum analyzer. The spectrum analyzer cursor signal was then displayed on the oscilloscope and the cursor was set to 1423. The cursor was then moved by turning a screw located at the rear of the spectrum analyzer amplifier unit until it was aligned with the $P_2(6)$ signal on the oscilloscope. All other lasing lines were then one by one passed through the amplifier and were identified by recording the cursor reading at which the cursor was aligned with the signal of each line. Table 7 presents all the calibration information necessary to identify the lasing lines.

3.5 LOW PRESSURE ZERO POWER GAIN MEASUREMENTS

The amplifier input power required to measure the zero power gain of each line ($P_{IN\ ZPG}$ or less) was established for both the Run 34 and Run 36 flow rates in the amplifier by measuring the amplification ratio as a function of input power at the point in the flow field (x,y), Fig. 28, corresponding to maximum amplification. The axis of the input beam was 1.0 mm downstream of the H_2 injectors. The zero power gain of each line was calculated from the measured amplification ratios and was then plotted as a function of input power. Figures 29, 30, 31 and 32 present gain versus input power data for lines $P_1(?)$ to $P_1(8)$ and $P_2(3)$ to $P_2(9)$ for the Run 34 flow rates in the amplifier. Figures 33, 34, 35, 36 and 37 present gain versus input power data for the same lines for the Run 36 flow rates in the amplifier. All of these graphs behave in a similar way in the sense that gain goes up as input power is decreased until a point is reached where the gain levels off; the gain at this point is the zero power gain. In some cases however ($P_2(5)$ in Fig. 31 is a good example), a decrease in gain was measured at powers lower

Line	Actual Wavelength (μm)	Spectrum Analyzer Cursor Reading ≈ λ/2 (μm)	Calibration Table Wavelengths (μm)
$P_1(1)$	2.5508	Not Lasing	Not Lasing
$P_1(2)$	2.5788	1292	2.5792
$P_1(3)$	2.6085	1307	2.6084
$P_1(4)$	2.6398	1323	2.6395
$P_1(5)$	2.6728	1340	2.6724
$P_1(6)$	2.7075	1358	2.7072
$P_1(7)$	2.7441	1377	2.7438
$P_1(8)$	2.7826	1397	2.7822
$P_1(9)$	2.8231	Not Lasing	Not Lasing
$P_1(10)$	2.8657	Not Lasing	Not Lasing
$P_1(11)$	2.9103	Not Lasing	Not Lasing
$P_1(12)$	2.9573	Not Lasing	Not Lasing
$P_2(1)$	2.6667	Not Lasing	Not Lasing
$P_2(2)$	2.6962	Not Lasing	Not Lasing
$P_2(3)$	2.7275	1368	2.7264
$P_2(4)$	2.7605	1386	2.7611
$P_2(5)$	2.7953	1404	2.7956
$P_2(6)$	2.8319	1423	2.8319
$P_2(7)$	2.8706	1444	2.8719
$P_2(8)$	2.9112	1465	2.9118
$P_2(9)$	2.9540	1487	2.9535
$P_2(10)$	2.9990	Not Lasing	Not Lasing
$P_2(11)$	3.0462	Not Lasing	Not Lasing
$P_2(12)$	3.0958	Not Lasing	Not Lasing

Table 7. Wavelength, spectrum analyzer cursor reading and calibration table wavelength corresponding to each cursor reading for each line that lased in the CL I with the single line optics for the Run 34 flow rates at 5.4 torr.

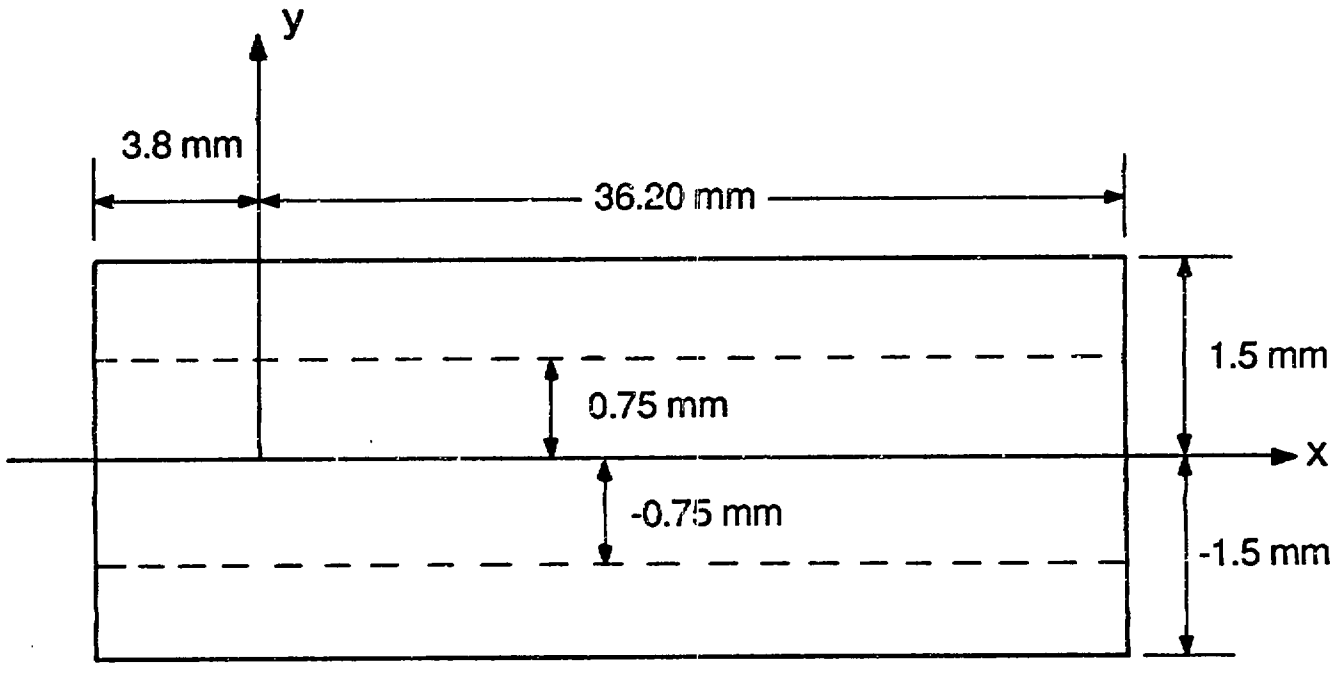

Figure 28. The clear aperture of the flow channel of the CL I and CL II lasers. H_2 is injected through sonic orifices in the upper and lower walls. The y axis is centered on these orifices. The x axis is the center line of the flow channel.

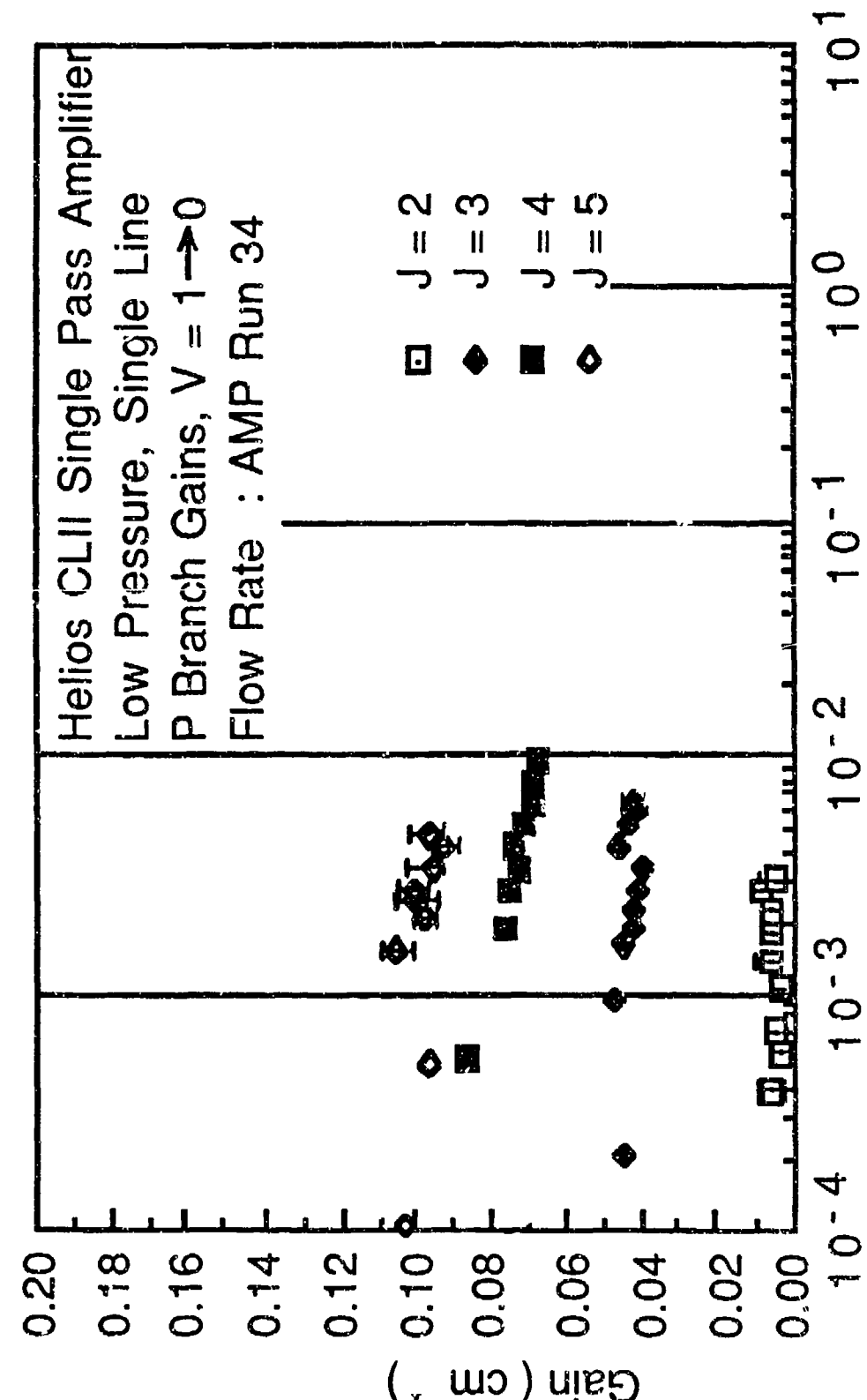

Figure 29. Variation of gain with input power for several $P_1(J)$ lines. Error bars smaller than the symbols are not shown.

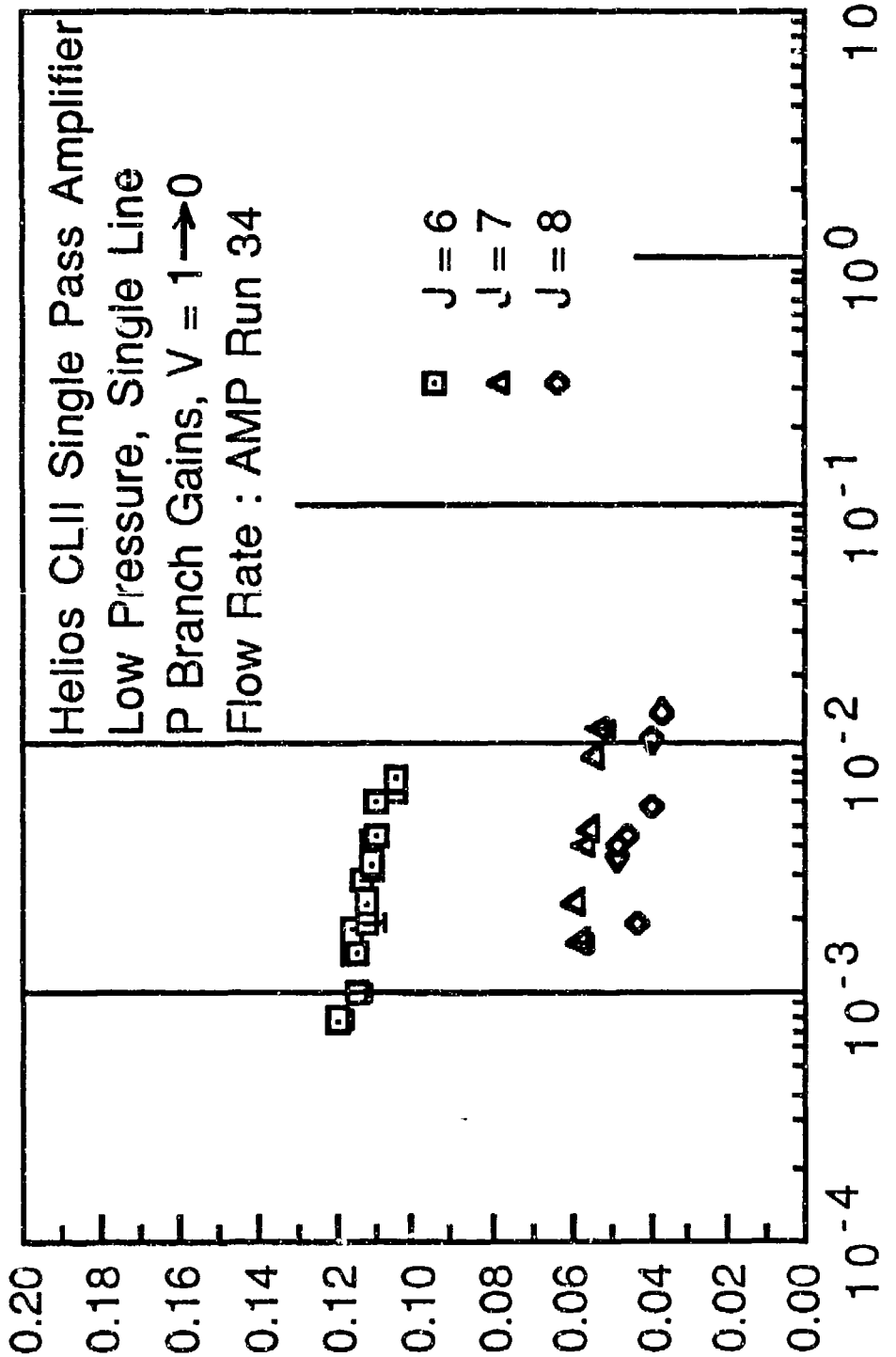

Figure 30. Variation of gain with input power for several $P_1(J)$ lines. Error bars smaller than the symbols are not shown.

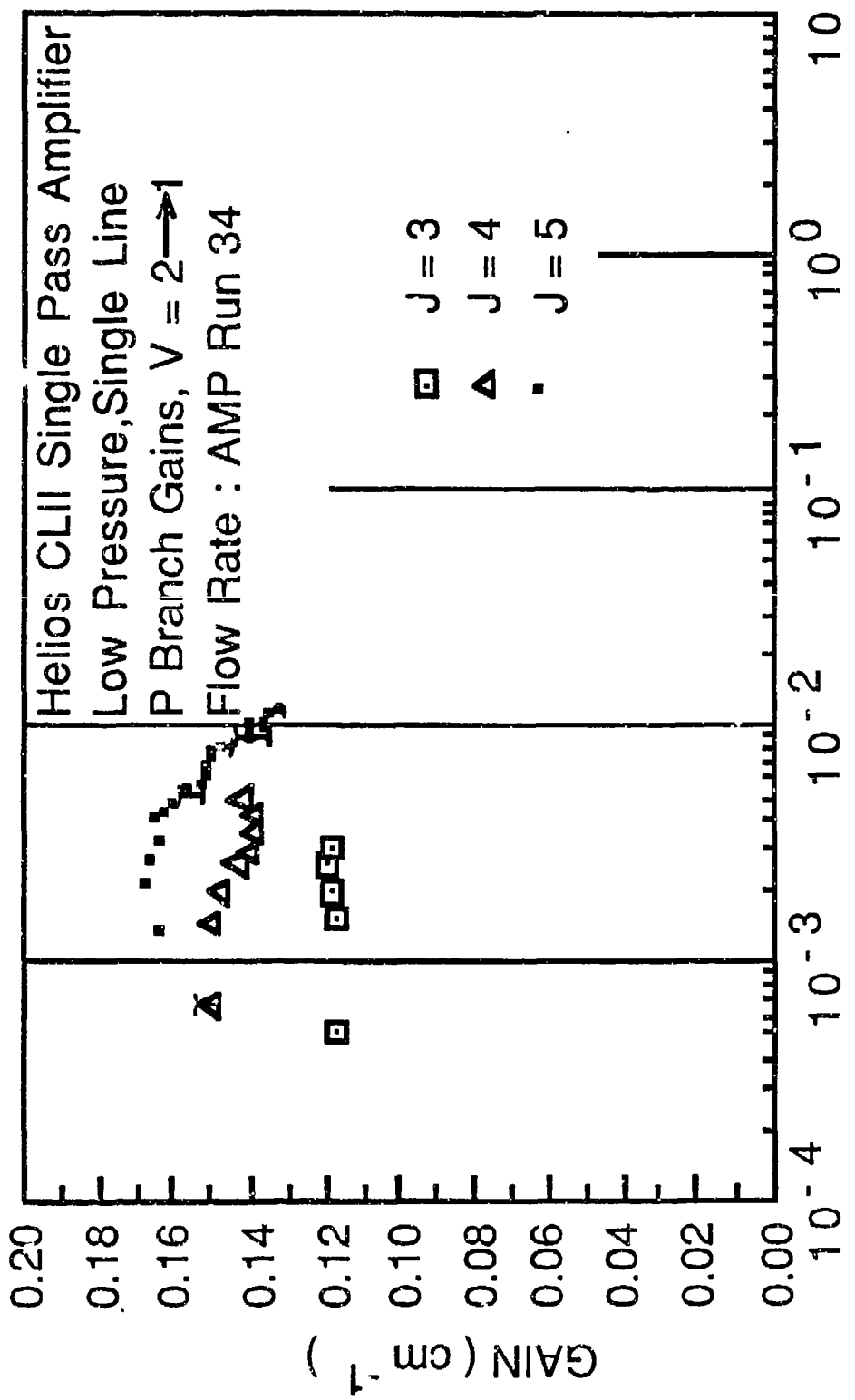

Figure 31. Variation of gain with input power for several $P_2(J)$ lines. Error bars smaller than the symbols are not shown.

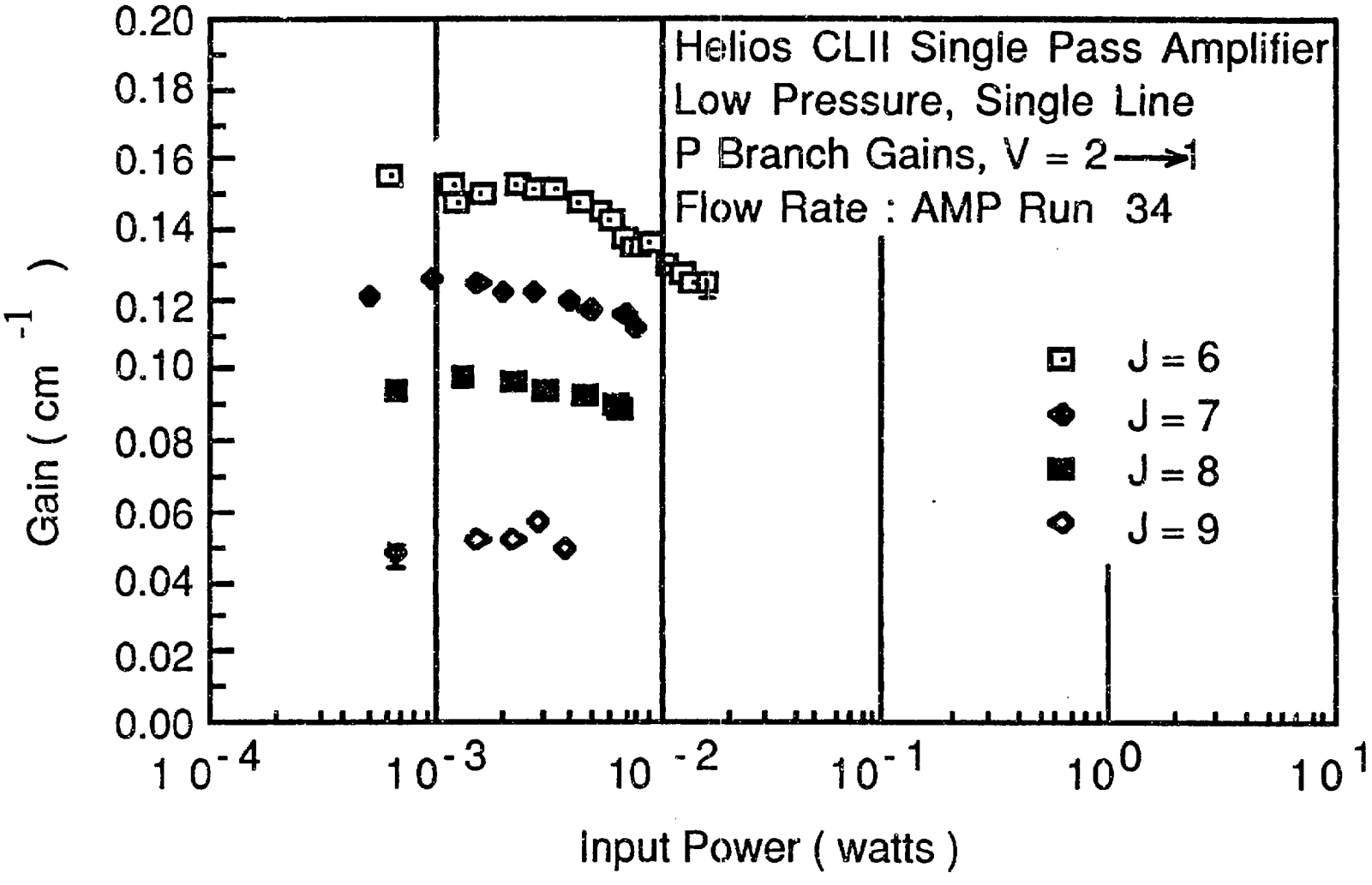

Figure 32. Variation of gain with input power for several $P_2(J)$ lines. Error bars smaller than the symbols are not shown.

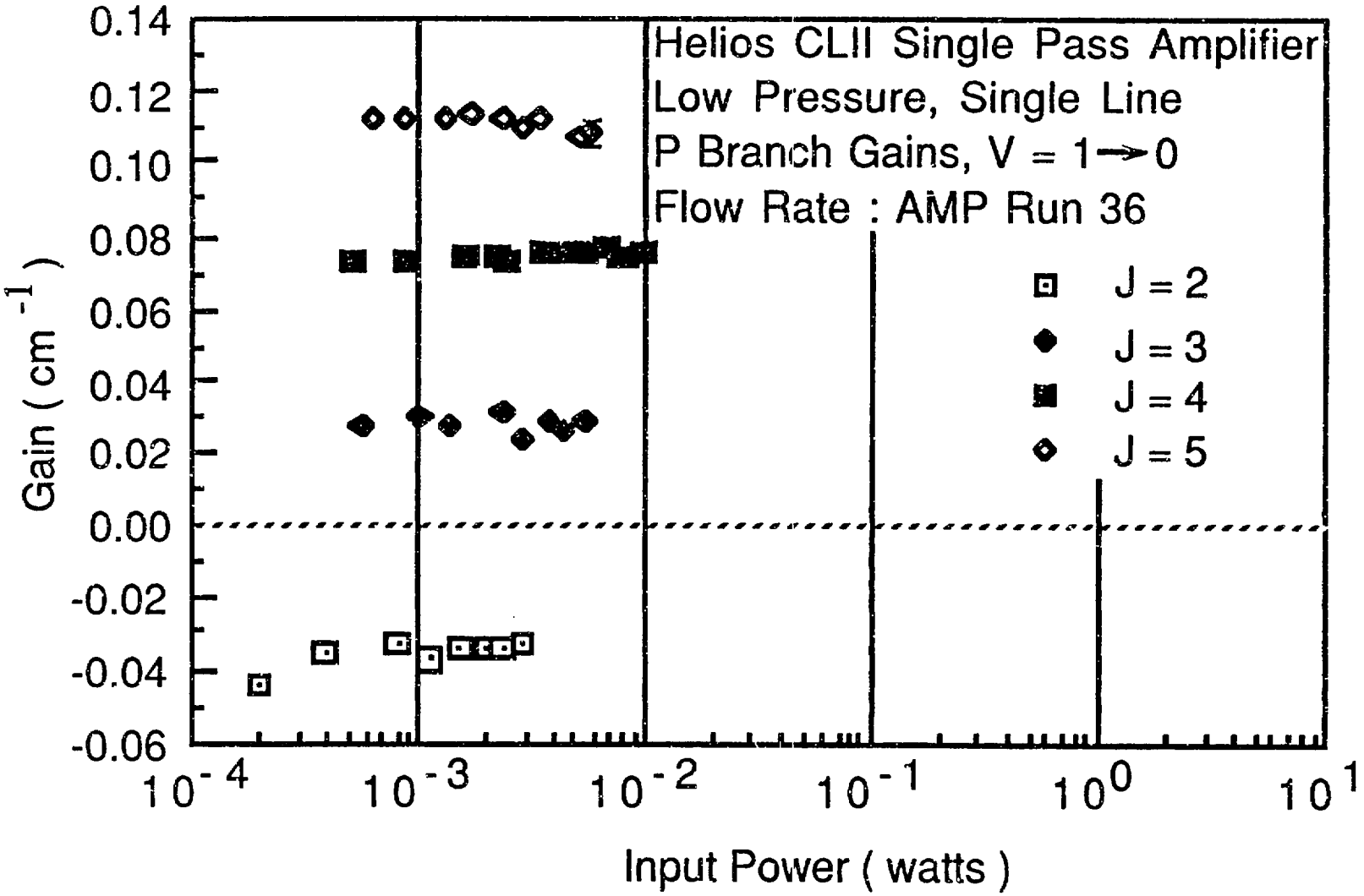

Figure 33. Variation of gain with input power for several $P_1(J)$ lines. Error bars smaller than the symbols are not shown.

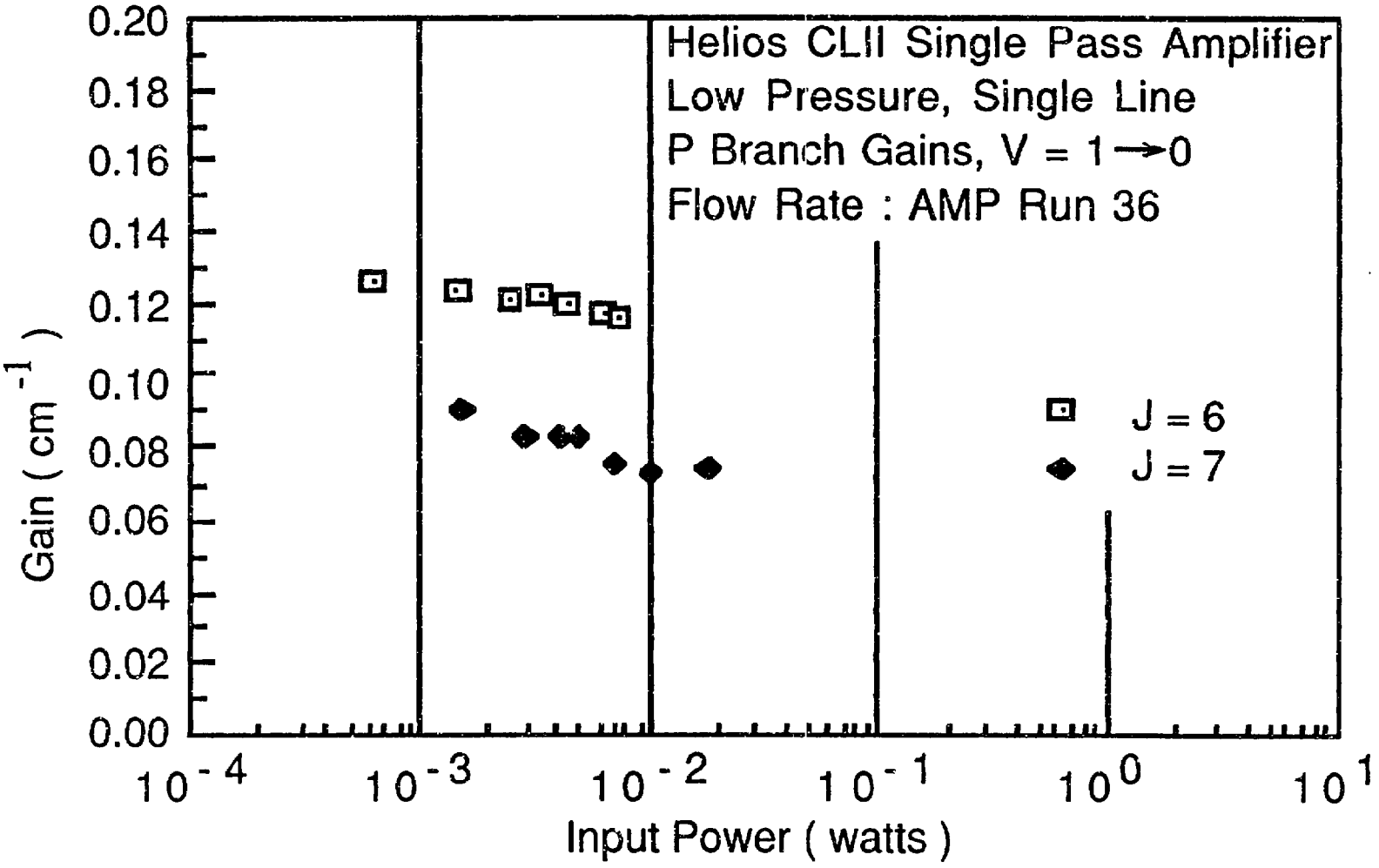

Figure 34. Variation of gain with input power for several $P_1(J)$ lines. Error bars smaller than the symbols are not shown.

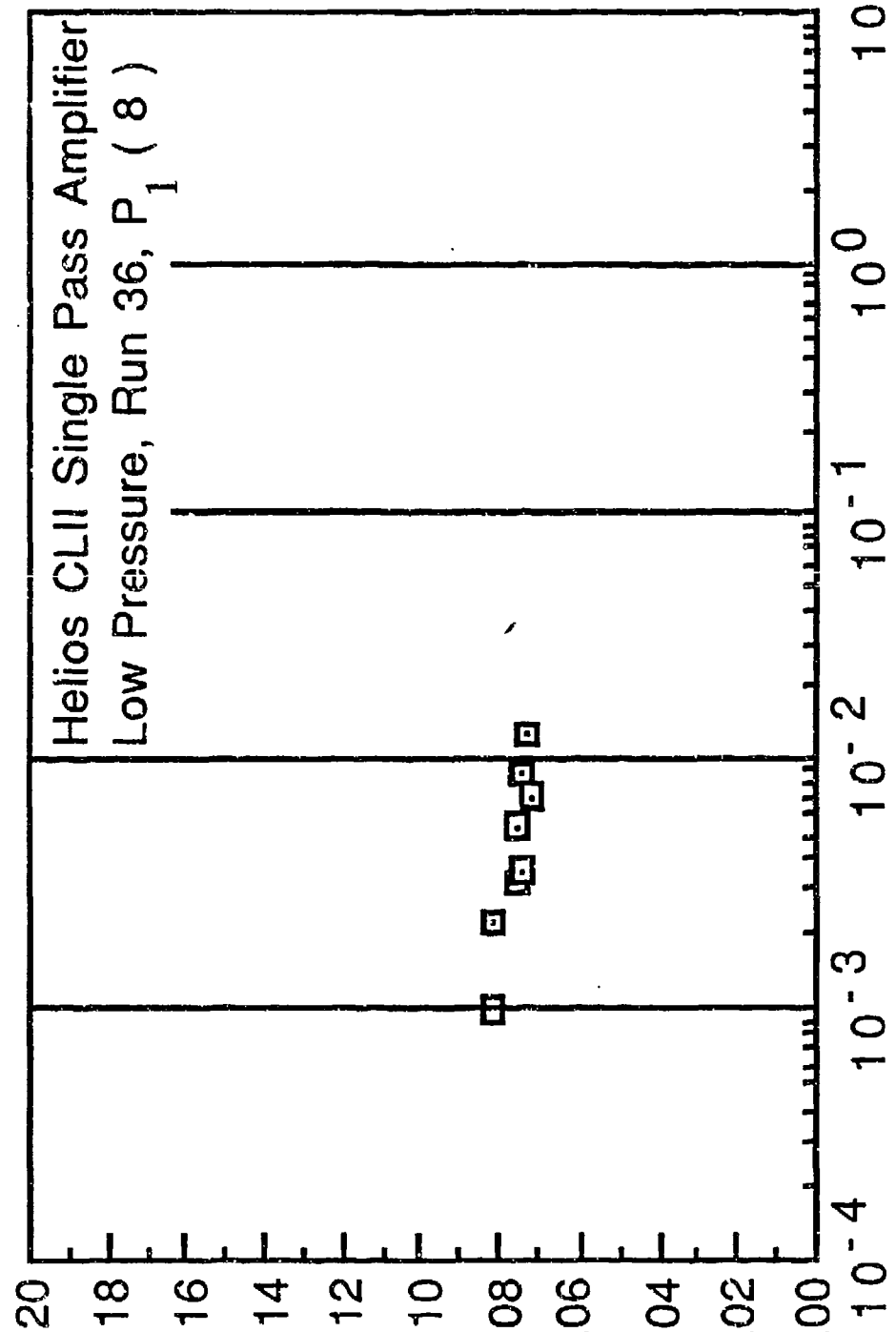

Figure 35. Variation of gain with input power for the $P_1(8)$ line. Error bars smaller than the symbols are not shown.

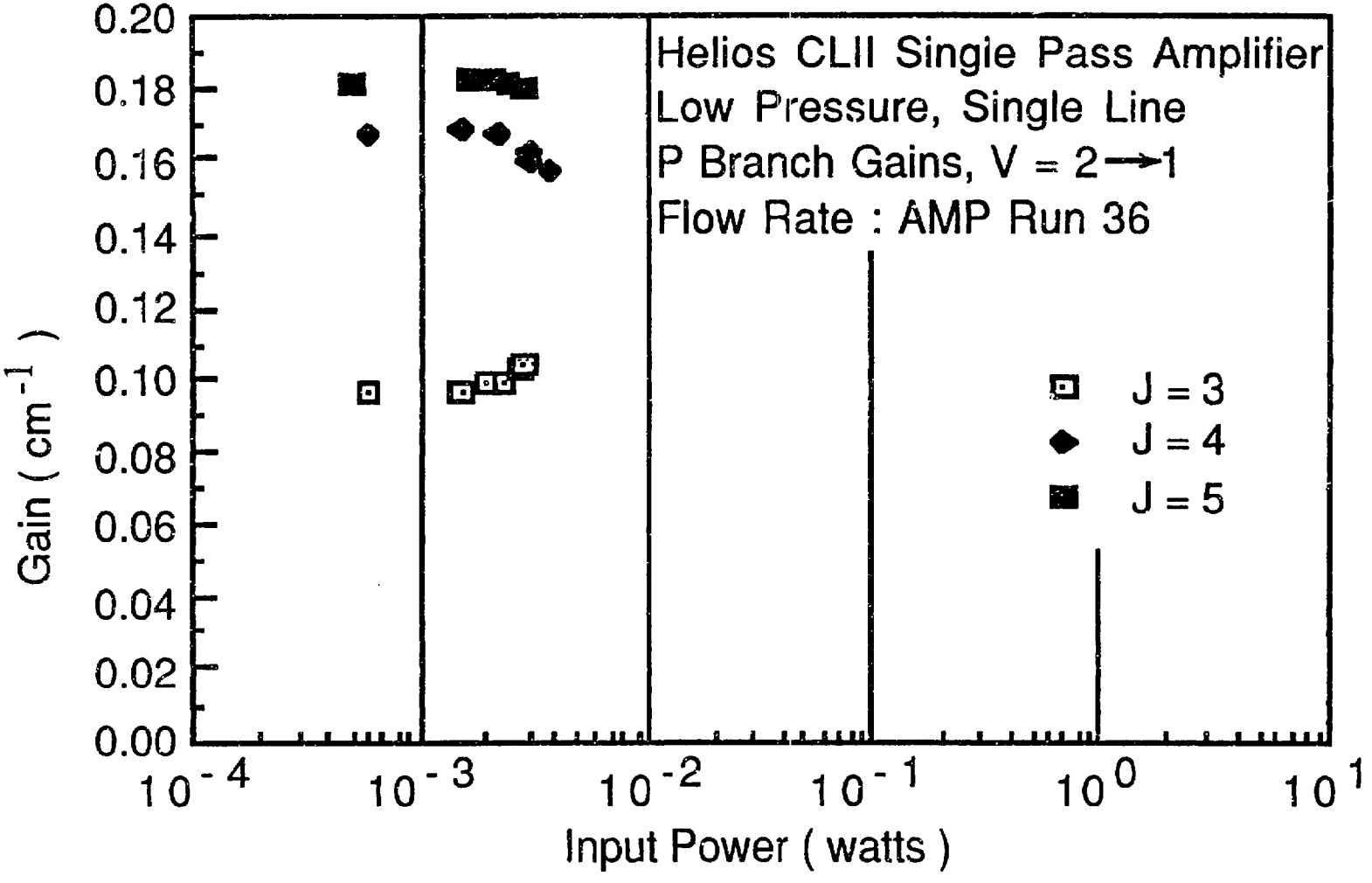

Figure 36. Variation of gain with input power for several $P_2(J)$ lines. Error bars smaller than the symbols are not shown.

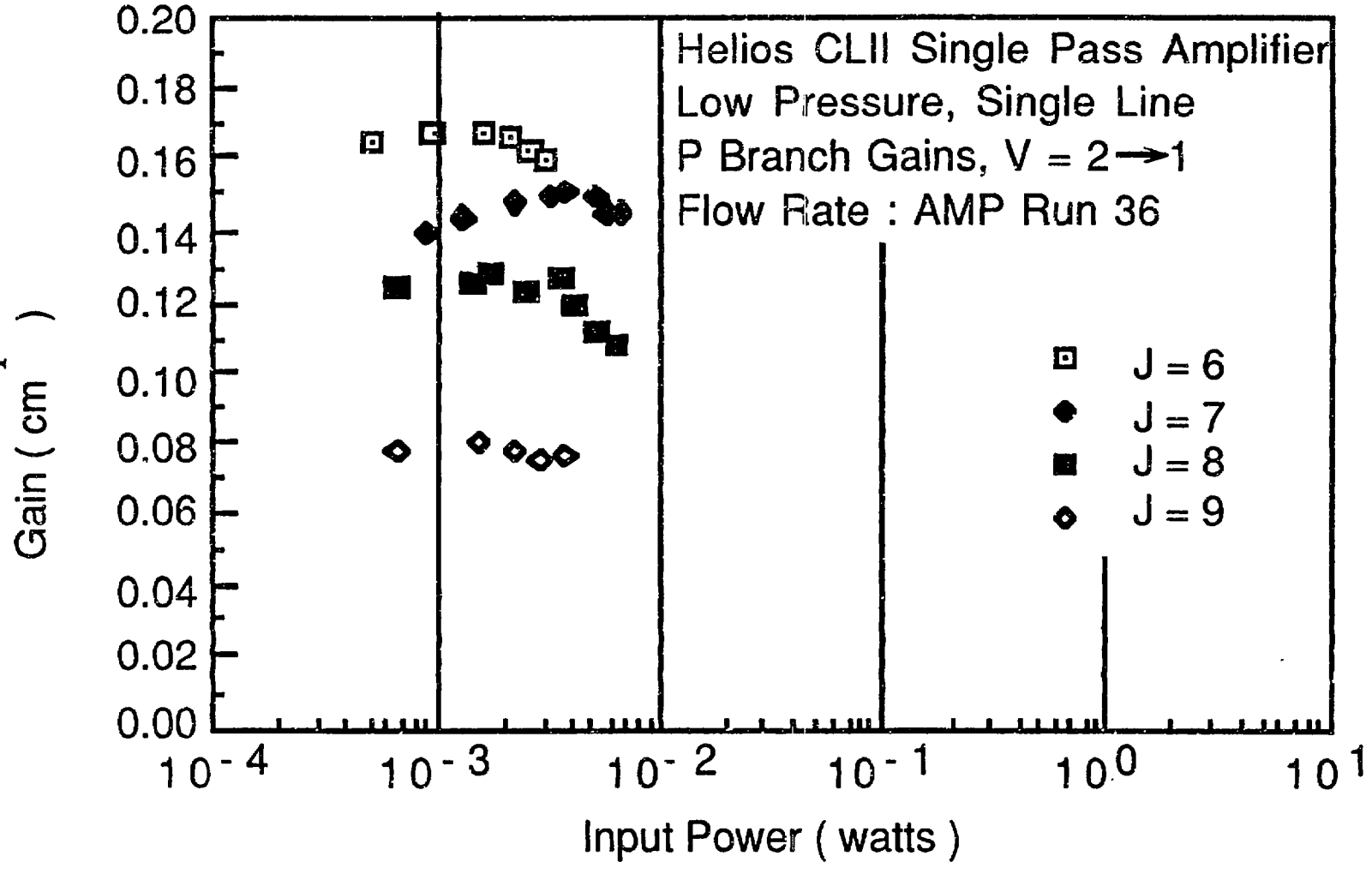

Figure 37. Variation of gain with input power for several $P_2(J)$ lines. Error bars smaller than the symbols are not shown.

than $P_{IN\ ZPG}$. This is a measurement error due to the low input power involved in these measurements. At low input power the $V_{H_2\ OFF}$ signal fluctuates between $V_{H_2\ OFF\ HIGH}$ and $V_{H_2\ OFF\ LOW}$, because of the low SF_6 flow rates in the CL I. As the SF_6 flow rate in the CL I is decreased further, the input power is decreased and the signal instability is increased until at some point $V_{H_2\ OFF\ LOW}$ becomes less than V_{NOISE} (the voltage of the noise in the signal). At this point the oscilloscope, when used to average the signal 800 times, takes averages between $V_{H_2\ OFF\ HIGH}$ and V_{NOISE}, and therefore it calculates an average $V_{H_2\ OFF}$ that is higher than the actual. This higher $V_{H_2\ OFF}$ signal then results in a gain that is lower than the zero power gain.

The zero power gain as a function of x was measured for both the Run 34 and the Run 36 flow rates in the amplifier. This was done by following the procedure described below. The input beam was passed through the amplifier 1.0 mm downstream of the H_2 injectors (x = 1.0 mm) and was aligned with the centerline of the flow channel (y = 0.0 mm). The monochromator was then aligned in both the x and the y directions until maximum amplification was obtained. The x location for maximum amplification was at the center of the beam (x = 1.0 mm) and the y location for maximum amplification was 0.75 mm above the center line (y = 0.75 mm). Both the optical bench and the monochromator were then moved 1.5 mm upstream. The amplification ratio was then measured as a function of x by translating both the optical bench and the monochromator in the downstream direction by increments of 0.5 mm. The amplification ratio of each line was measured in this way by using an input power equal to or less than the $P_{IN\ zpg}$ for that line. The zero power gain was then calculated from the amplification ratio of each line and plotted versus x. Figures 38 - 41 present zero power gain versus x data for $P_1(2)$ to

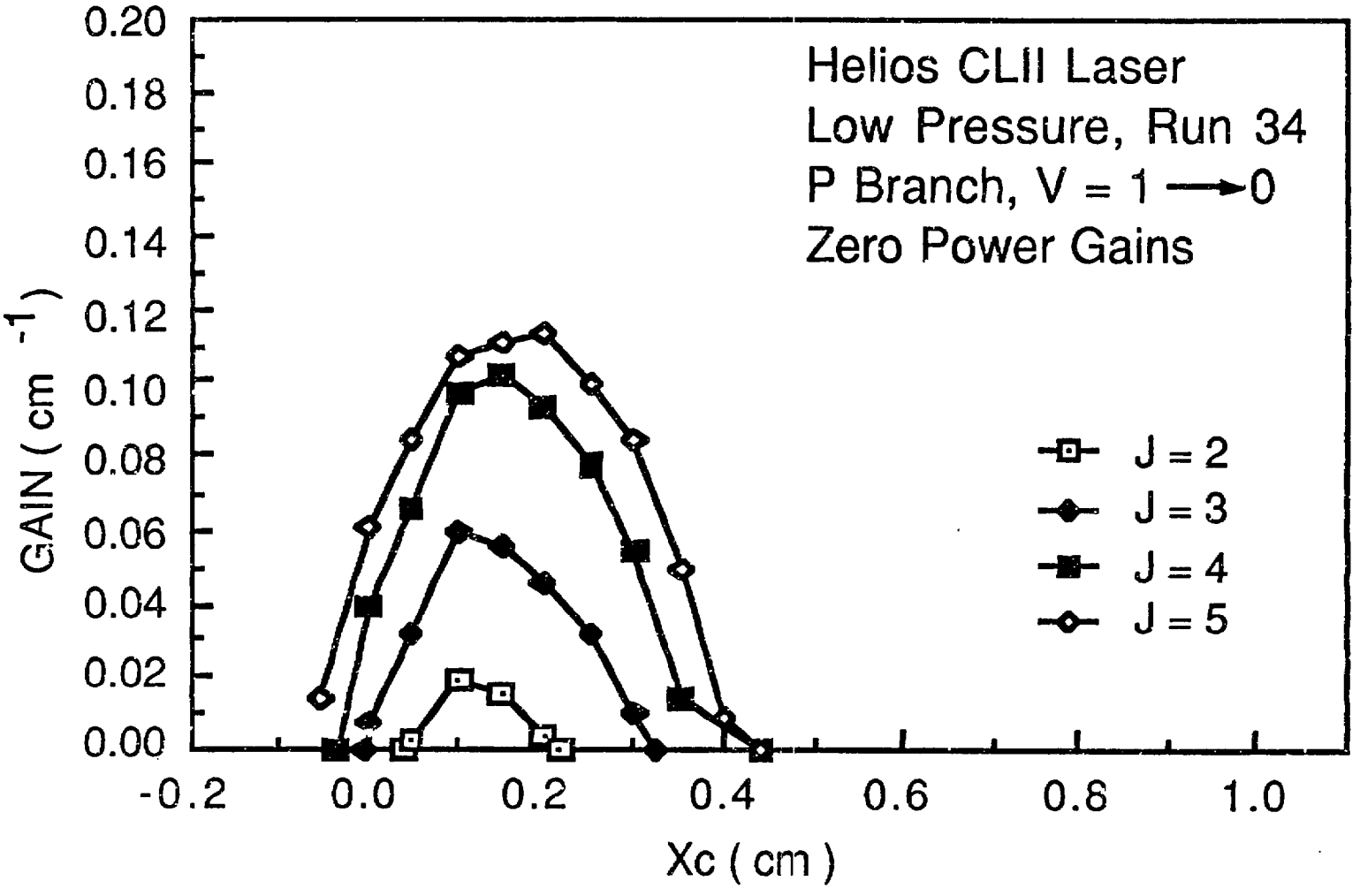

Figure 38. Variation of the zero power gain as a function of distance downstream of the H_2 injectors at y = 0.75 mm for several $P_1(J)$ lines. Error bars smaller than the symbols are not shown.

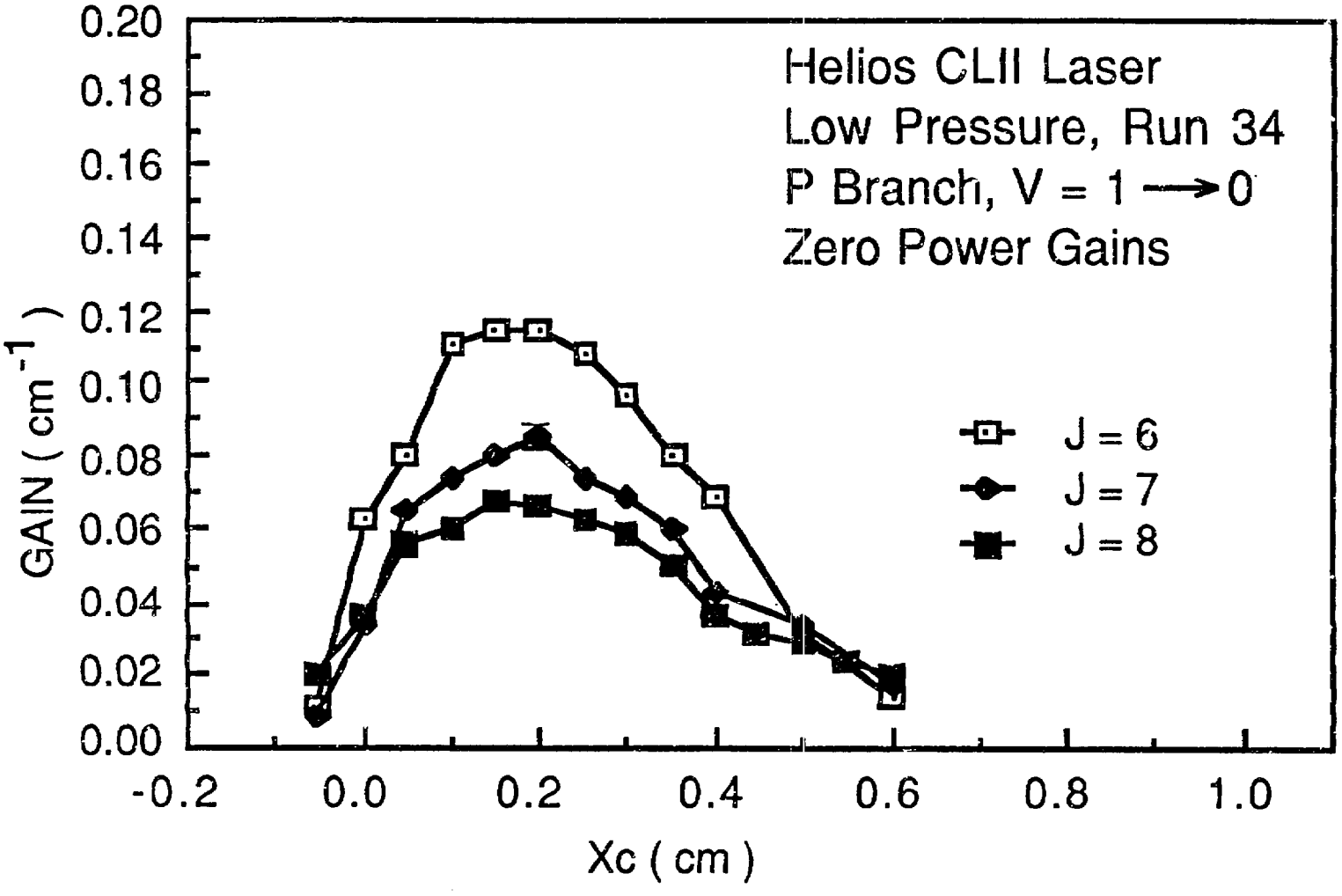

Figure 39. Variation of the zero power gain as a function of distance downstream of the H_2 injectors at y = 0.75 mm for several P_1(J) lines. Error bars smaller than the symbols are not shown.

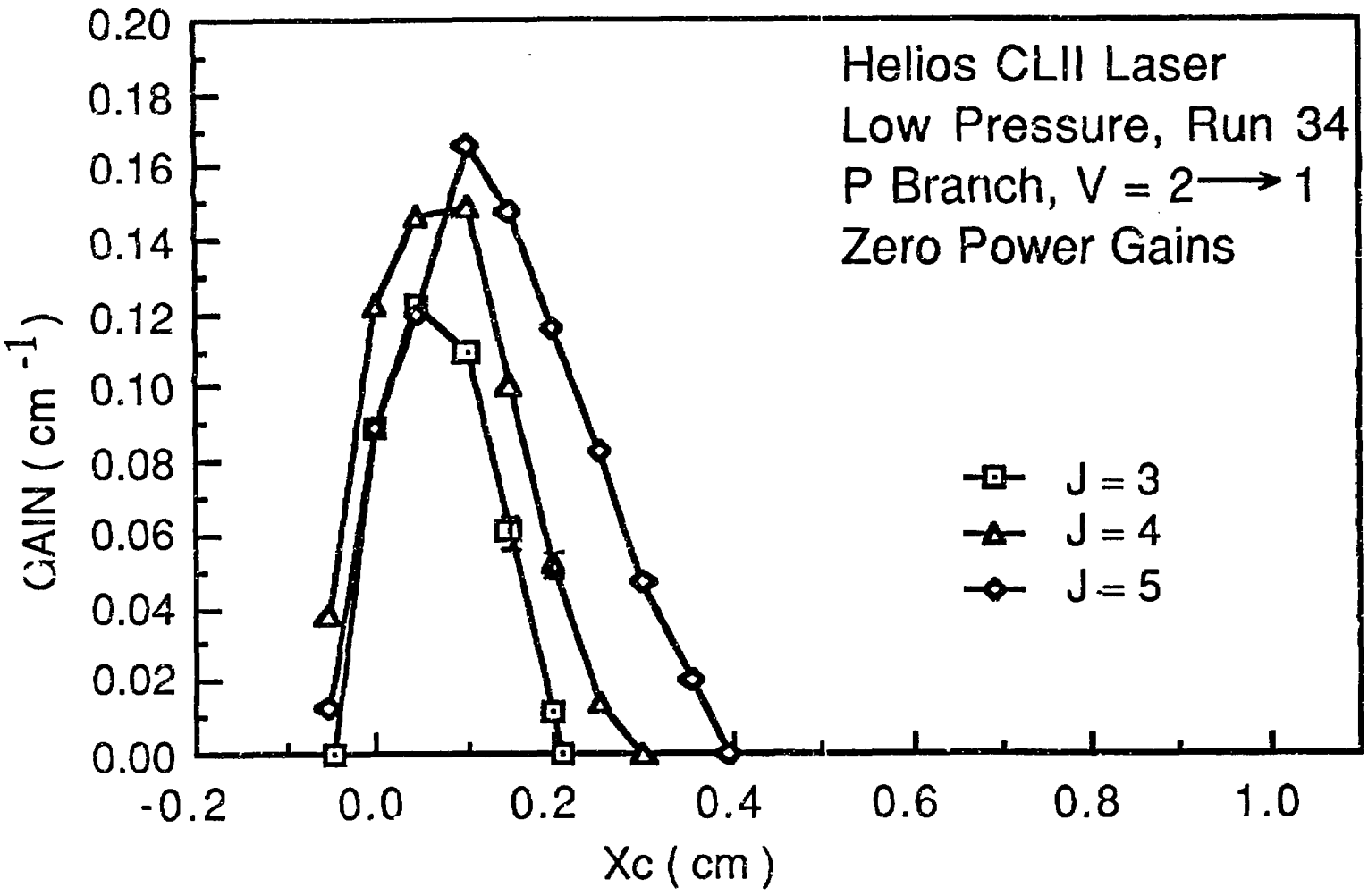

Figure 40. Variation of the zero power gain as a function of distance downstream of the H_2 injectors at y = 0.75 mm for several $P_2(J)$ lines. Error bars smaller than the symbols are not shown.

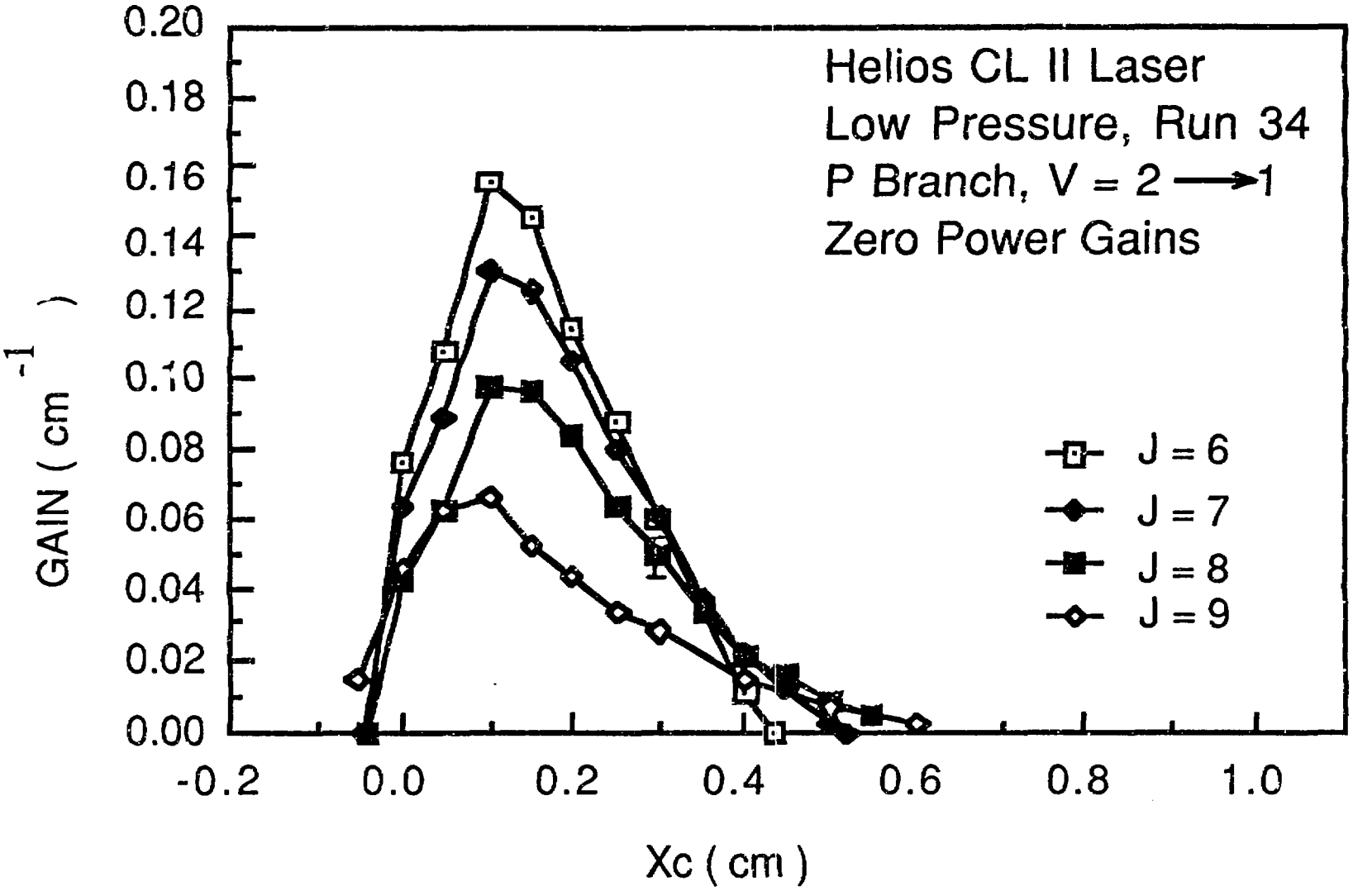

Figure 41. Variation of the zero power gain as a function of distance downstream of the H_2 injectors at y = 0.75 mm for several $P_2(J)$ lines. Error bars smaller than the symbols are not shown.

$P_1(8)$ and $P_2(3)$ to $P_2(9)$ for the Run 34 flow rates in the amplifier. Figures 42 - 45 present zero power gain versus x data for lines $P_1(5)$, $P_1(6)$, $P_1(7)$, $P_1(8)$, $P_2(5)$, $P_2(6)$, $P_2(7)$ and $P_2(8)$ for the Run 36 flow rates in the amplifier. Comparison of the above figures shows that the $P_2(J)$ peak zero power gains are about 1.55 times larger than the $P_1(J)$ peak zero power gains. The length of the gain zone of the $P_1(J)$ lines is about 1.3 times larger than that of the $P_2(J)$ lines. It can be seen from the figures that the zero power gains of all the $P_1(J)$ lines reach their peak 1.5 - 2.0 mm downstream of the H_2 injectors while the zero power gains of the $P_2(J)$ lines reach their peak 1.0 mm downstream of the H_2 injectors. In previous experiments[1] when the CL II was run as an oscillator with a stable resonator, peak power was obtained when the optical axis of the stable resonator was located 1.0 to 1.5 mm downstream of the H_2 injectors. This is consistent with the measured locations of the peaks of the zero power gain curves. The measured zero power gains are consistent with the results of similar measurements in combustion driven cw HF chemical lasers[8]. The lines with the highest zero power gains are $P_1(5)$ and $P_1(6)$ for the 1→0 vibrational band and $P_2(5)$ and $P_2(6)$ for the 2→1 vibrational band.

The variation of zero power gain with height in the flow channel was investigated by measuring the amplification ratio of $P_2(5)$ with the Run 34 flow rates in the amplifier at the flow channel cent line (y = 0.0) and at 0.75 mm below the centerline (y= -0.75). The zero power gain data corresponding to these measurements is presented as a function of x in Figs. 46 and 47 respectively. Comparison of Figs. 40, 45 and 47 shows that the zero power gain values obtained 0.75 mm and -0.75 mm from the center of the flow channel, Fig. 28, are almost identical and are higher than the values of the zero power gain measured on the flow channel centerline. Because H_2 is

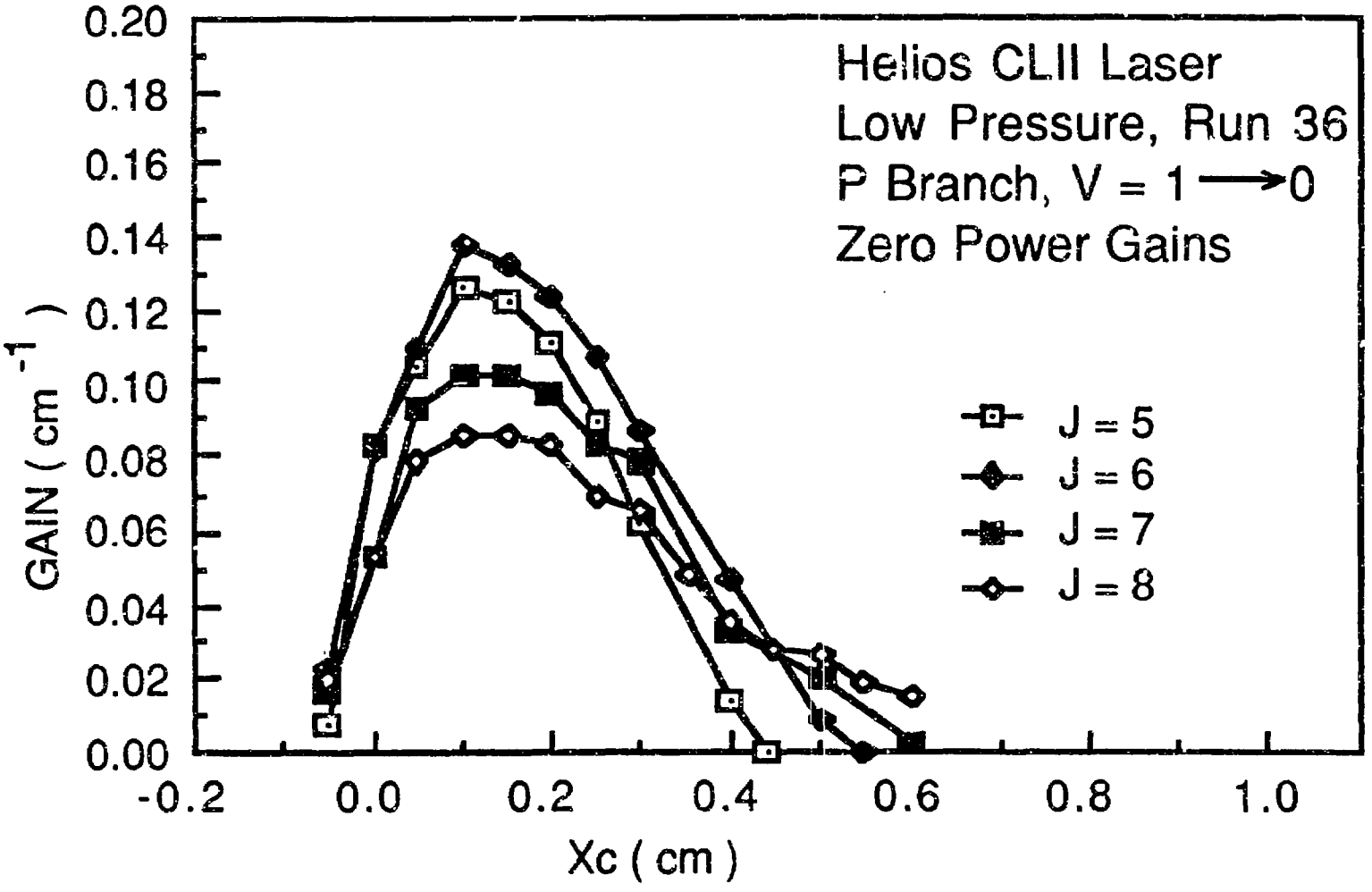

Figure 42. Variation of the zero power gain as a function of distance downstream of the H_2 injectors at y = 0.75 mm for several $P_1(J)$ lines. Error bars smaller than the symbols are not shown.

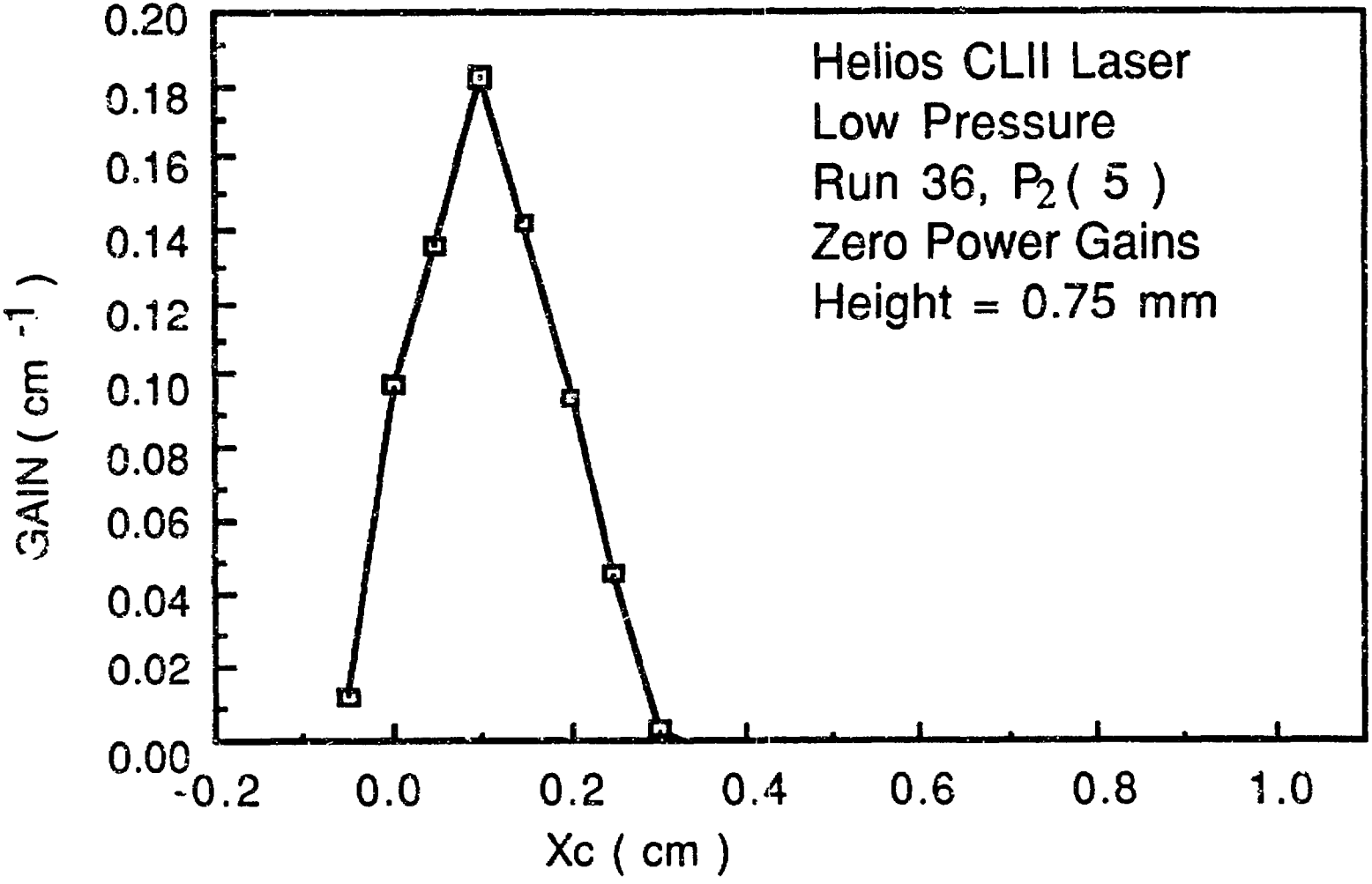

Figure 43. Variation of the zero power gain as a function of distance downstream of the H_2 injectors at y = 0.75 mm for the $P_2(5)$ line. Error bars smaller than the symbols are not shown.

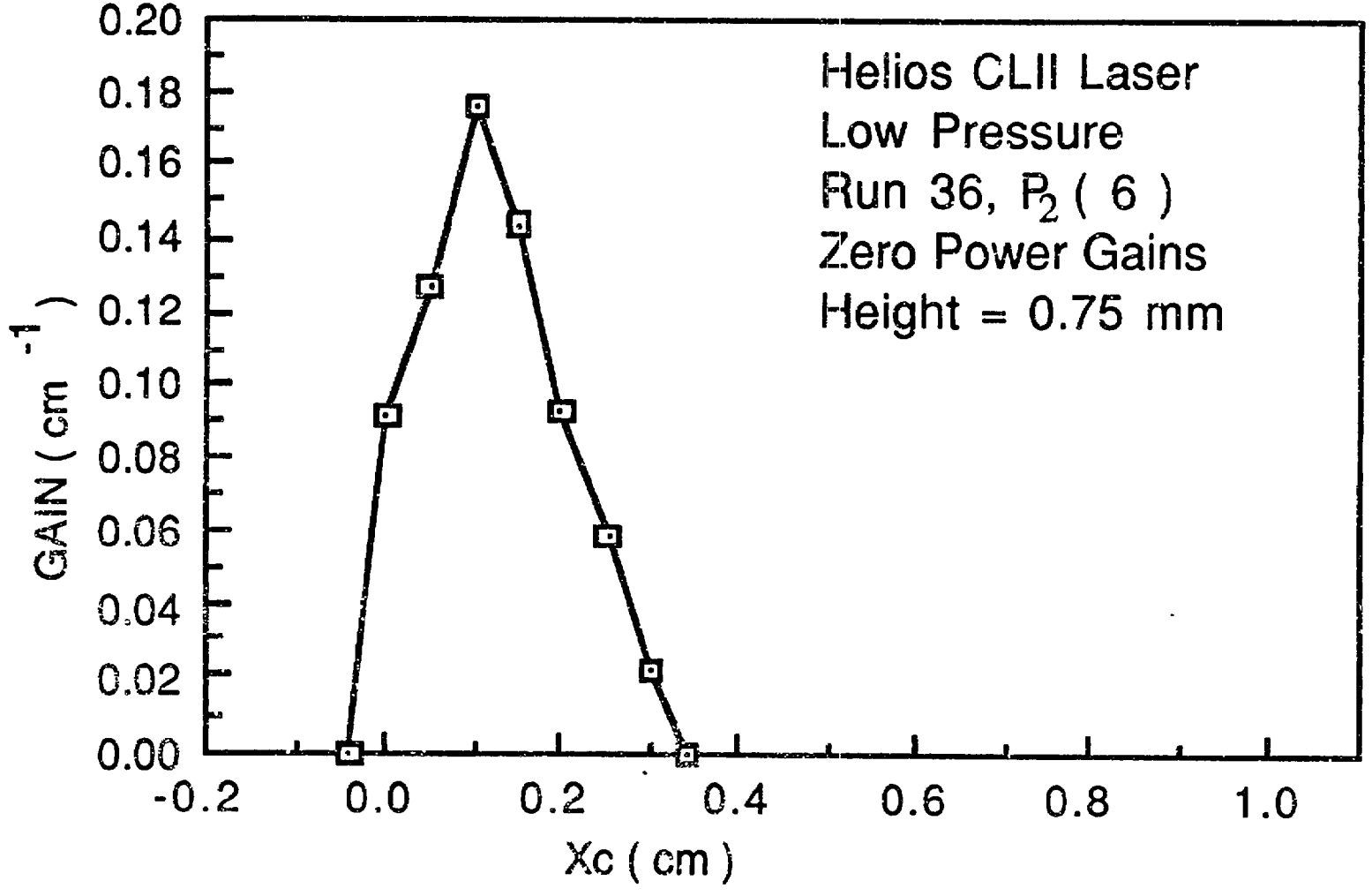

Figure 44. Variation of the zero power gain as a function of distance downstream of the H_2 injectors at y = 0.75 mm for the $P_2(6)$ line. Error bars smaller than the symbols are not shown.

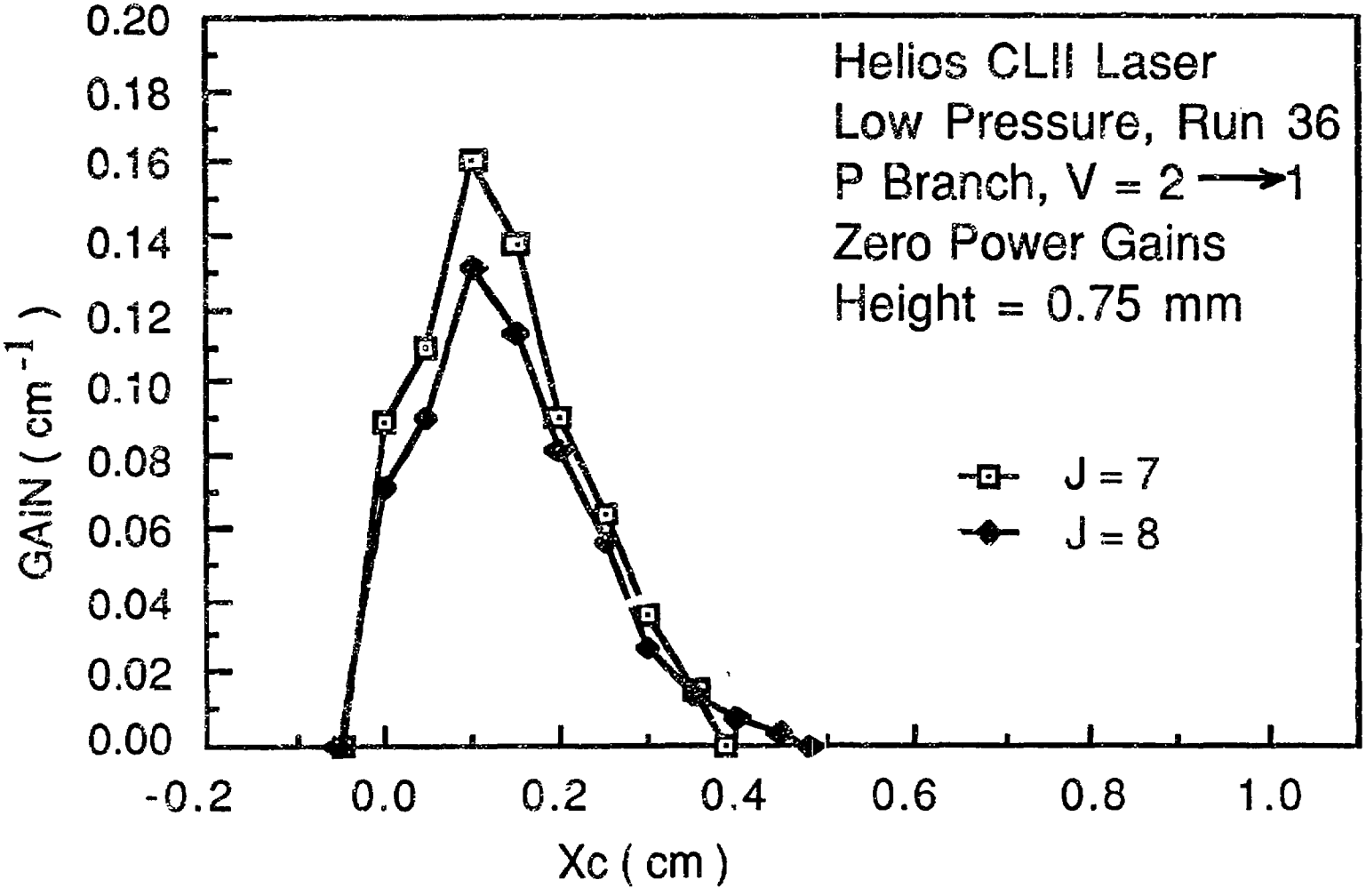

Figure 45. Variation of the zero power gain as a function of distance downstream of the H_2 injectors at y = 0.75 mm for lines $P_2(7)$ and $P_2(8)$. Error bars smaller than the symbols are not shown.

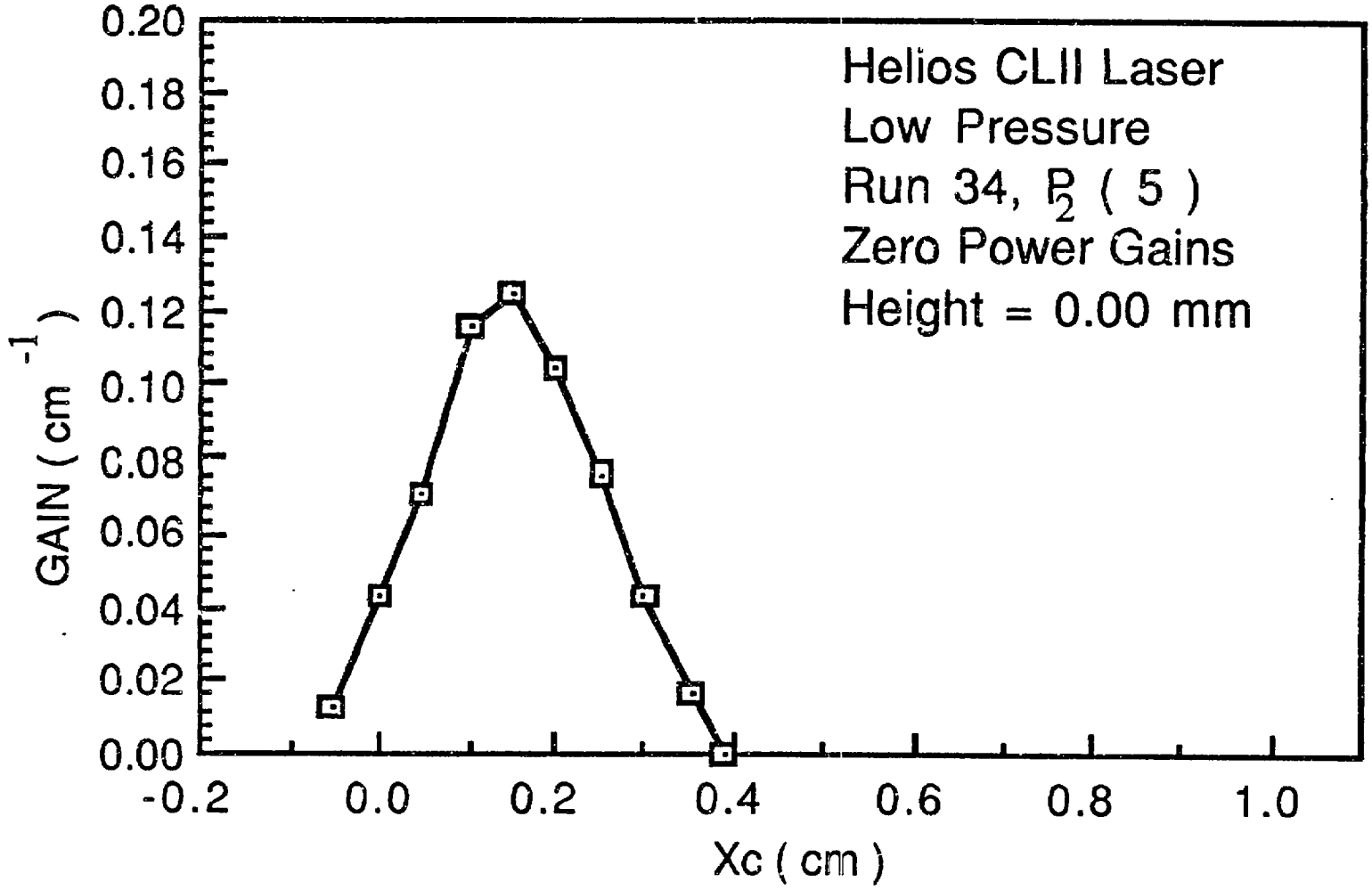

Figure 46. Variation of the zero power gain as a function of distance downstream of the H_2 injectors at y = 0.00 mm for the $P_2(5)$ line. Error bars smaller than the symbols are not shown.

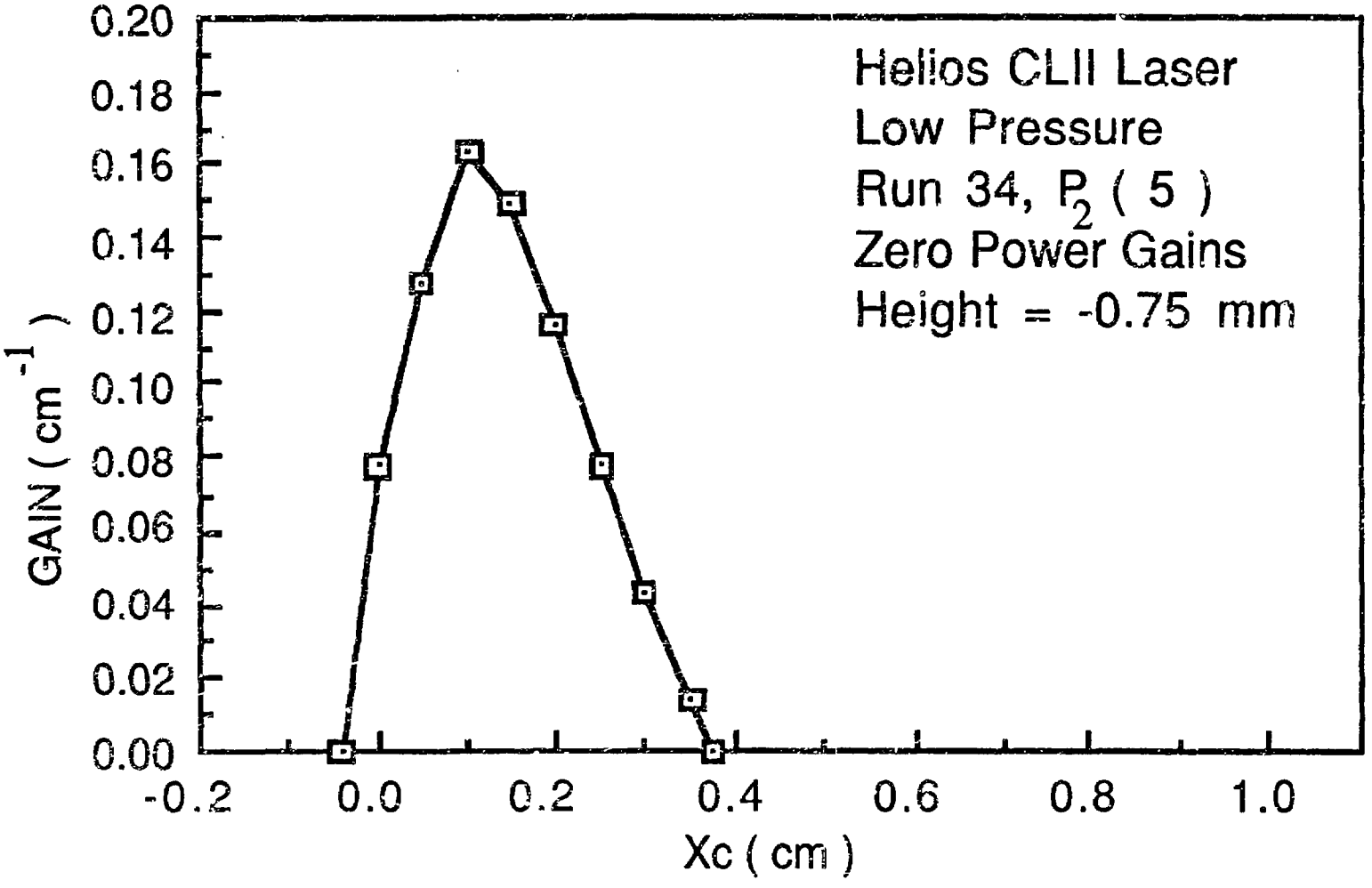

Figure 47. Variation of the zero power gain as a function of distance downstream of the H_2 injectors at y = - 0.75 mm for the $P_2(5)$ line. Error bars smaller than the symbols are not shown.

injected from the upper and lower flow channel walls, the mixing occurs so that the vertical flow field location for the highest zero power gain is 0.75 mm above or below the centerline of the 3.0 mm flow channel.

3.6 HIGH PRESSURE ZERO POWER GAIN MEASUREMENTS

The effect of high pressure on zero power gain was investigated for lines $P_1(6)$, $P_2(5)$ and $P_2(6)$. The amplifier was run at the Run 34 flow rates at a cavity pressure of 10.0 torr. The high pressure zero power gains of these three lines were measured as a function of the distance from the H_2 injectors, Figs. 48, 49 and 50, by using the same input powers that were used to measure the low pressure zero power gains of these lines. Comparison of Figs. 48, 49 and 50 to Figs. 39, 40 and 41 respectively, shows that high pressure results in zero power gain zones that are considerably shorter than those measured in the case of low pressure. The peak zero power gain of $P_1(6)$ was not affected by high pressure but the peak zero power gains of $P_2(5)$ and $P_2(6)$ were decreased by about 22.5%. This is a result of the fact that the increased deactivation of HF(2) repopulates HF(1) thereby keeping the population difference between HF(1) and HF(0) about the same whereas the population difference between HF(2) and HF(1) decreased. High pressure caused the location of the peak zero power gain to occur 0.5 mm closer to the H_2 injectors for all three lines.

3.7 EFFECT OF POLARIZATION ON ZERO POWER GAIN

The Brewster windows used in the previous zero power gain measurements polarized the beam vertically. The effect of polarization on zero power gain was investigated by taking zero power gain measurements with non-Brewster windows (which do not polarize the beam) on both the oscillator and the amplifier and with a Brewster window on the oscillator (set to polarize the

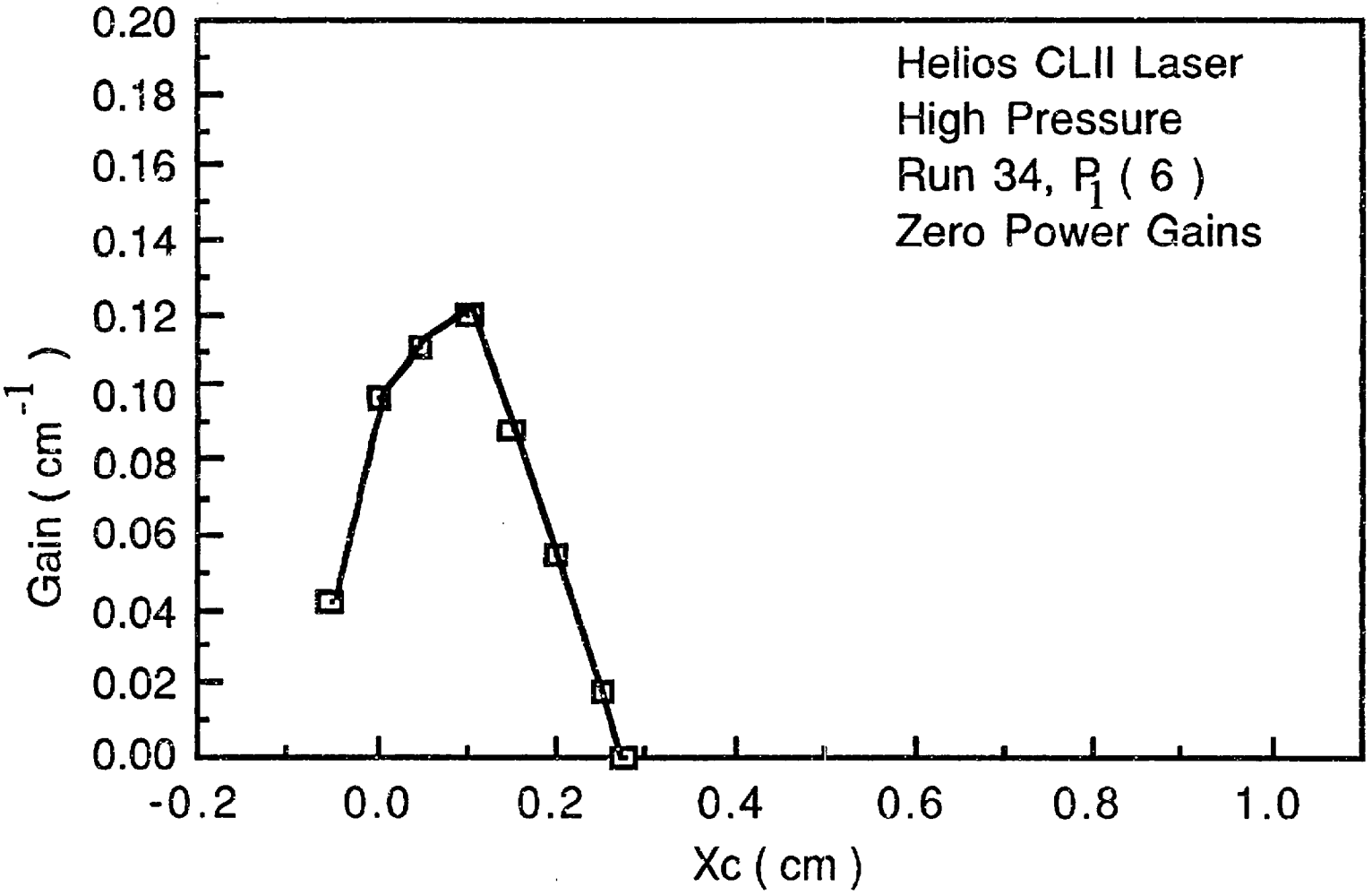

Figure 48. Variation of the zero power gain as a function of distance downstream of the H_2 injectors at y = 0.75 mm for the $P_1(6)$ line. Error bars smaller than the symbols are not shown.

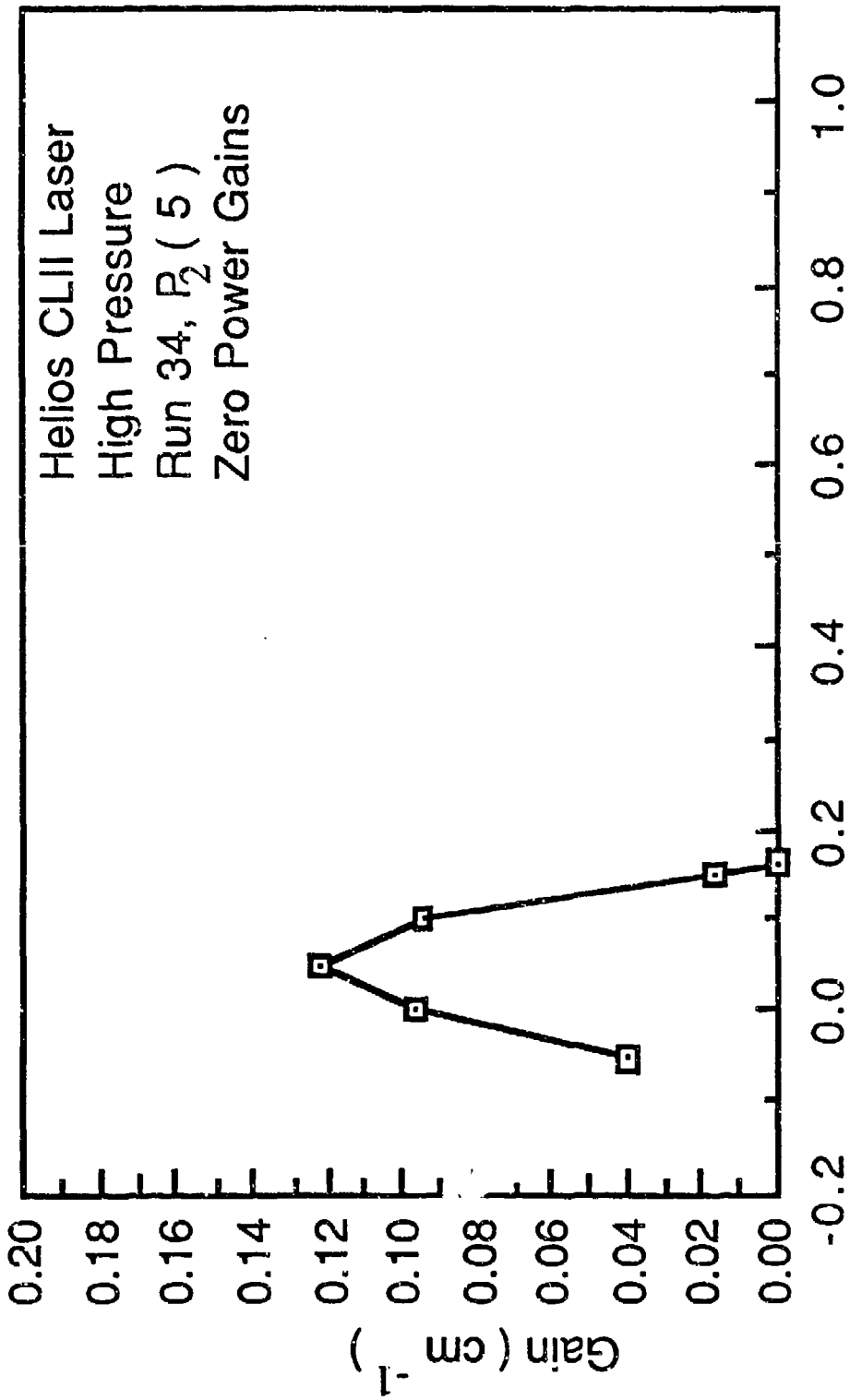

Figure 49. Variation of the zero power gain as a function of distance downstream of the H_2 injectors at y = 0.75 mm for the $P_2(5)$ line. Error bars smaller than the symbols are not shown.

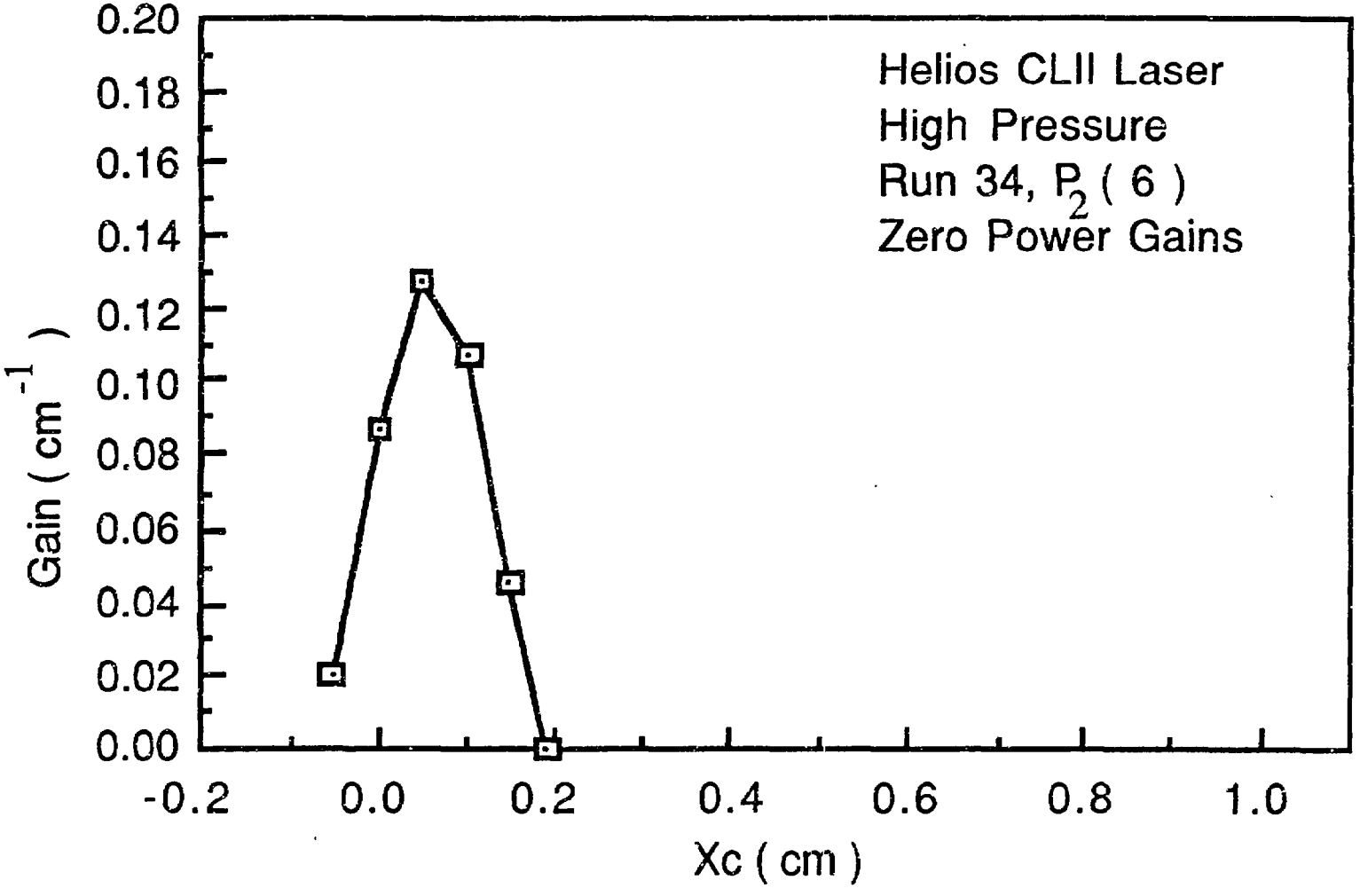

Figure 50. Variation of the zero power gain as a function of distance downstream of the H_2 injectors at y = 0.75 mm for the $P_2(6)$ line. Error bars smaller than the symbols are not shown.

beam horizontally) and non-Brewster windows on the amplifier.

When the non-Brewster windows were placed on the amplifier, an interesting phenomenon was observed. The non-Brewster windows acted as a Fabry-Perot resonator, causing the amplifier to lase. The amplifier output beam was passed through the ROFIN spectrum analyzer and it was found that the lasing lines were $P_2(4)$ and $P_2(5)$. Figure 51 presents a copy of the oscilloscope CRT, showing the whole spectrum of the ROFIN spectrum analyzer. The two strong peaks (they look like one peak but they are actually two peaks close to each other) on the right represent lines $P_2(4)$ and $P_2(5)$. The peaks of lines $P_2(4)$ and $P_2(5)$ can be separated by expanding the oscilloscope time scale ten times, Figs. 52 and 53. Figure 52 presents a copy of the oscilloscope CRT, showing the peaks corresponding to lines $P_2(4)$ and $P_2(5)$ and the spectrum analyzer cursor that was used in this case to identify $P_2(4)$. Figure 53 shows the peaks for lines $P_2(4)$ and $P_2(5)$, but this time the cursor was used to identify $P_2(5)$. The weak peak on the far left side of Fig. 51 is also shown in Fig. 54, aligned with the spectrum analyzer cursor. The cursor reading (which is approximately half the wavelength of the signal) is 45 nm. This signal is a spurious reflection or a higher order reflection of either $P_2(4)$ or $P_2(5)$. Since Figs. 51, 52, 53 and 54 are copies of the oscilloscope CRT, the horizontal scale that was originally on them was the time scale of the oscilloscope. This time scale was converted to a wavelength scale by using the known wavelengths and the location of the peaks of lines $P_2(4)$ and $P_2(5)$. The negative wavelength in Fig. 51 is due to the fact that the zero wavelength position on the signal was not aligned with the voltage axis shown in Figs. 51 to 54. The discrepancy in Fig. 54 between the actual wavelength of the signal and the cursor reading (the cursor reading should be equal to about one half of the actual wavelength) is due to the fact that the

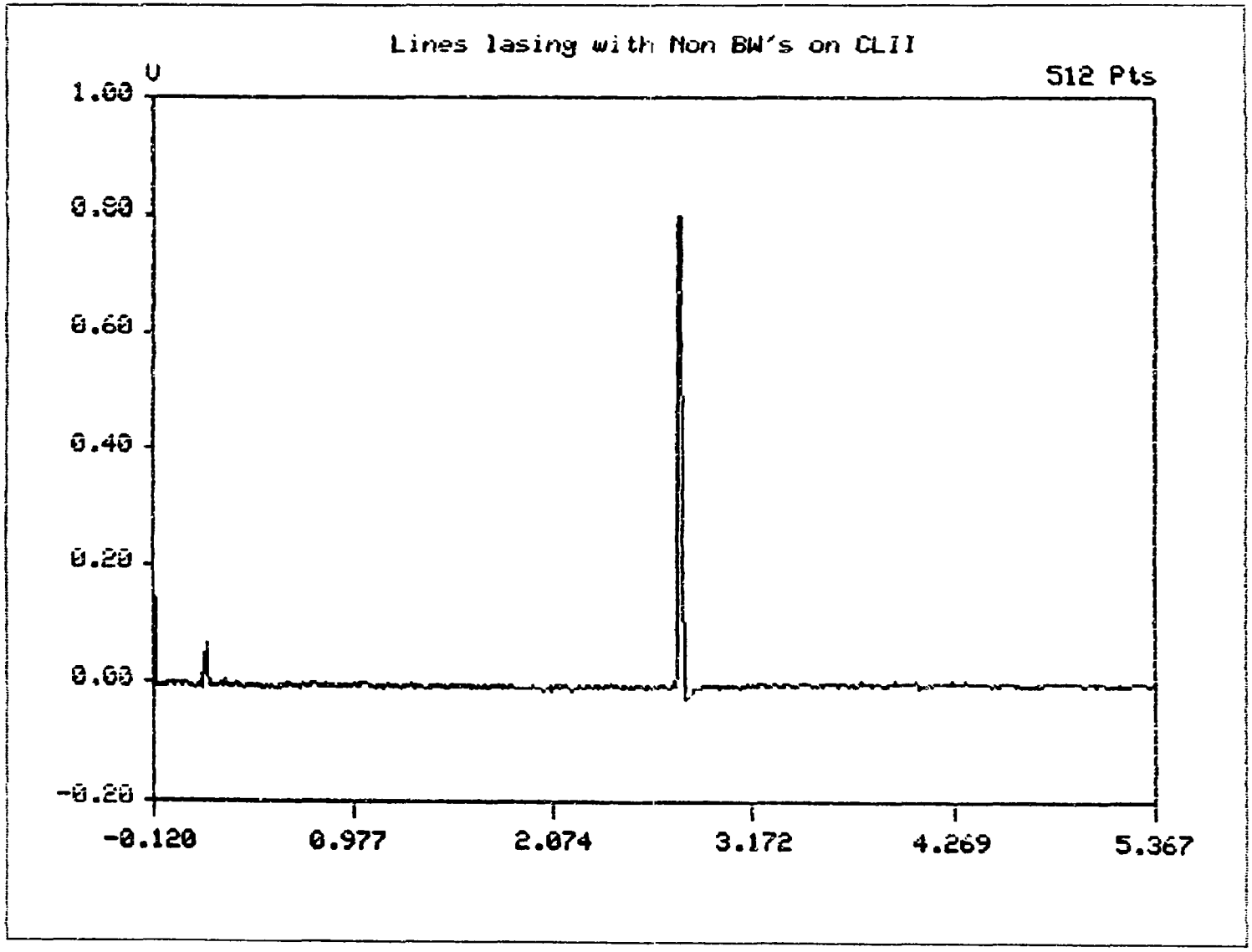

Figure 51. Oscilloscope CRT showing the whole spectrum of the ROFIN spectrum analyzer. The two peaks located at the center of the CRT represent lines $P_2(4)$ and $P_2(5)$.

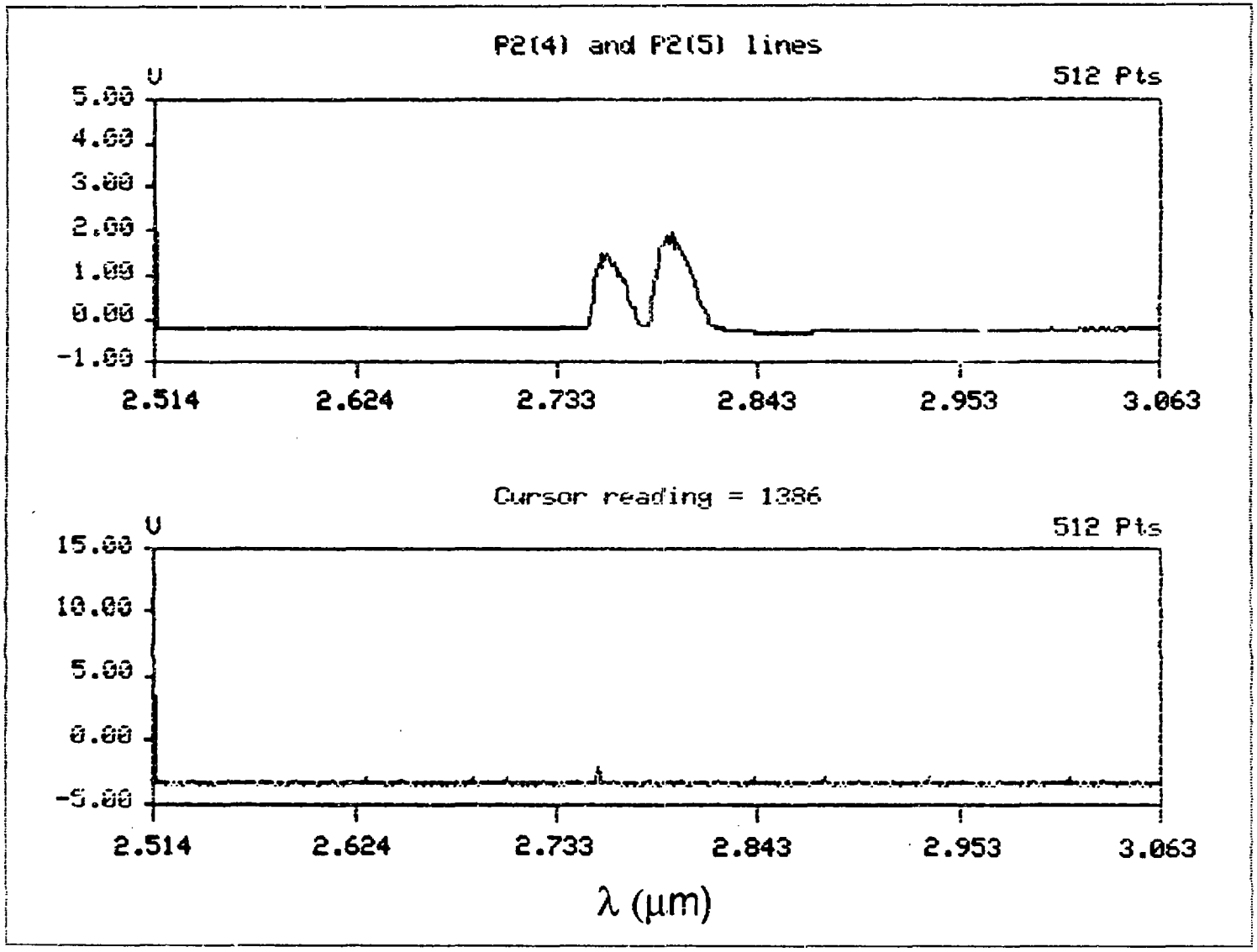

Figure 52. Oscilloscope CRT showing the two peaks corresponding to lines $P_2(4)$ and $P_2(5)$ and the spectrum analyzer cursor that was used to identify $P_2(4)$.

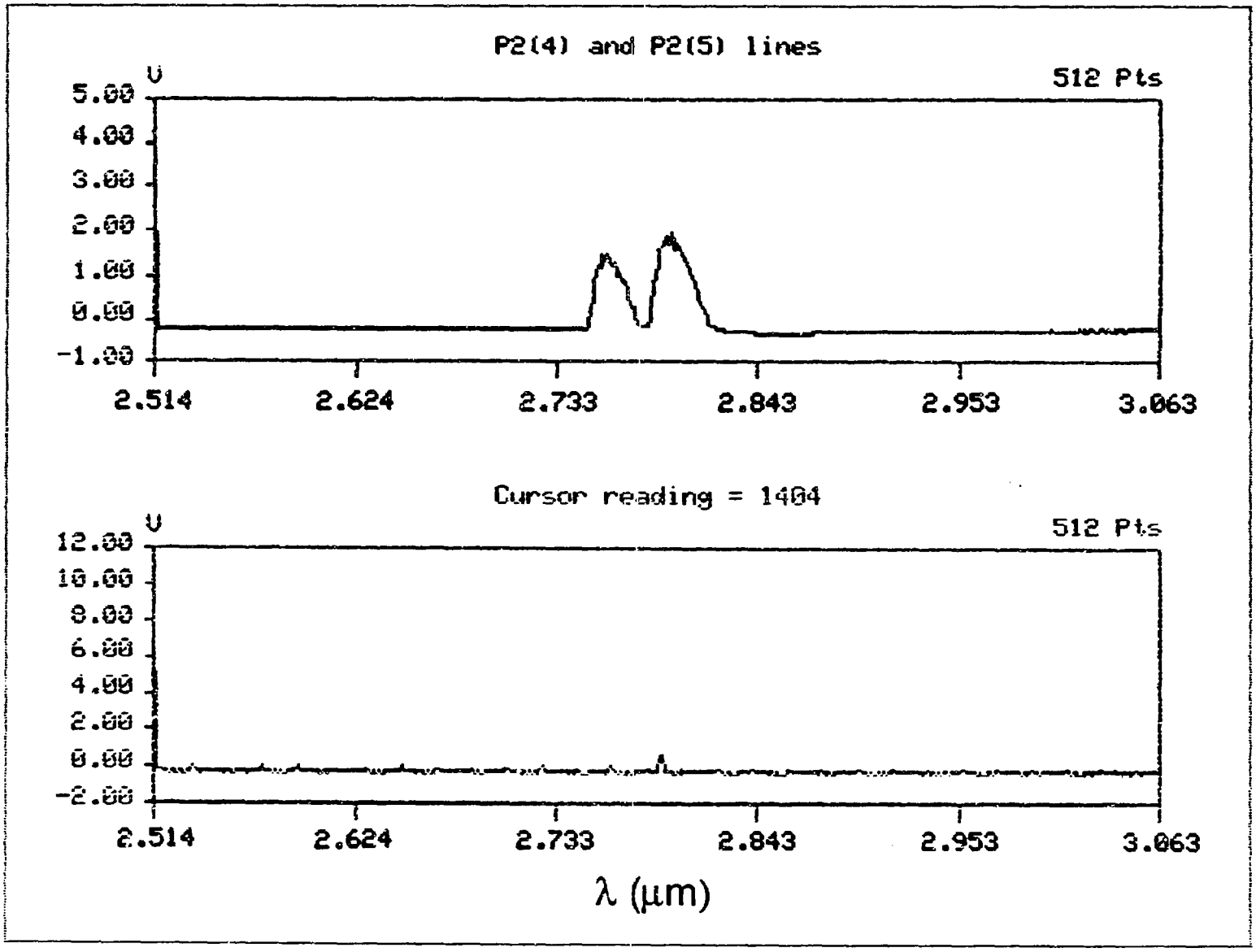

Figure 53. Oscilloscope CRT showing the two peaks corresponding to lines $P_2(4)$ and $P_2(5)$ and the spectrum analyzer cursor that was used to identify $P_2(5)$.

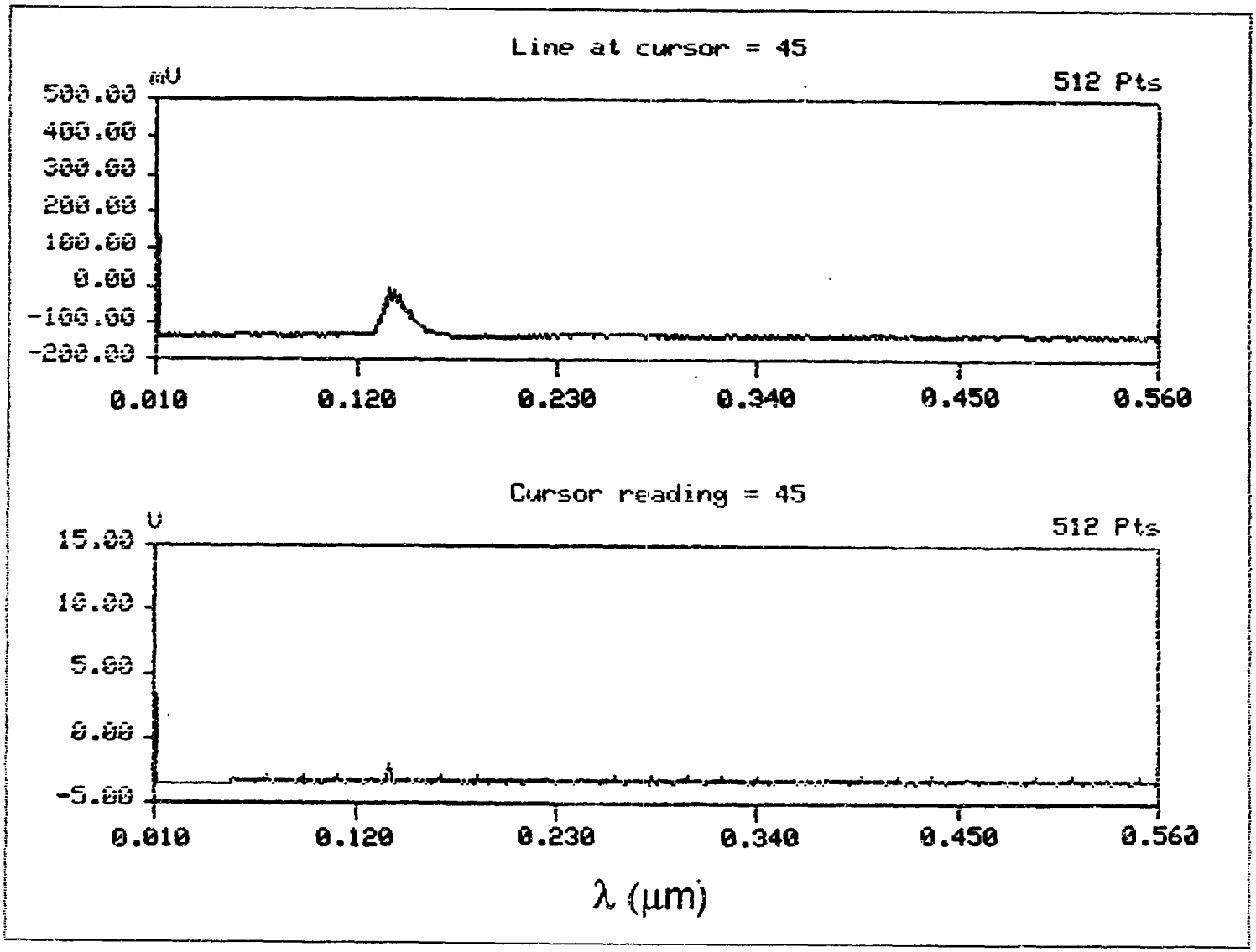

Figure 54. Oscilloscope CRT showing a peak corresponding to a spurious reflection or a higher order reflection of either $P_2(4)$ or $P_2(5)$ and the spectrum analyzer cursor that was used to estimate its wavelength.

instrument behaves non-linearly at the very high or very low wavelengths of its range. The fact that the lines $P_2(4)$ and $P_2(5)$ lased with the non-Brewster windows on the amplifier supports the zero power gain data because it suggests that $P_2(4)$ and $P_2(5)$ have the highest gains, which is in agreement with the experimental results that show $P_2(5)$ to have the highest zero power gain followed by lines $P_2(4)$ and $P_2(6)$, whose zero power gains are about equal.

The amplifier lasing was stopped by tilting the right non-Brewster window by about 0.5 degree, which misaligned the Fabry-Perot resonator. An unpolarized input beam was obtained by using non-Brewster windows on both the oscillator and the amplifier. Figures 55 and 56 present gain versus input power data; Figs. 57 and 58 present gain as a function of x for lines $P_1(5)$, $P_1(6)$, $P_2(5)$ and $P_2(6)$. These data were obtained with an unpolarized input beam with the low pressure Run 34 flow rates in the amplifier. Comparison of the gains obtained in this case with the zero power gains of the same lines obtained with a vertically polarized beam, Figs. 38, 39, 40 and 41 shows that the gains obtained with the unpolarized input beam were considerably lower.

The fact that the gains measured with the unpolarized beam are lower than the zero power gains measured with the vertically polarized beam suggests that either polarization affects zero power gain or that the right amplifier non-Brewster window (in the case of the unpolarized input beam) reflects into the cavity enough power to perturb the media. The effective reflectivity of the non-Brewster windows was calculated as follows.

$$\alpha_{sat} = - \frac{1}{2\,Le} \ln (r_0\, r_L) \qquad (3.7\text{-}1)$$

where α_{sat} is the saturated gain which has a value slightly lower than the

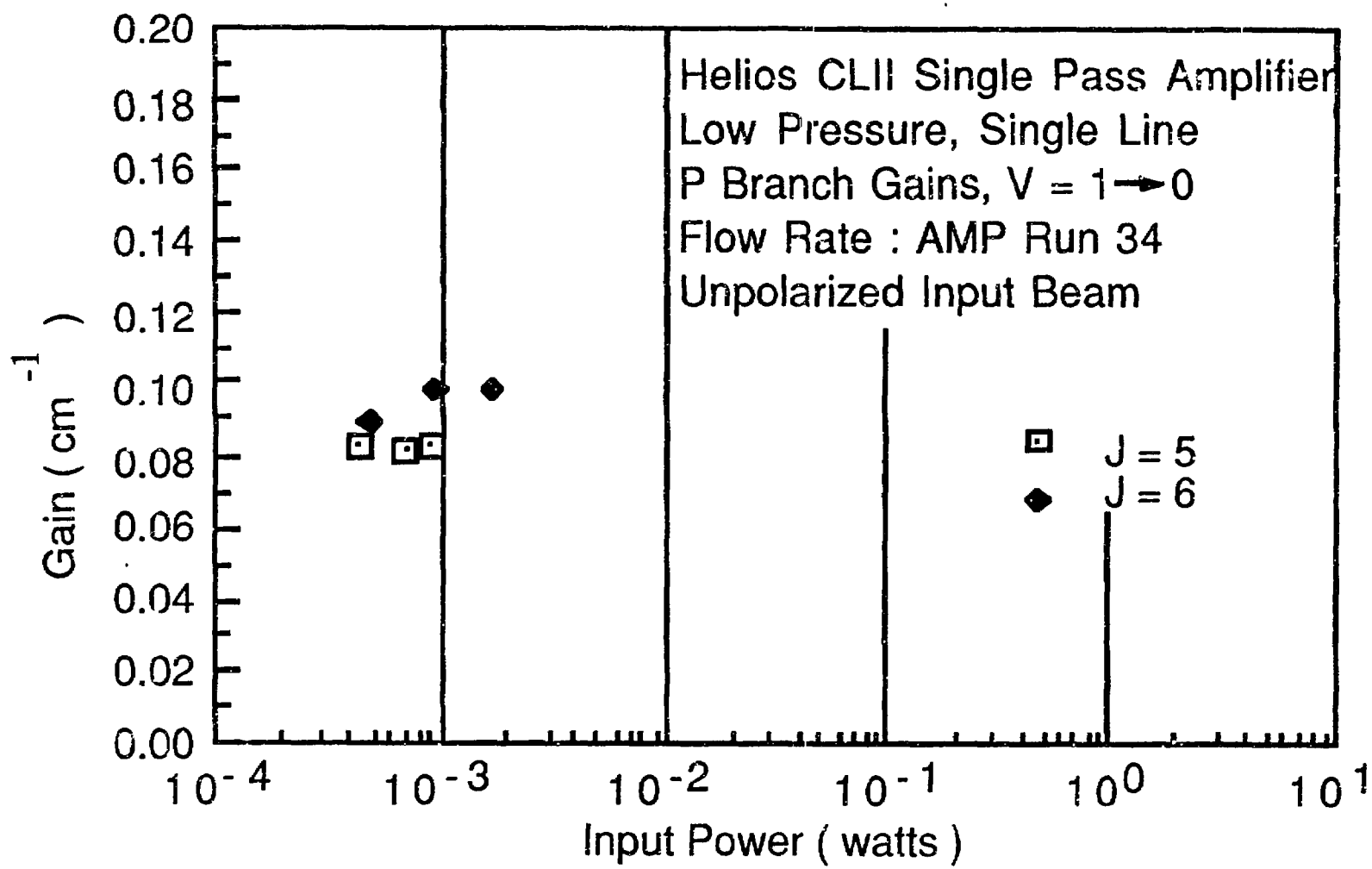

Figure 55. Variation of gain with input power for lines $P_1(5)$ and $P_1(6)$. The zero power gain region is reached when $P_{IN} < 0.002$ watts. Error bars smaller than the symbols are not shown.

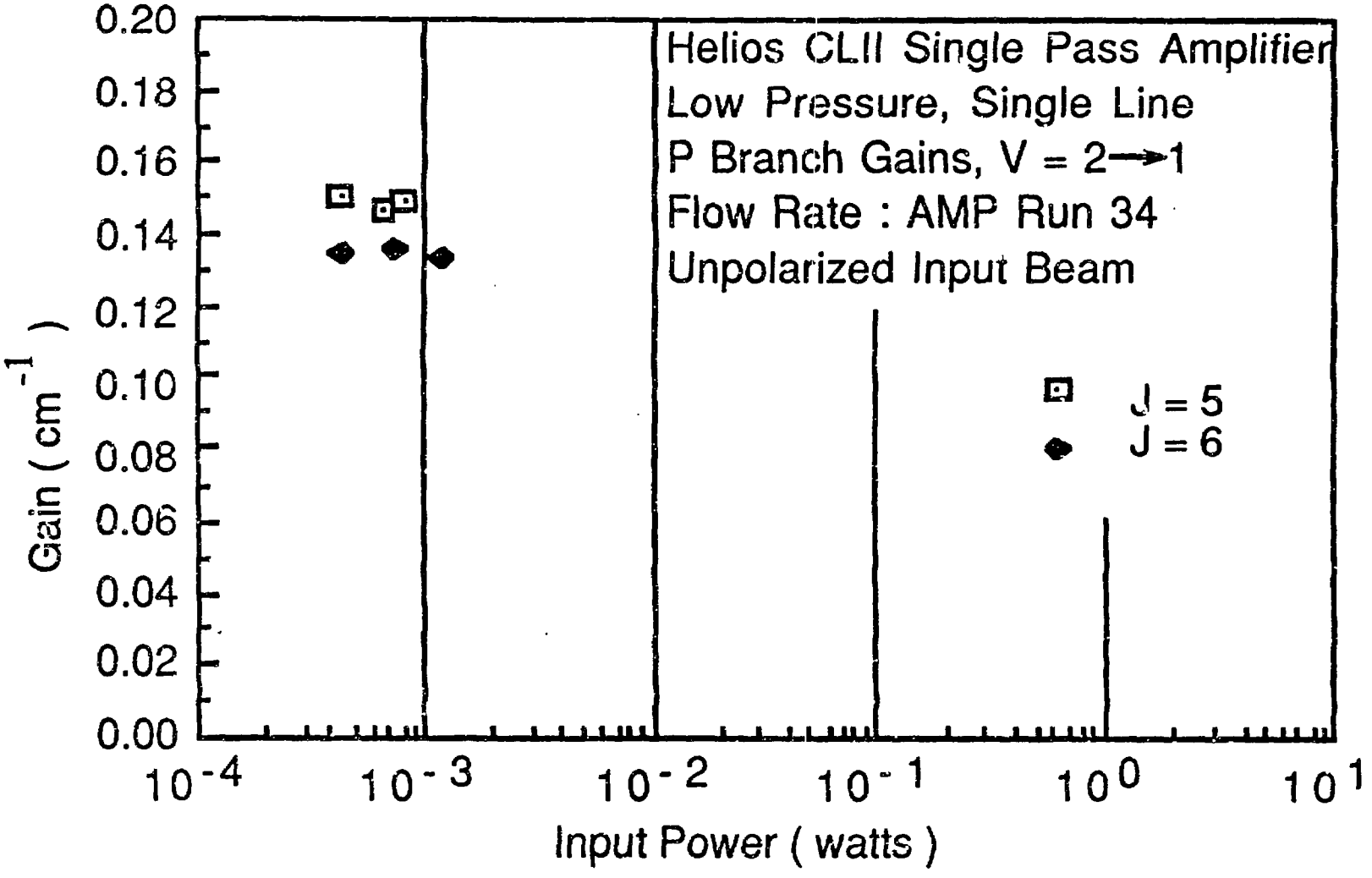

Figure 56. Variation of gain with input power for lines $P_2(5)$ and $P_2(6)$. The zero power gain region is reached when $P_{IN} < 0.001$ watts. Error bars smaller than the symbols are not shown.

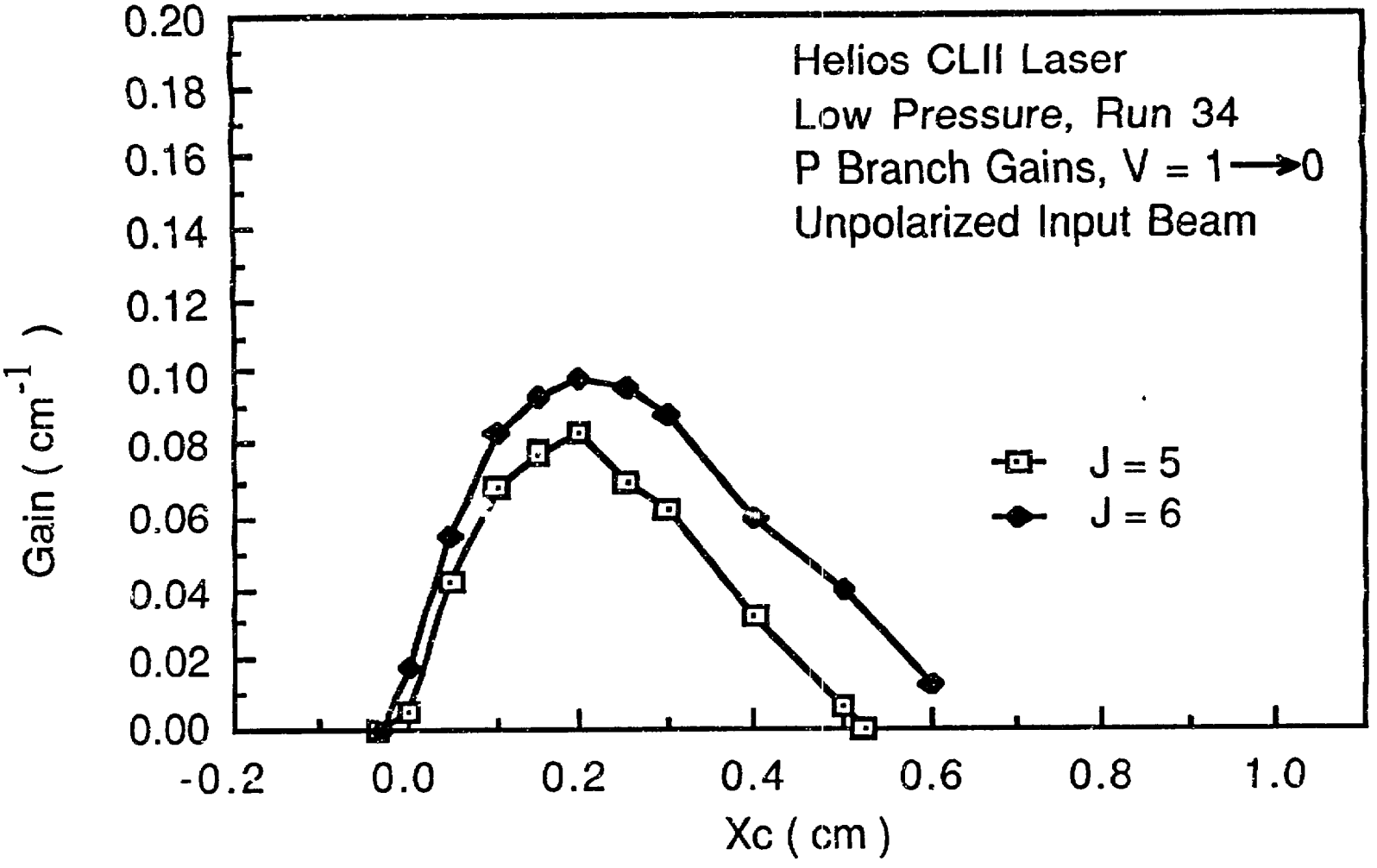

Figure 57. Variation of the gain as a function of distance downstream of the H_2 injectors at y = 0.75 mm for lines $P_1(5)$ and $P_1(6)$. The zero power gain was not reached because of the high input power. Error bars smaller than the symbols are not shown.

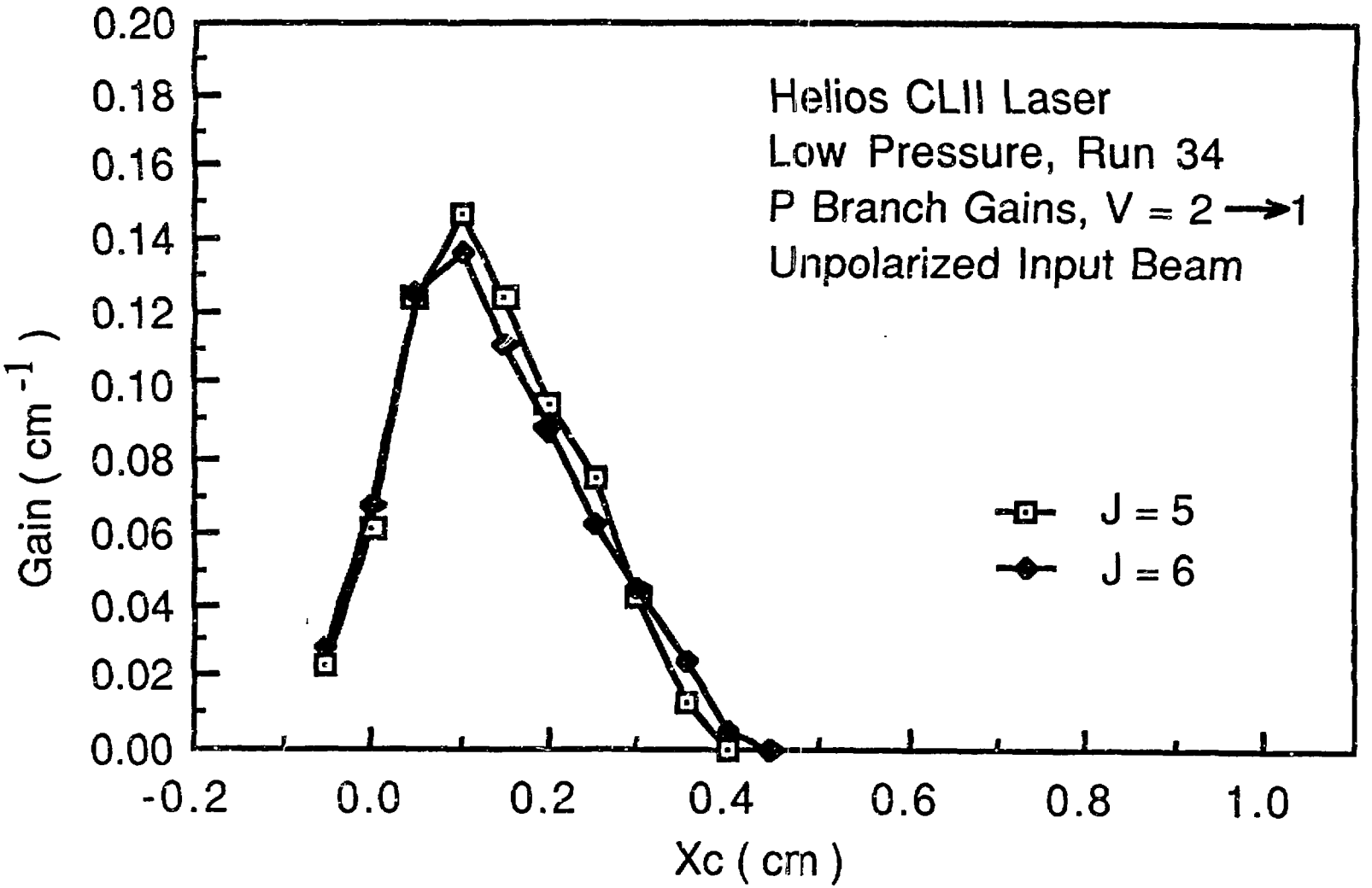

Figure 58. Variation of the gain as a function of distance downstream of the H_2 injectors at y = 0.75 mm for lines $P_2(5)$ and $P_2(6)$. The zero power gain was not reached because of the high input power. Error bars smaller than the symbols are not shown.

peak gain measured in the amplifier. In the case of the unpolarized beam, the peak $P_2(5)$ gain measured in the amplifier is ~.03%/cm, and therefore α_{sat} was assumed to have a value of 14.0%/cm. The effective reflectivities of the left and the right non-Brewster windows can be assumed to be equal, thus

$$r_0 = r_L = r_{eff} \tag{3.7-2}$$

so that

$$\alpha_{sat} = -\frac{1}{2Le} \ln r_{eff}^2 \tag{3.7-3}$$

Equation (3.7-3) can be solved for r_{eff} as

$$r_{eff} = e^{-Le\,\alpha_{sat}} \tag{3.7-4}$$

With Le equal to 24.4 cm and α_{sat} equal to 0.14 cm^{-1}, Eq. (3.7-4) gives an effective reflectivity of 3.3%. In an attempt to solve this problem, the right non-Brewster window on the amplifier was tilted by about 1.0 degree more so that its reflection would not go through the amplifier.

The zero power gain measurements were then repeated for line $P_2(5)$ with the low pressure Run 34 flow rates in the amplifier, Figs. 59 and 60. Comparison of Figs. 60 and Fig. 40 shows that the gain measured in this case is equal to the zero power gain measured with the Brewster windows on the amplifier. This indicates that polarization does not affect the zero power gain.

To insure that zero power gain is independent of polarization, the right non-Brewster window on the oscillator was replaced by a Brewster window oriented so that it would polarize the beam horizontally. Zero power gain measurements were made for lines $P_1(5)$ and $P_2(5)$. Figures 61 and 62 present gain versus input power and Figs. 63 and 64 present zero power gain as a

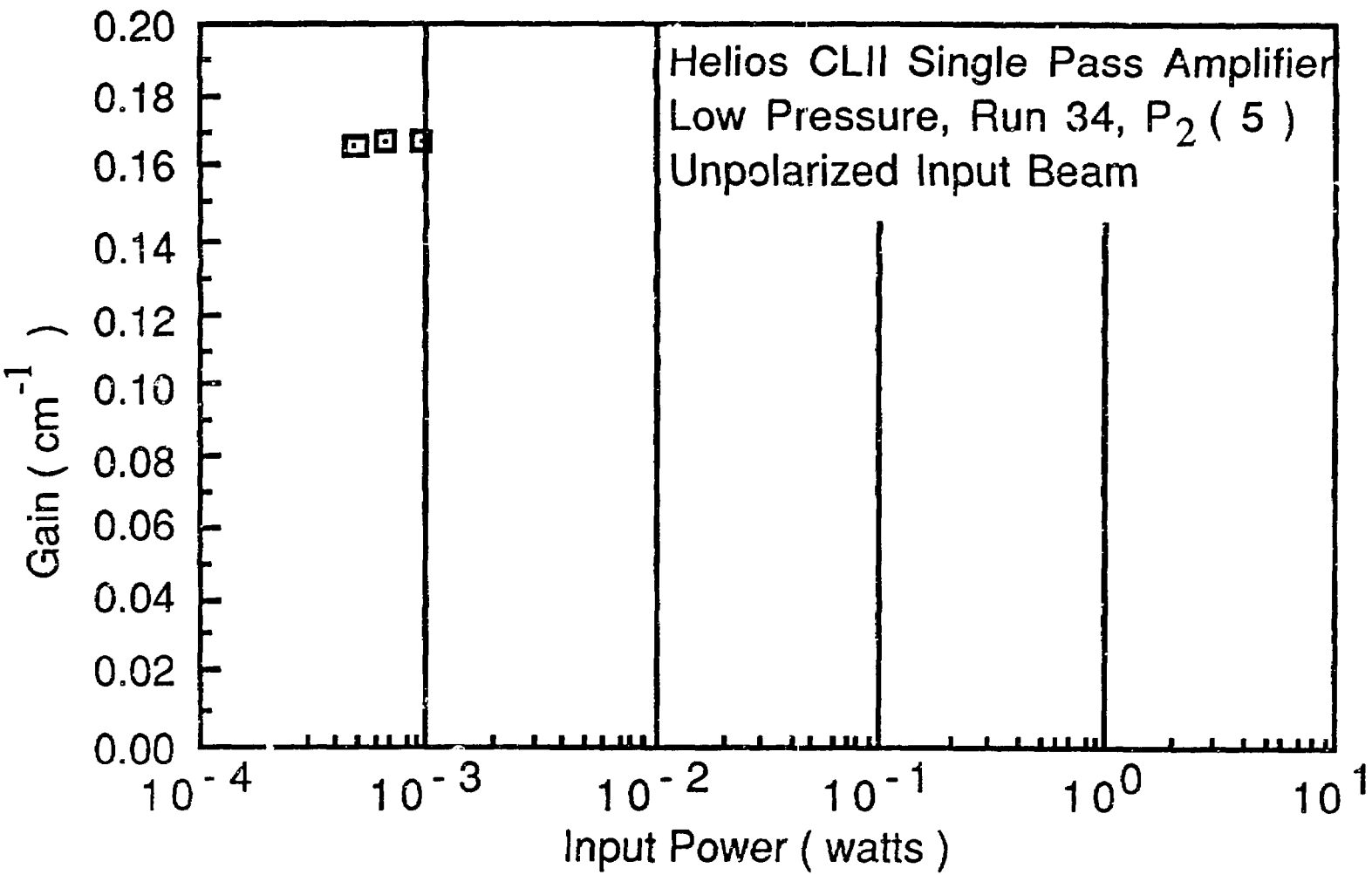

Figure 59. Variation of gain with input power for the $P_2(5)$ line with the right amplifier non-Brewster window tilted 1.5 degrees. Error bars smaller than the symbols are not shown.

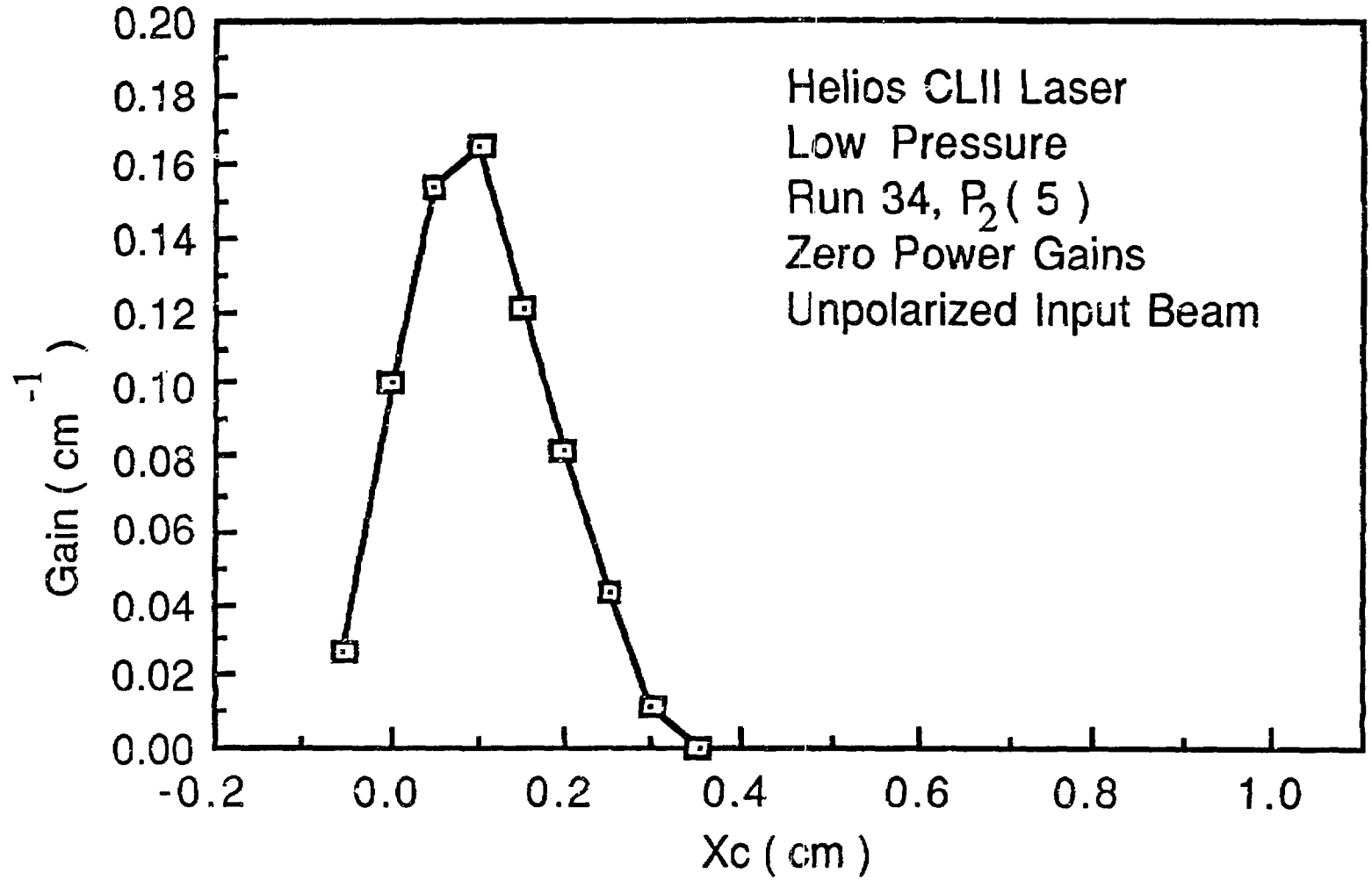

Figure 60. Variation of the zero power gain as a function of distance downstream of the H_2 injectors at y = 0.75 mm for the $P_2(5)$ line with the right amplifier non-Brewster window tilted 1.5 degrees. Error bars smaller than the symbols are not shown.

function of x. As can be seen from Figs. 61 and 62, the input powers required for these measurements are considerably lower than the input powers used in zero power gain measurements with Brewster windows on both the oscillator and the amplifier, Figs. 29 and 30. This is because the power reflected by the non-Brewster window back into the cavity is higher when the beam is horizontally polarized than when the beam is unpolarized. Zero power gain measurements are possible only when the average intensity, I_{AV}, is low enough that it does not perturb the media. Since I_{OUT} can be expressed as

$$I_{OUT} = I_{IN} \cdot AR \tag{3.7-5}$$

I_{AV} can be written as

$$I_{AV} = \frac{1}{2}\left(I_{IN} + I_{IN} \cdot AR\right) + \frac{1}{2}\left(r_{eff} \cdot I_{IN} \cdot AR + r_{eff} \cdot I_{IN} \cdot AR^2\right) \tag{3.7-6}$$

Since I_{AV} is proportional to input intensity, I_{IN}, low input powers were required in order to reach zero power gain levels. If the zero power gain data of Figs. 63 and 64 (horizontal polarization) is compared to zero power gain data obtained with Brewster windows on both the oscillator and the amplifier (vertical polarization), Figs. 38 and 40, it can be seen that polarization does not affect the zero power gain.

3.8 COMPARISON OF BLAZE II ZERO POWER GAIN CALCULATIONS WITH ZERO POWER GAIN DATA

In a study of unstable resonator modeling of the CL II laser[2], the effect of the % SF_6 dissociation and the secondary mixing length on zero power gain was investigated. The best agreement between the data and the zero power gains calculated in Ref. 2 was obtained for 3.2% SF_6 dissociation and 2.5 cm secondary mixing length, Figs. 65 and 66. Comparison of the calculated (Figs. 65 and 66) and measured (Figs. 35-41) peaks of the zero power gains showed

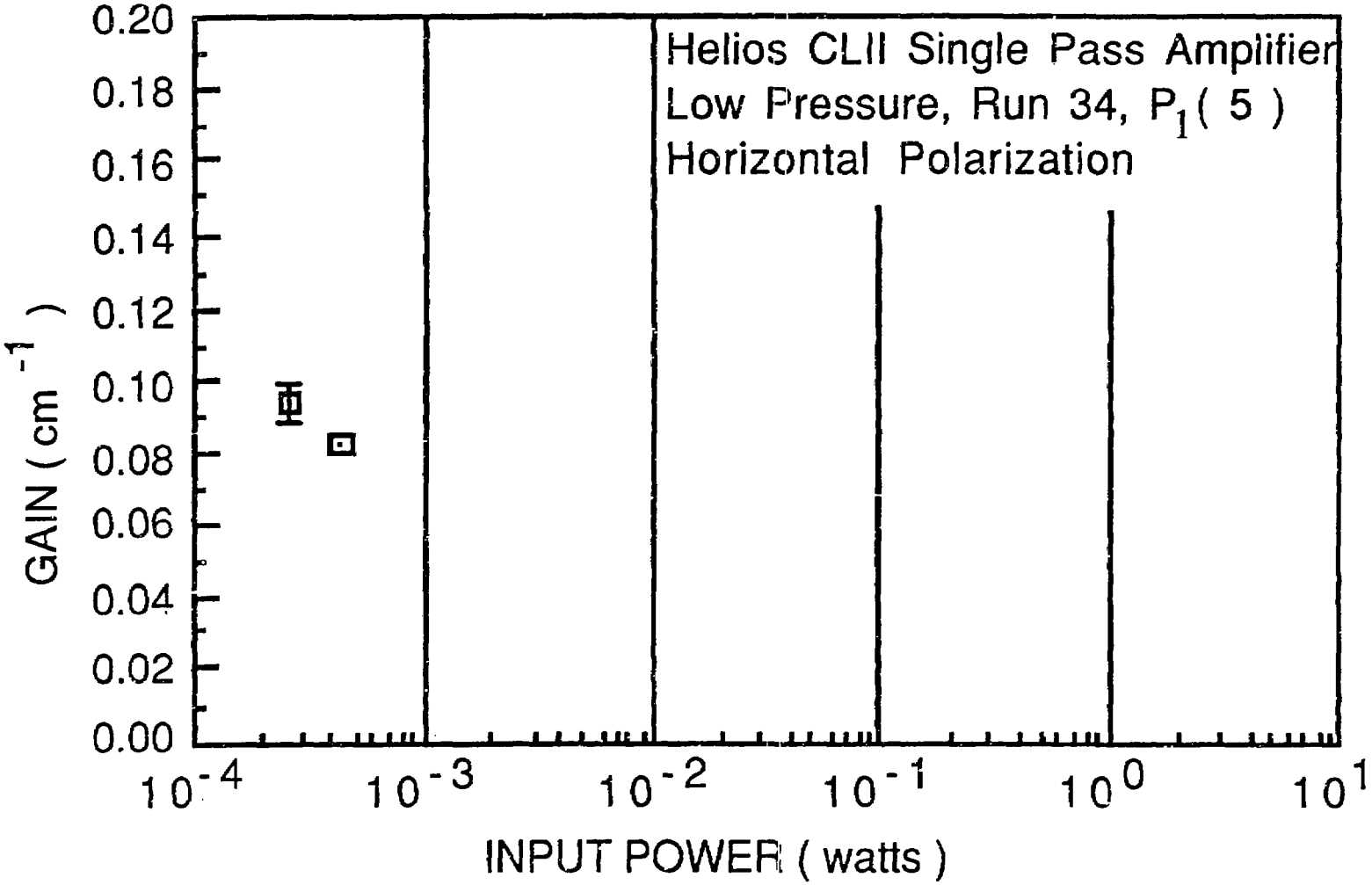

Figure 61. Variation of gain with input power for the $P_1(5)$ line. Error bars smaller than the symbols are not shown.

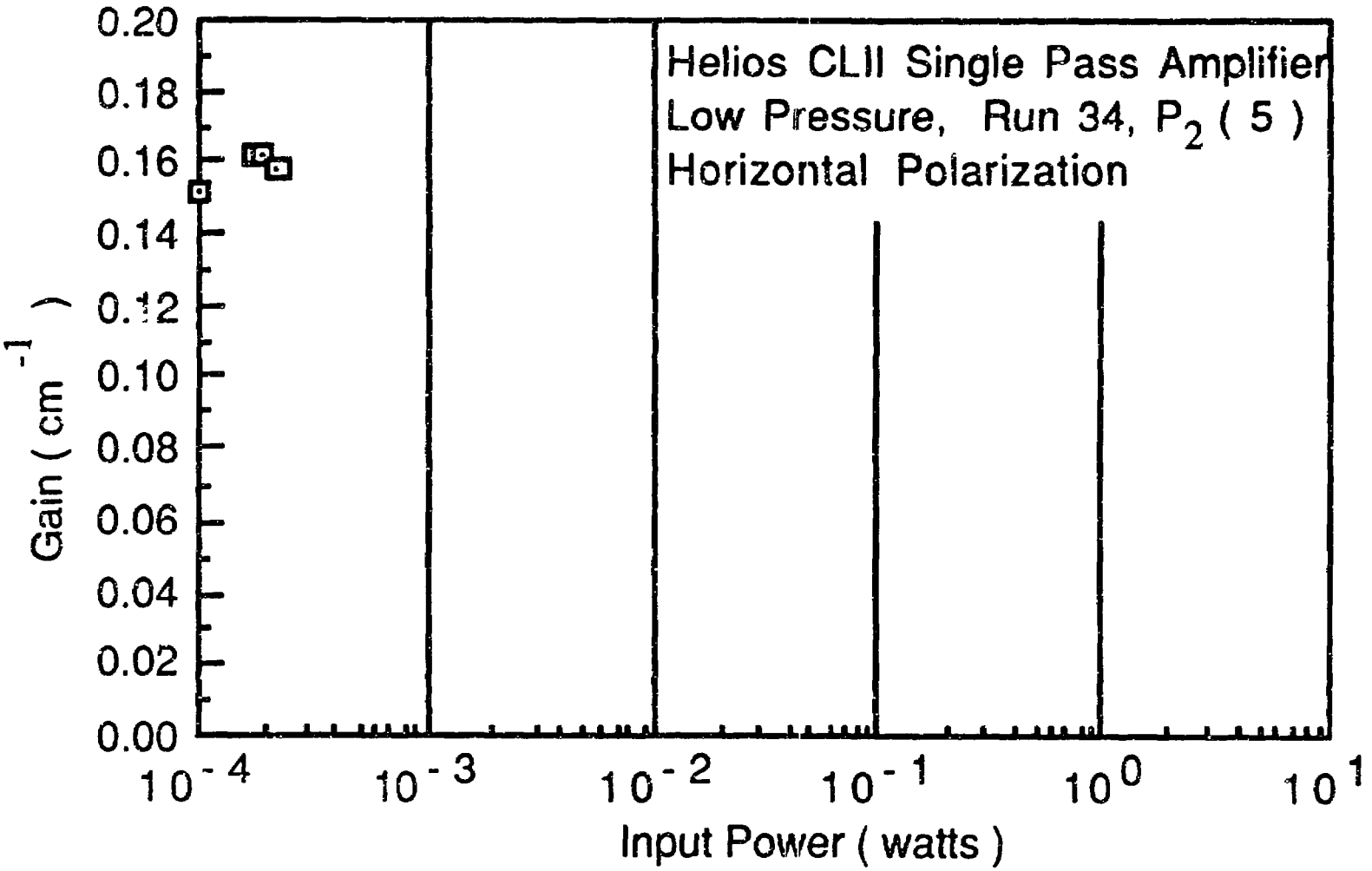

Figure 62. Variation of gain with input power for the $P_2(5)$ line. Error bars smaller than the symbols are not shown.

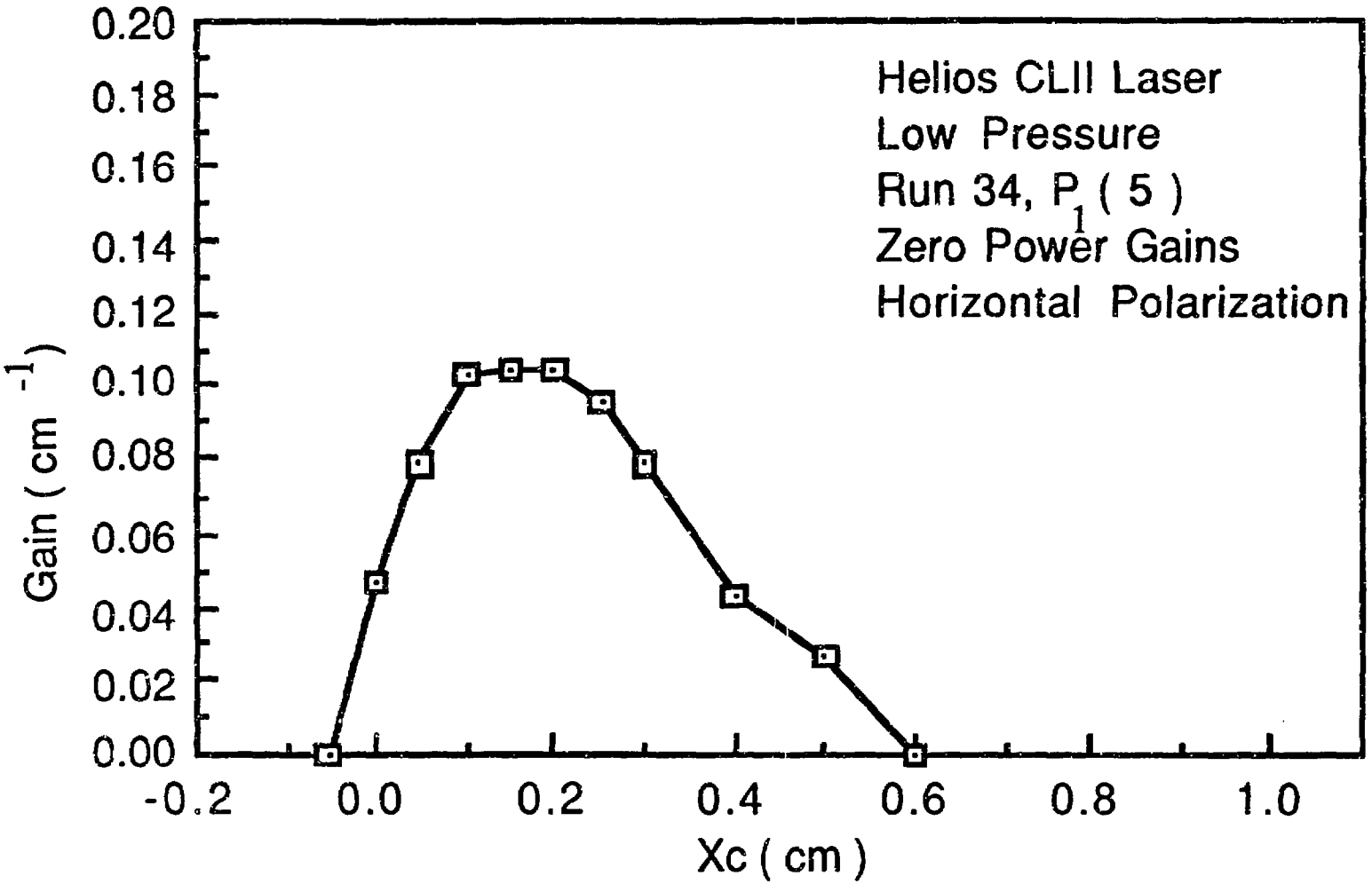

Figure 63. Variation of the zero power gain as a function of distance downstream of the H_2 injectors at y = 0.75 mm for the $P_1(5)$ line. Error bars smaller than the symbols are not shown.

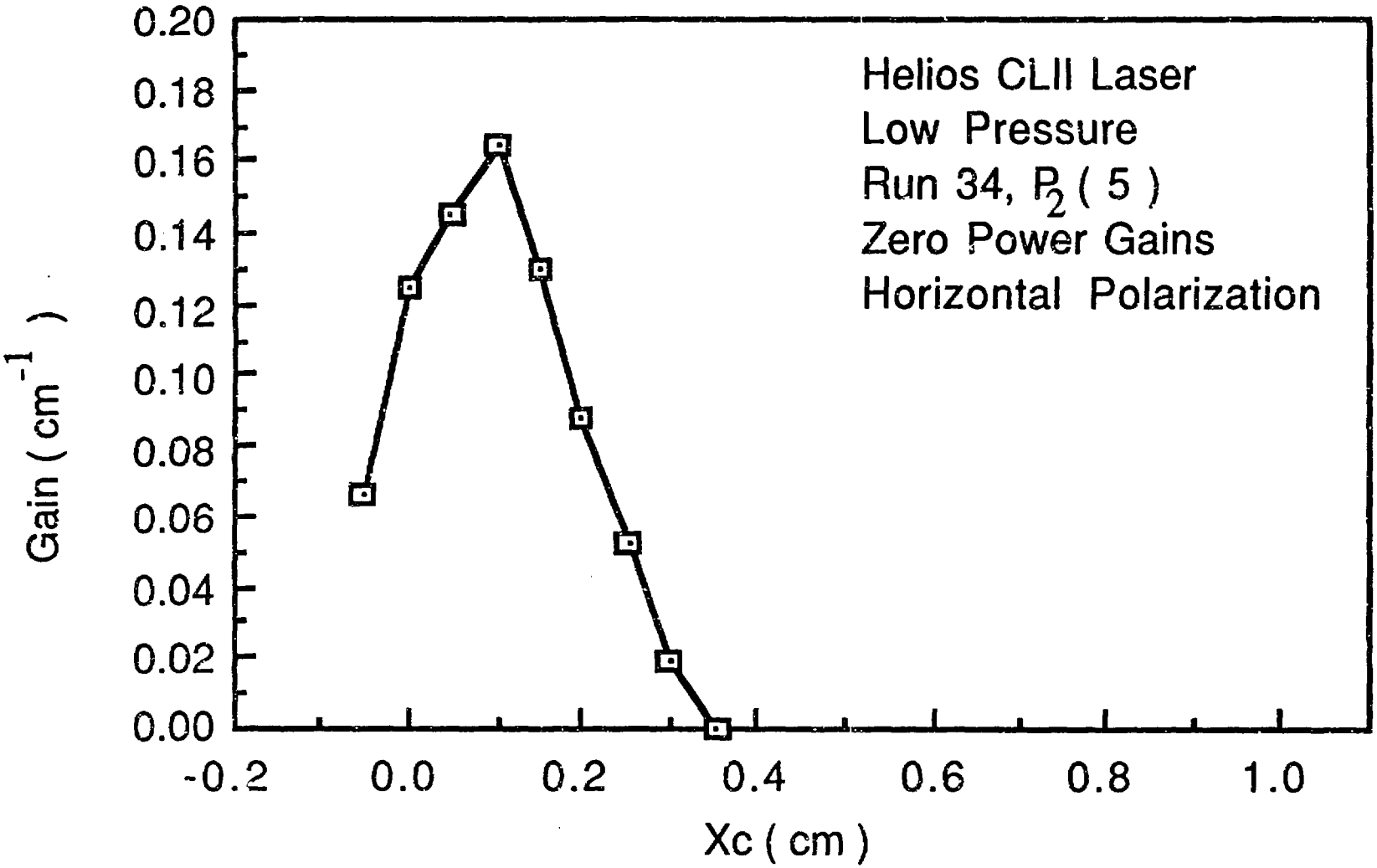

Figure 64. Variation of the zero power gain as a function of distance downstream of the H_2 injectors at y = 0.75 mm for the $P_2(5)$ line. Error bars smaller than the symbols are not shown.

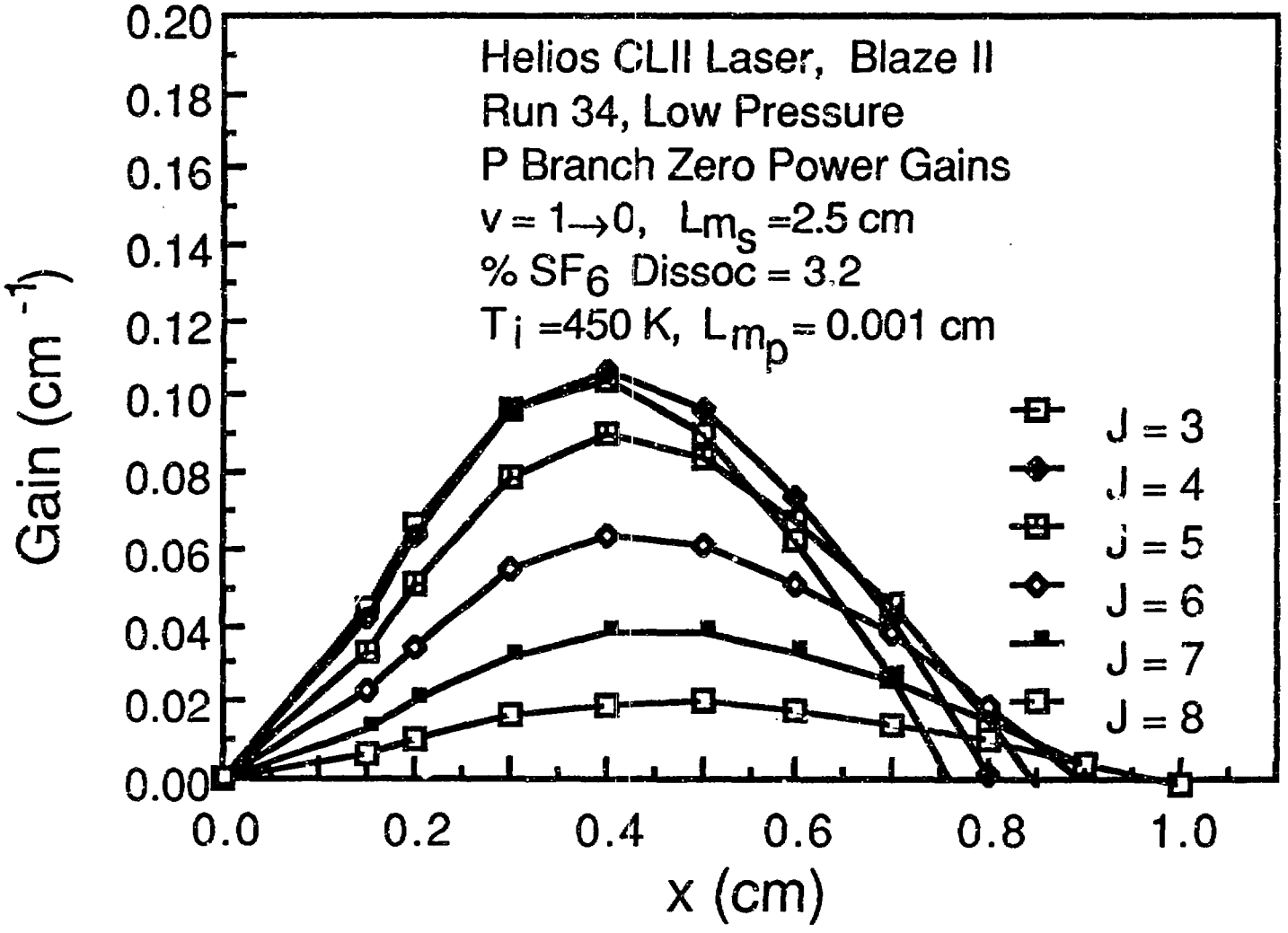

Figure 65. Variation of the zero power gain as a function of distance downstream of the H_2 injectors from the Blaze II model of the CL II laser[2]. L_{mp} is the mixing length of the primary stream, L_{ms} is the mixing length of the secondary stream, T_i is the static temperature of the flow at the H_2 injectors.

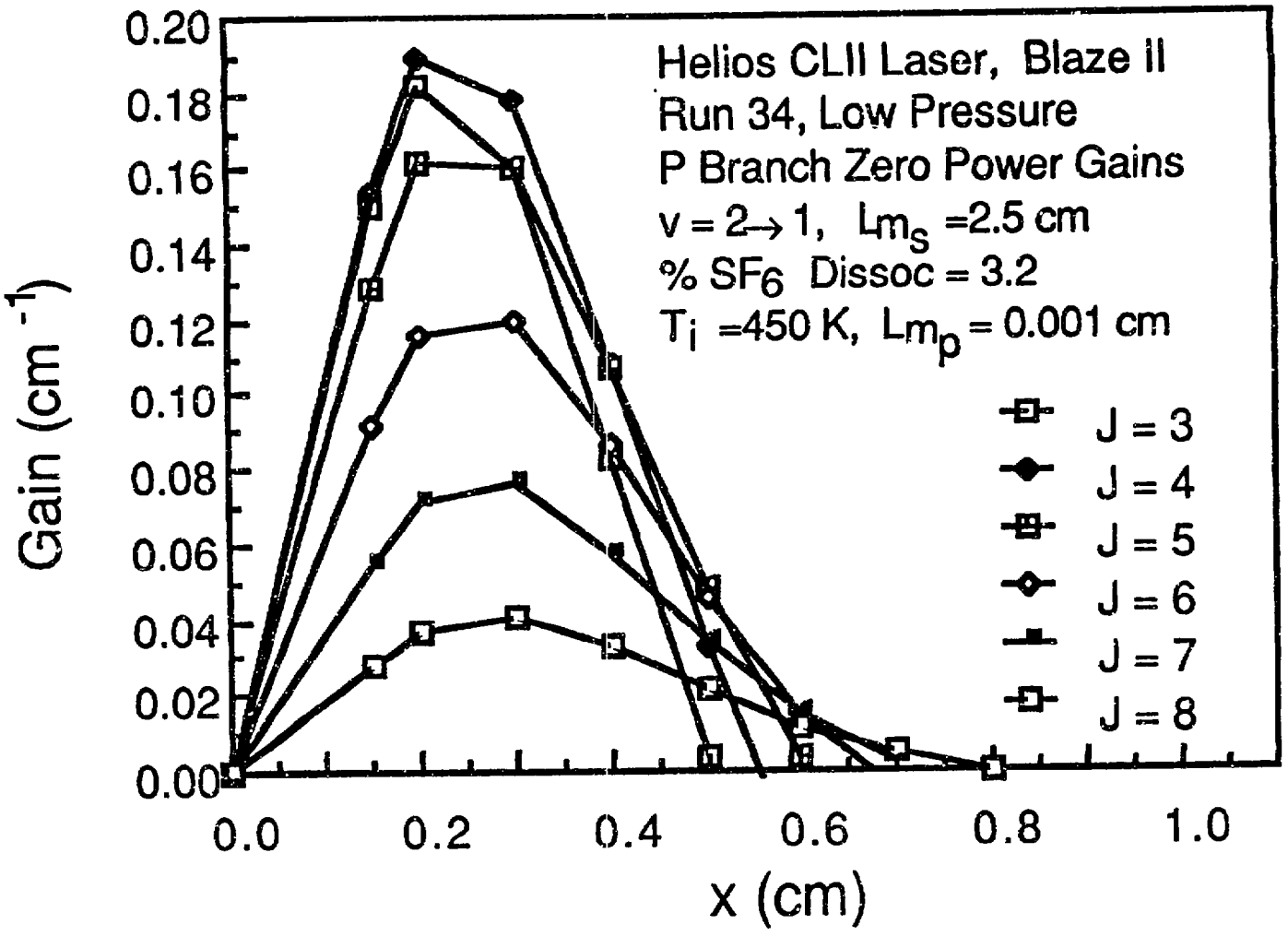

Figure 66. Variation of the zero power gain as a function of distance downstream of the H_2 injectors from the Blaze II model of the CL II laser[2]. L_{mp} is the mixing length of the primary stream, L_{ms} is the mixing length of the secondary stream, T_i is the static temperature of the flow at the H_2 injectors.

that the calculated $P_1(J)$ peaks are about 9% smaller than the measured peaks and the calculated $P_2(J)$ peaks are about 13% larger than the measured peaks. Comparison of the length of the calculated and measured zero power gain zones showed that the calculations predict gain zones that are about 30% longer than the data. The calculated $P_1(J)$ zero power gains peak 4.0 mm downstream of the H_2 injectors, while the experimental ones peak 1.5 to 2.0 mm downstream of the H_2 injectors. The calculated $P_2(J)$ zero power gains peak 2.0 mm downstream of the H_2 injectors while the experimental ones peak 1.0 mm downstream of the H_2 injectors. The calculations predict that the peak zero power gain lines are two J's lower than the data. The differences between the calculated and measured zero power gains are probably a consequence of approximating the three dimensional flow field with a one dimensional scheduled mixing model[2].

3.9 SUMMARY

Low pressure zero power gain data showed that the $P_2(J)$ peak zero power gains are about 1.55 times larger than the $P_1(J)$ peak zero power gains. The length of the gain zone of the $P_1(J)$ lines is about 1.3 times larger than that of the $P_2(J)$ lines. The zero power gains of all the $P_1(J)$ lines reach their peak 1.5 - 2.0 mm downstream of the H_2 injectors while the zero power gains of the $P_2(J)$ lines reach their peak 1.0 mm downstream of the H_2 injectors. The locations of both the $P_1(J)$ and the $P_2(J)$ peak zero power gains are close to the location of the optical axis for peak power when the CL II was run as an oscillator with a stable resonator[1]. The lines with the highest zero power gains are $P_1(5)$ and $P_1(6)$ for the $1\rightarrow0$ vibrational band and $P_2(5)$ and $P_2(6)$ for the $2\rightarrow1$ vibrational band.

The variation of zero power gain with height in the flow channel was investigated and it was found that the zero power gain values obtained 0.75 mm above and 0.75 mm below the center of the flow channel are almost identical

and higher than the values of the zero power gain measured on the flow channel centerline. This is due to the way the primary and the secondary streams mix after injecting H_2 from the upper and lower flow channel walls.

The effect of high pressure on zero power gain was investigated for lines $P_1(6)$, $P_2(5)$ and $P_2(6)$. It was found that high pressure results in zero power gain zones that are considerably shorter than those measured in the case of low pressure. The peak zero power gain of $P_1(6)$ was not affected by high pressure but the peak zero power gains of $P_2(5)$ and $P_2(6)$ were decreased by about 22.5%. This is a result of the fact that the increased deactivation of HF(2) repopulates HF(1) thereby keeping the population difference between HF(1) and HF(0) about the same whereas the population difference between HF(2) and HF(1) decreased. High pressure caused the location of the peak zero power gain to occur 0.5 mm closer to the H_2 injectors for all three lines.

The effect of polarization on zero power gain was investigated by using an unpolarized and a horizontally polarized input beam and non-Brewster windows on the amplifier. The non-Brewster windows acted as a Fabry-Perot resonator, causing the amplifier to lase on lines $P_2(4)$ and $P_2(5)$. The fact that the lines $P_2(4)$ and $P_2(5)$ lased with the non-Brewster windows on the amplifier supports the zero power gain data because it suggests that $P_2(4)$ and $P_2(5)$ have the highest gains, which is in agreement with the experimental results that show $P_2(5)$ to have the highest zero power gain followed by lines $P_2(4)$ and $P_2(6)$ whose zero power gains were about equal. The amplifier lasing was stopped after tilting the right non-Brewster window by about 0.5 degree. Then gain versus x data was obtained for lines $P_1(5)$, $P_1(6)$, $P_2(5)$ and $P_2(6)$ using an unpolarized beam. Comparison of the gains obtained in this case with the zero power gains of the same lines obtained with a vertically polarized beam showed that the gains obtained with the unpolarized input beam were

considerably lower. The gains obtained with the unpolarized beam were lower than the zero power gains obtained with the vertically polarized beam because the right amplifier non-Brewster window reflected (the non-Brewster window reflectivity was calculated to be 3.3%) back into the cavity enough power to cause a significant increase of the average intensity that the media sees. This increased I_{AV} was enough to perturb the media and cause the amplifier gain to decrease from the zero power gain levels measured with a vertically polarized beam to the gains measured with an unpolarized beam. The right amplifier non-Brewster window was then tilted 1.0 degree more, and the gain was measured as a function of x. The gain measured in this case was equal to the zero power gain measured with the Brewster windows on the amplifier. Zero power gain measurements were then made for lines $P_1(5)$ and $P_2(5)$ using a horizontally polarized input beam. The input powers required for these measurements (in order to reach the zero power gain levels) were considerably lower than the input powers used in zero power gain measurements with a vertically polarized input beam. Comparison of the zero power gain measured with an unpolarized and with a horizontally polarized input beam with the zero power gain measured with a vertically polarized input beam showed that polarization does not affect the zero power gain.

Zero power gain Blaze II calculations[2] showed that best agreement between the experimental and the calculated zero power gains was obtained for 3.2% SF_6 dissociation and 2.5 cm secondary mixing length. Comparison of the calculated and experimental peak zero power gains showed that the calculated $P_1(J)$ peak zero power gains are about 9% smaller than the experimental ones, while the calculated $P_2(J)$ peak zero power gains are about 13% larger than the experimental ones. Comparison of the gain zones of the calculated and the experimental zero power gains showed that calculations predict gain zones that

are about 30% longer than the data. The calculated $P_1(J)$ zero power gains peak 4.0 mm downstream of the H_2 injectors, while the experimental $P_1(J)$ zero power gains peak 1.5 to 2.0 mm downstream of the H_2 injectors. The calculated $P_2(J)$ zero power gains peak 2.0 mm downstream of the H_2 injectors, while the experimental ones peak 1.0 mm downstream of the H_2 injectors. The calculations predicted that the peak zero power gain lines were two J's lower than the data.

IV. CONCLUDING REMARKS

Preliminary amplifier experiments with 0% and 50% aperturing of the input beam by the flow channel showed that flow channel aperturing caused a significant reduction (an average of 16%) in the amplification ratio. An investigation of the multiline amplifier absorption of the input beam showed that He and O_2 did not absorb and that the SF_6 absorption was less than 0.005 cm^{-1}. Thus, all amplifier experiments were performed with no flow channel aperturing of the input beam and the effect of SF_6 absorption could be neglected.

Multiline amplification experiments showed that the peak amplification ratios occurred at an X_c that is both close to the value of X_c for peak power when a stable resonator is used on the CL II, and close to the values of X_c at which the peak zero power gains of the $P_1(J)$ and $P_2(J)$ lines were measured. Thus, to obtain maximum amplification, the input beam should be passed through the amplifier at the X_c location corresponding to peak amplifier gain. Higher amplification ratios were obtained when both the oscillator and the amplifier were run at the Run 34 flow rates than when both were run at the Run 36 flow rates. This was a consequence of the higher input intensity that was used in the case of the Run 36 flow rates.

Preliminary single-line amplification experiments showed that the peak $P_1(6)$ and $P_2(6)$ amplification ratios occurred at the same X_c at which the zero power gains are a maximum. Thus, to obtain maximum single-line amplification, the input beam should be passed through the amplifier at the X_c for maximum zero power gain. The single-line amplification ratios were considerably lower than the multi-line amplification ratios that were measured using the same input power. This was a result of the fact that in the multiline case, the total input power was distributed among the different lasing lines, which

means that the input intensity on each line was less than the input intensity in the single-line case. This fact resulted in higher amplification ratios for each line, because each line's gain in the amplifier was depressed less than in the single-line case for the same total input power.

The multiline amplifier performance was measured as a function of input power. It was found that about 1/3 of the oscillator output needs to be input to obtain amplifier output equal to the oscillator performance.

The amplifier input power required to measure the zero power gain of each line was obtained by measuring the amplification ratio as a function of input power at the point in the flow field corresponding to maximum amplification. When the amplification ratio became independent of input power, the zero power gain region had been reached. The zero power gain of each line was then measured for the low pressure Run 34 and Run 36 flow rates as a function of x and it was found that the $P_2(J)$ peak zero power gains are about 1.55 times larger than the $P_1(J)$ peak zero power gains. The length of the gain zone of the $P_1(J)$ lines is about 1.3 times larger than that of the $P_2(J)$ lines.

The zero power gains of all the $P_1(J)$ lines reached their peak 1.5 - 2.0 mm downstream of the H_2 injectors while the zero power gains of the $P_2(J)$ lines reached their peak 1.0 mm downstream of the H_2 injectors. The lines with the highest zero power gains are $P_1(5)$ and $P_1(6)$ for the 1→0 vibrational band and $P_2(5)$ and $P_2(6)$ for the 2→1 vibrational band. The variation of zero power gain with height in the flow field was investigated by taking $P_2(5)$ zero power gain measurements with the Run 34 flow rates in the amplifier at the center line of the flow channel, and ± 0.75 mm above and below the center line of the flow channel. The zero power gain values obtained 0.75 mm above and below the center line of the flow channel were almost identical and higher than the zero power gain values measured on the flow channel centerline. This

was due to the way the primary and the secondary streams mix after injecting H_2 from the upper and lower flow channel walls.

The effects of high pressure on zero power gain were investigated for lines $P_1(6)$, $P_2(5)$ and $P_2(6)$; it was found that high pressure results in gain zones that are considerably shorter than those measured in the case of low pressure. The peak zero power gain of $P_1(6)$ was not affected by high pressure but the peak zero power gains of $P_2(5)$ and $P_2(6)$ were decreased by almost 22.5%. High pressure caused the location of the peak zero power gain to occur 0.5 mm closer to the H_2 injectors for all three lines.

The effect of polarization on zero power gain was studied by comparing zero power gain data taken with vertically polarized, horizontally polarized, and unpolarized beams. It was found that polarization does not affect zero power gain.

The best agreement between the experimental and the calculated[2] zero power gains was obtained when a 3.2% SF_6 dissociation and a secondary mixing length of 2.5 cm were used. Comparison of the experimental and the calculated peak zero power gains showed that the calculated $P_1(J)$ peak zero power gains are about 9% smaller than the experimental ones. The calculated $P_2(J)$ peak zero power gains are about 13% larger than the experimental ones. Calculations predicted gain zones that are about 30% longer than those measured experimentally. The calculated $P_1(J)$ zero power gains peak 4.0 mm downstream of the H_2 injectors, while the experimental $P_1(J)$ zero power gains peak 1.5 to 2.0 mm downstream of the H_2 injectors. The calculated $P_2(J)$ zero power gains peak 2.0 mm downstream of the H_2 injectors, while the experimental ones peak 1.0 mm downstream of the H_2 injectors. Calculations predicted that the peak zero power gain lines are two J's lower than the data. The differences between the calculated and measured zero power gains are probably

a consequence of approximating the three dimensional flow field with a one dimensional scheduled mixing model.

REFERENCES

1. L. H. Sentman and M. H. Nayfeh, "Nonlinear Interaction Between the Pumping Kinetics, Fluid Dynamics and Optical Resonator of cw Fluid Flow Lasers," AAE TR 83-5, UILU Eng. 83-0505, Aeronautical and Astronautical Engineering Dept., University of Illinois, Urbana, IL, March 1983.

2. L. H. Sentman and J. O. Gilmore, "Computer Simulation of cw HF Chemical Laser Unstable Resonator Performance," AAE TR 87-5, UILU Eng. 87-0505, Aeronautical and Astronautical Engineering Dept., University of Illinois, Urbana, IL, August 1985.

3. L. H. Sentman, D. L. Carroll, P. Theodoropoulos and A. Gumus, "Scale Effects in a cw HF Chemical Laser," AAE TR 86-5, UILU Eng. 86-0505, Aeronautical and Astronautical Engineering Dept., University of Illinois, Urbana, IL, September 1986.

4. Helios Models CL I and CL II Laboratory Chemical Laser Systems Installation and Operating Manual, Helios Incorporated, 1822 Sunset Place, Longmont, CO 80501.

5. Infared Industries Type 5035 Lead Selenide Detector Manual, Infared Industries, 12151 Research Parkway, Orlando, FL 32826.

6. Rofin RS 600 Series Optical Spectrum Analyzer Manual, Rofin Sinar, Hamm Moor Lane, Weybridge, Surrey KT152SN, England.

7. L. H. Sentman, P. F. Schmidt and G. M. Marinos, "Effects of the HF Rate Package and the Optical Resonator on cw HF Chemical Laser Performance," AAE TR 88-6, UILU, Eng. 83-0506, Aeronautical and Astronautical Engineering Dept., University of Illinois, Urbana, IL, June 1983.

8. R. Driscoll et al., "DF/HF Chemical Laser Technology," AFWL TR 81-69, November 1981.